

NASA-CR-168509
1982 0011894

A Reproduced Copy
OF

DUPLICATE COPY

1982
LUNAR TECHNOLOGY CENTER
4000 GOLF COURSE ROAD
HOUSTON, TEXAS

Reproduced for NASA
by the
NASA Scientific and Technical Information Facility

STAR (113)

Optimum Employment of Satellite Indirect Soundings as Numerical Model Input

Department of Meteorology
University of Wisconsin-Madison
1225 W. Dayton Street
Madison, Wisconsin 53706



Contributions by

J. C. Derber
L. H. Horn
T. L. Koehler
B. D. Schmidt

L. H. Horn, Principal Investigator

FINAL REPORT

The research in this report has been supported
by the Goddard Laboratory for Atmospheric Sciences of the
National Aeronautics and Space Administration under Grant NSG-5252

December 1981

(NASA-CR-168509) OPTIMUM EMPLOYMENT OF
SATELLITE INDIRECT SOUNDINGS AS NUMERICAL
MODEL INPUT Final report (Wisconsin Univ. -
Madison.) 112 p HC AC6/ME A01 CSCL 04B

882-19768
TH&U
882-19771
JNC&S
09172
63/47

N82-19768
+hrw
N82-19771



Optimum Employment of Satellite Indirect Soundings as Numerical Model Input

Department of Meteorology
University of Wisconsin-Madison
1225 W. Dayton Street
Madison, Wisconsin 53706



Contributions by

J. C. Derber
L. H. Horn
T. L. Koehler
B. D. Schmidt

L. H. Horn, Principal Investigator

FINAL REPORT

The research in this report has been supported
by the Goddard Laboratory for Atmospheric Sciences of the
National Aeronautics and Space Administration under Grant NSG-5252

December 1981

NSG-19768-NR-19771

TABLE OF CONTENTS

	Page
Introduction	111
I. A Case Study of Height and Temperature Analyses Derived from Nimbus-6 Satellite Sounding, by Thomas L. Koehler . . .	1
II. Evaluation of TIROS-N and NOAA-6 Satellite Data: Comparisons of Colocated Soundings and Analyses for a January Case, by Brian D. Schmidt, Thomas L. Koehler and Lyle H. Horn	51
III. A Numerical Evaluation of TIROS-N and NOAA-6 Analyses in a High Resolution Limited Area Model, by John C. Derber, Thomas L. Koehler and Lyle H. Horn	82

INTRODUCTION

This report serves as the Final Report for research supported by the National Aeronautics and Space Administration, Goddard Laboratory for Atmospheric Sciences under Grant NSG-5252. (Optimum Employment of Satellite Indirect Soundings as Numerical Model Input.) The fundamental goal of this project was to identify characteristics of satellite-derived temperature soundings that would significantly affect their use as input for numerical weather prediction models.

Many of the previous sounding evaluations involved model impact studies that mixed satellite soundings with conventional data, before the error characteristics of the satellite soundings were fully defined. In contrast, our work has emphasized independent evaluations of satellite soundings to better define these error characteristics. The article by Koehler presents a Nimbus-6 sounding study from February 1976 (during the winter Data Systems Test). His results reveal an underestimation of the strength of synoptic scale troughs and ridges, and associated gradients in isobaric height and temperature fields. The most significant errors occur near the earth's surface and the tropopause. The instruments carried aboard Nimbus-6 were prototypes for those carried aboard the TIROS-N and NOAA-6 satellites, which provided the global distribution of satellite-derived temperature profiles during the important FGGE year observational study (from December 1978 through November 1979).

Soundings from the TIROS-N and NOAA-6 satellites are evaluated in Schmidt, Koehler and Horn. Their results are remarkably similar to those from Koehler, again showing an underestimation of upper level trough amplitudes leading to weaker thermal gradient depictions in satellite-only fields. These errors show a definite correlation to the synoptic flow patterns.

Derber, Koehler and Horn used one of Schmidt et al.'s satellite-only analysis to initialize a numerical model forecast, and found that these synoptically correlated errors are retained in the forecast sequence. If the sounding errors were not retained or were more random in nature, they could be more easily combined with conventional data in data rich regions. However, the correlated nature of these sounding errors complicates their incorporation into conventional data sets. Thus, this knowledge of the nature of the satellite errors should be used in additional efforts to develop methods which can facilitate the inclusion of satellite-sounding information into the observational data mix.

N82

19769

UNCLAS

A Case Study of Height and Temperature Analyses

Derived from Nimbus-6 Satellite Soundings

Thomas L. Koehler

Department of Meteorology
University of Wisconsin-Madison, WI 53706

Abstract

Height and temperature analyses were constructed on a subset of the LFM grid using only Nimbus-6 satellite temperature profiles from approximately 1800 GMT 22 Feb. 1976. Several experiments were performed to evaluate various features of these satellite-derived analyses. Fields derived from the bracketing LFM analyses provide the verification data. Results from this study provide insight into possible reasons for the inconclusive results from the DST-6 impact studies.

The results indicate that Nimbus-6 soundings were able to correctly position the major troughs and ridges, but underestimate gradients in the analyses due primarily to the soundings being too warm in the troughs. No advantage could be found in using a set of satellite soundings with a greater horizontal resolution than the DST soundings.

While the satellite soundings for this period were degraded due to a loss of one set of infrared channels, results from this study are quite similar to those presented in Phillips et al. (1979), Schlatter (1981) and Schmidt et al. (1981) with more recent TIROS-N and NOAA-6 sounding data. This suggests inherent limitations in the methods used to derive these soundings, and in their incorporation into conventional data sets.

1. Introduction

The ability to provide accurate synoptic scale weather predictions from one to several days has been hampered by the lack of conventional data over large regions of the globe, especially ocean regions. During the last decade considerable effort has been expended to alleviate this problem by providing truly global data sets. The culmination of this effort was reached in the collection of the FGGE year data sets (December 1978 to November 1979). Vertical temperature profiles derived from satellite measurements comprise an integral part of these global data sets.

During the periods 18 August to 4 September 1975 and 2 February to 4 March 1976, the National Aeronautics and Space Administration (NASA) conducted Data Systems Tests (DST-5 and DST-6, respectively) to evaluate several components of the special FGGE observing systems in an operational mode. During the DST periods, atmospheric temperature profiles were derived from radiometric data measured by instruments aboard the Nimbus-6 satellite. These instruments were prototypes of those carried aboard the TIROS-N and NOAA-6 satellites during the FGGE year.

As part of the DST evaluations, several research institutions completed impact studies designed to assess the effect of Nimbus-6 satellite soundings on Northern Hemispheric model predictions. Two and three day forecasts started from initial states with and without satellite temperature profile data were verified. The results from these studies, as presented by Miyakoda et al. (1977) for the Geophysical Fluid Dynamics Laboratory (GFDL), Halem et al. (1978) for the Goddard Institute for Space Studies (GISS) and Desmarais et al. (1978) for the National Meteorological Center (NMC), were inconclusive. Considerable debate was generated between these groups concerning the reasons for the lack of significant impact. While the poor quality of satellite soundings may have been a major cause for the lack of impact, other design features of the studies may have contributed. For example, impact was primarily determined using two to three day forecasts from relatively coarse mesh (~400 km grid spacing) numerical models. Finer resolution model runs over shorter periods are known to be more accurate. Also, satellite soundings were mixed with data from other sources for these studies. Since satellite soundings have different characteristics than radiosonde soundings, care must be taken to combine them properly. The results from the DST experiments raised serious questions concerning the ability of satellite soundings to provide the

additional, reliable information over data-sparse regions needed for improved numerical weather prediction.

In this paper, a case study approach is used to evaluate Nimbus-6 satellite soundings over the data-dense region of North America for one day from the winter DST-6 period. Analyses of mandatory pressure level heights were constructed on a subset of the Limited-area Fine Mesh (LFM) model grid of NMC, which had a grid spacing of 190.5 km. This grid permitted a better resolution of synoptic scale patterns than the coarser grids used in the DST impact studies. The height fields were constructed using only satellite soundings and conventional surface data, eliminating the problems involved with mixing satellite soundings with conventional upper air data. In addition to evaluating the ability of satellite soundings to define height fields, other investigations were undertaken. These included using both the DST resolution and a higher horizontal resolution data set, manually checking the soundings for horizontal consistency, and subjecting the satellite-derived analyses to the LFM model initialization procedure.

Several factors have limited the applicability of the results from this study to the soundings collected during the FGGE year. This paper presents the results from research conducted in 1977 and 1978, a period when the DST impact studies were appearing, and before TIROS-N and NOAA-6 soundings became available. The operational retrieval methods used to process TIROS-N soundings were modified as a result of the experience gained from the DST results. Also, the instruments aboard the TIROS-N model satellites have wider scan angles than those aboard Nimbus-6, decreasing the wide gaps between adjacent satellite passes. Finally and more importantly, measurements in the 15 μm infrared channels were degraded by an instrument malfunction during the winter DST period, and were not used in the Nimbus-6 sounding retrievals.

Despite all of these limitations, useful information can be gleaned from the results presented. The soundings evaluated in the DST impact tests were derived in the same manner as those applied in this study. Since satellite soundings were not mixed with conventional upper air data, certain properties exhibited by Nimbus-6 soundings that may have led to the lack of model impact may be identified. It is also interesting to compare these "degraded" results to those from more recent studies with TIROS-N soundings such as Schmidt et al. (1981), Schlatter (1981) and Phillips et al. (1979). These comparisons may indicate whether the improvements made in the TIROS-N processing have had a significant

effect on the thermal fields defined by satellite soundings.

The presentation of this study proceeds in the following manner. The pertinent characteristics of the satellite sounding data are presented in Section 2, followed by a description of the study's design in Section 3. The data screening and analysis method appear in Section 4. Section 5 presents the results, which are summarized in the conclusions (Section 6).

2. The satellite sounding data

The orbital characteristics of the Nimbus-6 satellite, and the retrieval methods used to determine temperatures from the measured radiances, played an important role in the design of this study. The Nimbus-6 satellite was placed in a nearly sun-synchronous polar orbit, with the northbound orbital segments passing overhead at local noon (approximately 1800 GMT over the U.S.). Consecutive northbound passes cross the equator about 107 minutes apart, with passes progressing from east to west. Thus, satellite soundings are available in continuous swaths circling the globe, a limited number of which are available at the same time as conventional synoptic upper air observations. This asynchronous nature of satellite-derived temperature profiles has presented complex problems in both their application and evaluation.

Two instruments aboard the Nimbus-6 satellite provided the raw radiance data used to derive tropospheric temperature soundings: the High-resolution Infrared Sounder (HIRS) and the Scanning Microwave Spectrometer (SCAMS). Both instruments had scanning capabilities allowing them to provide fields of data. The HIRS scanning geometry is described in great detail because it served as a basis for the method used to convert radiance to temperatures.

As Nimbus-6 moved along its orbital path, both the HIRS and SCAMS instruments scanned from left to right (see Srith and Woolf, 1976). HIRS had a much smaller field of view (29.1 km diameter at nadir) compared to SCAMS (144 km). Also, HIRS required frequent inflight calibrations which resulted in gaps within the HIRS radiance data called calibration intervals. Each calibration interval covered an area equivalent to that of four scan lines and was thus approximately 120 km wide in the direction along the orbital path. Twenty scans were made between calibration intervals, each scan consisting of 42 individual fields of view. Thus, if a temperature retrieval was made for each individual HIRS field of view, 840 soundings would appear between calibration intervals, over an area 619 km by 1821 km (roughly equivalent to

one-seventh the area of the adjacent 48 states). The high density of possible HIRS soundings is both impractical and unmanageable for most purposes. Also, factors such as clouds, varying surface emissivities, pronounced surface elevation changes, and instrument noise cause some of the radiances to be unsuitable for temperature retrievals. Therefore, HIRS data from several adjoining fields were combined to decrease the total number of soundings and to remove unsuitable radiances.

The following description of the method used to combine the radiance data in the operational retrieval process is based on the HIRS scanning geometry illustrated in Figure 1. In this schematic diagram individual fields of view between two calibration intervals are depicted as circles. (The actual field of view would have an elliptical footprint which increases in size as the scan angle measured from nadir increases.)

The first step in obtaining a manageable data set was to subdivide this set of 840 fields of view into 30 subset arrays of 28 fields of view each. These subsets are called HIRS 4x7 blocks because each contains four fields of view along the orbital path by seven fields of view across the orbital path (see Fig. 1). Within a 4x7 block, each HIRS measurement is checked for consistency using SCAMS measurements interpolated to the HIRS fields of view. Acceptable radiances are then combined using a method described by Smith and Woolf (1976), designed to minimize the effect of cloud contamination. This combination yields a set of clear column (cloud-free) HIRS radiances representative of the 4x7 blocks, located by X's in Fig. 1. These clear column radiances are supplemented by SCAMS microwave radiances interpolated to the cloud-free radiance locations.

NESS had originally planned to provide temperature retrievals derived at these 4x7 locations during the DST data collection periods. An optimum of 30 soundings between calibration intervals would then have been available. Normal distances between these soundings would have been either 120 km or 240 km along the orbital path, and 300 km normal to the orbital path. (The longer 240 km distance along the orbital path is the distance between two soundings on either side of a calibration interval.) NMC, however, found the number of 4x7 soundings to be too large for operational data handling purposes. A maximum of 12 rather than 30 soundings between calibration intervals was deemed a more manageable number. To implement this reduction, averaging of the clear column infrared and interpolated microwave radiances for adjacent 4x7 blocks along the orbital path was performed.

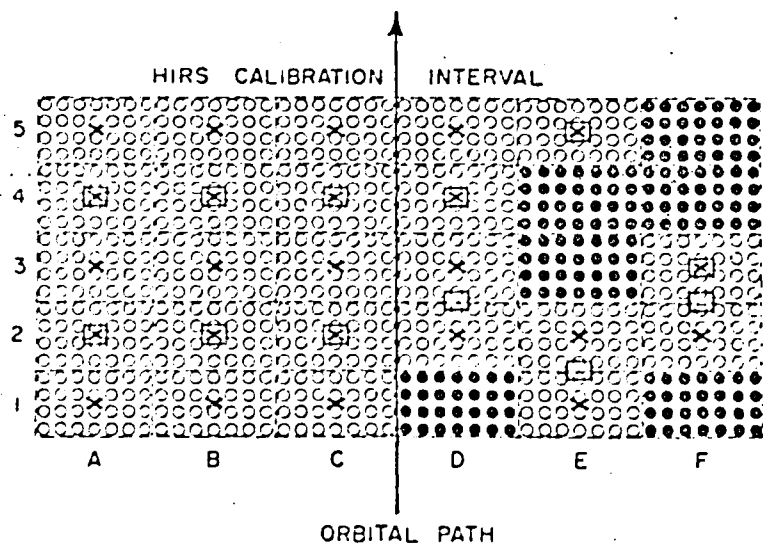


Figure 1. A simplified schematic of the HIRS data averaging process. Circles represent individual HIRS fields of view. The dashed lines outline HIRS 4x7 blocks. The 4x7 soundings are indicated by X's and the DST soundings by \square 's. Shaded circles represent 4x7 blocks with an inadequate number of HIRS measurements for sounding retrievals.

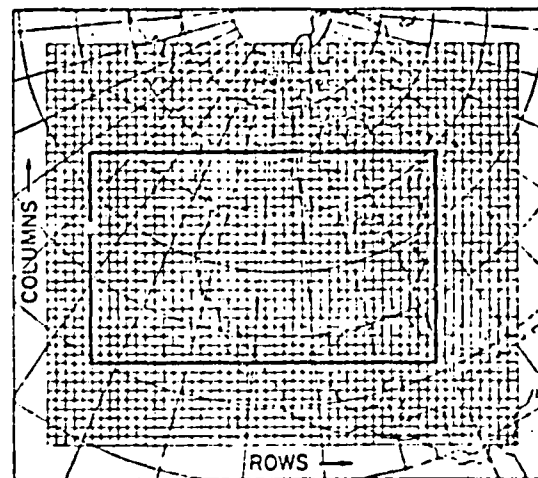


Figure 2. The LFM grid and the subset grid used for the satellite-derived analyses.

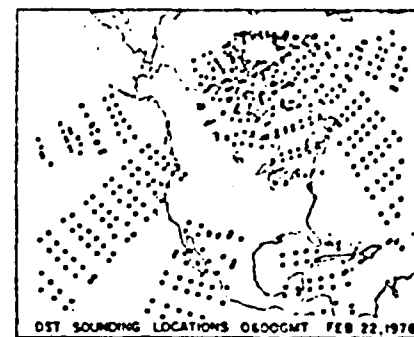


Figure 3. Nimbus-6 soundings at about 0600 GMT 22 Feb. 1976.

With only five 4x7 blocks available along the orbital path between calibration intervals, overlapping averages were required. In column A (Fig. 1) for example, cloud free radiances from blocks 1, 2 and 3 were averaged to yield a DST sounding (□) centered in block 2. Likewise, radiances from blocks 3, 4 and 5 were also averaged to create another DST sounding in block 4. The conversion from averaged radiances to temperature profiles was accomplished with an eigenvector approach also described by Smith and Woolf (1976). In an ideal situation, with no unacceptable HIRS data, twelve DST soundings would thus have been produced between calibrations with a spacing of 240 km along the orbital path within that region, and a spacing of 480 km across the calibration interval. The spacing in the other direction would remain at 300 km.

Examples to the right of the orbital path in Fig. 1 illustrate how this averaging was affected when adequate acceptable HIRS sounding pairs were unavailable within certain 4x7 blocks. These blocks are indicated by shaded circles. In column D, two DST soundings result from averaging radiances from blocks 2 and 3, and 3, 4 and 5 respectively. Note that the DST sounding is positioned at the center of the blocks being averaged. DST soundings also appear in blocks E1 and F3 because only the one block was available for the average.

Both DST and 4x7 temperature soundings are evaluated in this study. The main difference between the 4x7 and DST sounding sets is horizontal resolution. There are also other differences. In the DST data set, microwave only soundings were generated in regions where clear column radiances were unavailable, and the microwave data were acceptable. Also, in recalculating the 4x7 soundings from the original radiance data, more stringent acceptance criteria were used in the clear column infrared radiance determinations. Thus, if DST soundings appeared in regions where no 4x7 soundings were made, those soundings were either microwave only soundings or ones that passed the less stringent DST acceptance requirements.

3. The study design

As mentioned earlier a case study approach was used in this investigation. DST and 4x7 satellite soundings from five consecutive Nimbus-6 satellite passes over North America at local noon 22 February 1976, along with 1800 GMT surface observations, comprise the raw data for the experiment. While

the DST data set was made generally available for the DST impact tests conducted at several research institutions, the higher resolution 4x7 soundings for this February case were generated upon special request by the NESS group here at Wisconsin, and are unique to this study. The only previous study employing 4x7 soundings was by Elechman and Horn (1981), who investigated the use of higher resolution soundings in delineating a jet streak over North America on 25 August 1975.

Both the DST and 4x7 data sets were carefully inspected to detect inconsistent soundings, which were removed from these sets yielding two additional data sets, the screened DST and screened 4x7 sets. Analyses of heights on the mandatory pressure levels were constructed for each of the four resulting sounding sets (both screened and unscreened) on a subset of the LFM grid. These analyses were then passed through the LFM model initialization process. Finally, the satellite analysis and initialization fields were compared to equivalent LFM fields using methods designed to evaluate both magnitude and gradient information.

Results from these comparisons can provide insight into the following pertinent questions. How well do height and temperature fields prepared from DST-6 satellite soundings and surface data describe atmospheric features relevant to numerical prediction? What effect does increasing the horizontal resolution of satellite temperature soundings have upon these fields? Are the fields considerably improved by a careful manual screening of the temperature soundings? And to what degree are satellite thermal analyses affected by LFM model initialization? Answers to these questions, even if they are only partial answers, could prove valuable in developing better methods for combining satellite soundings with data from other sources. The remainder of this section is devoted to explaining the development of this experimental design.

Common sense dictates that satellite soundings must be evaluated over regions with dense conventional data coverage. Since model initializations were also to be evaluated, it seemed logical to employ an existing numerical model over a data-dense region for this study. The LFM model fulfilled not only these requirements, but also had a 190.5 km grid spacing (true at 60°N) that allowed better resolution of important synoptic scale features than the roughly 400 km grid meshes employed in the DST impact tests. Another advantage in using the LFM is its familiarity in the meteorological community. The analysis subset grid employed in this study is superimposed on the complete LFM grid in Figure 2.

Several factors influenced the choice of time period studied. A case from DST-6 with strong winter temperature gradients would enable a better evaluation of satellite capabilities than a case from the summer DST-5. However the HIRS instrument malfunctioned before the start of DST-6, degrading the longwave infrared channels and the resultant temperature profiles. Also, LFM tapes for the DST-6 period were available here at the University of Wisconsin due to a special arrangement with NMC. These tapes are not routinely archived and are therefore not readily available for use in case studies.

Daily weather maps from the DST-6 period were studied to find an interesting synoptic case suitable to this investigation. A case with two troughs in the analysis region appeared from 21 February through 23 February 1976. The DST sounding locations were extracted from the NESS sounding archive tapes from 16 February through 23 February. These locations were plotted over a region slightly larger than the LFM grid to get a general idea of the data distribution available. Nimbus-6 passed overhead at local noon and midnight, and thus passed over North America a few hours on either side of 0600 GMT and 1800 GMT. Unfortunately, no observations were processed during data readouts over the United States at roughly 0600 GMT, resulting in large data gaps over the region of interest. This is illustrated in Figure 3 for satellite passes at roughly 0600 GMT 22 February 1976. The lack of adequate data coverage over the United States at 0600 GMT precluded any attempt to study the time continuity of satellite analyses. It was finally decided to use the 1800 GMT 22 February soundings in this case study. The distribution of DST and 4x7 satellite sounding locations for this period are shown in Figure 4.

Two properties of the satellite sounding data sets complicated the verification procedures used in this evaluation. First, the satellite soundings in the analysis region were taken at roughly 1800 GMT (± 3 hours), nearly midway between the conventional 1200 GMT and 0000 GMT synoptic times, as shown schematically in Figure 5. In addition, consecutive passes are 107 minutes apart, which leads to a 6 hour time difference between the easternmost and westernmost soundings in the analysis region. This problem is better illustrated in Figure 6, an observation time analysis from the unscreened DST data set. Another problem is also depicted in this figure. The shading denotes the wedge-shaped satellite data-void regions between consecutive passes that appear south of about 55°N. These data gaps cause unique analysis problems.

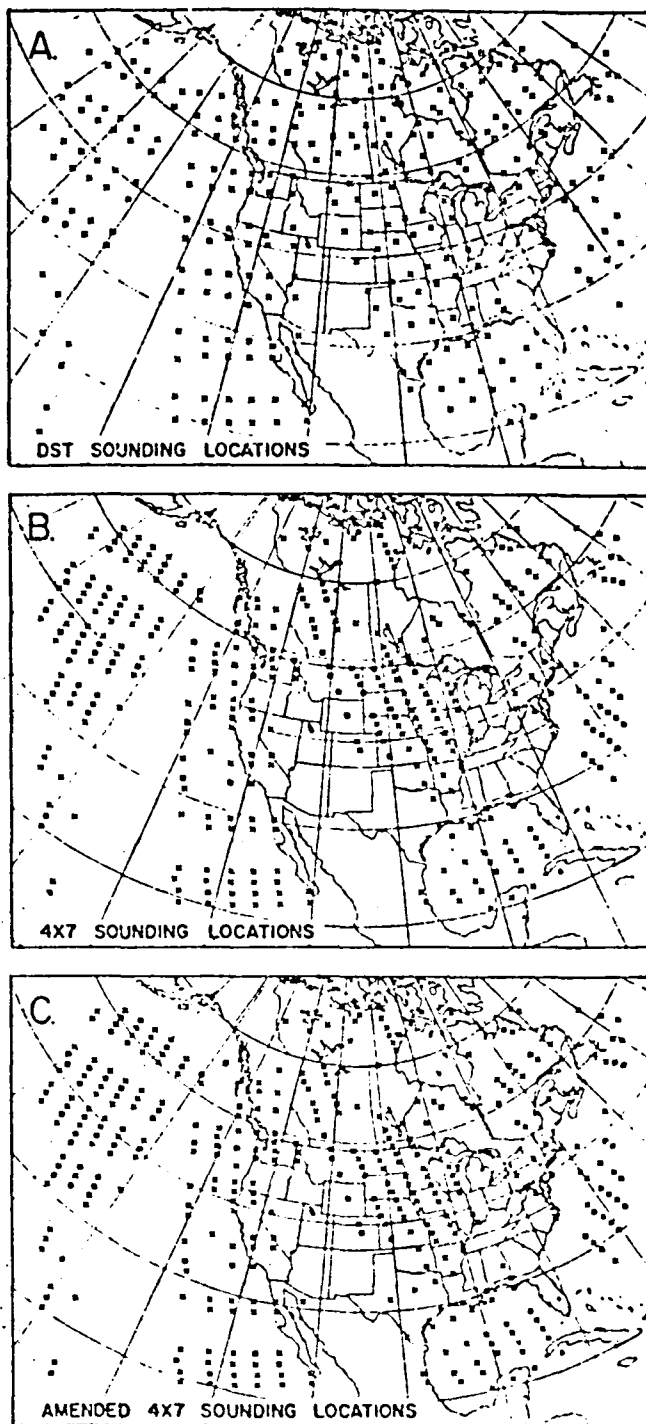
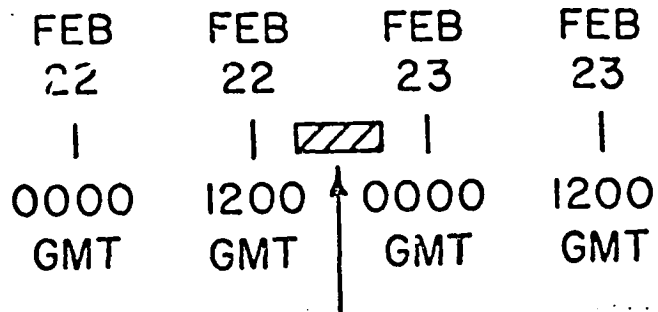


Figure 4. Nimbus-6 satellite soundings around 1800 GMT 22 Feb. 1976. Panel A - DST sounding locations, panel B - 4x7 sounding locations and panel C - final 4x7 sounding locations supplemented with qualifying DST soundings (see text). indicates soundings removed in the screening process.



SATELLITE SOUNDING OBSERVATION TIMES

Figure 5. A schematic illustrating the time interval of the satellite soundings in relation to the four synoptic times used to derive the verification data.

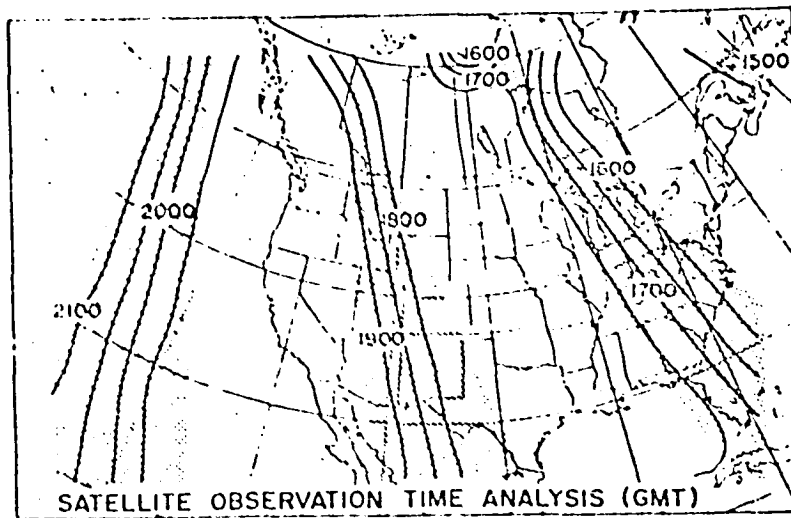


Figure 6. An analysis of satellite sounding observation times. The gaps between consecutive satellite passes are shaded.

Rather than just comparing the satellite results at roughly 1800 GMT to the bracketing 1200 GMT and 0000 GMT values, as done by Horn et al. (1976) and Petersen and Horn (1977), bogus LFM verification fields were generated which incorporated these limiting features of the satellite sounding data sets, namely data gaps and asynoptic times. The first step in constructing bogus LFM analyses was to remove the time differences between the satellite and LFM analyses. This was performed by interpolation to satellite sounding times from the four bracketing LFM analyses using overlapping quadratic polynomials. Two sets of bogus LFM analyses were constructed. The first simply interpolated grid point values in time using the grid point analysis of satellite observation time illustrated in Figure 6. The generation of the second bogus set involved a more complicated two step procedure. In the first step, grid point values were interpolated in space to the satellite observation locations for all four bracketing LFM analyses, and then interpolated to the reported satellite sounding time. (These soundings were used as the verification data in the colocated comparisons.) The bogus LFM set was then derived by interpolating these colocated values in space back to the grid points using the same analysis and filtering procedure applied in the satellite sounding thickness analyses.

The first bogus LFM analysis set derived from time interpolation only provides an estimate of the LFM fields valid at the times of the satellite observations. In the second bogus LFM set, both time and space interpolations are employed to further simulate inherent spatial limitations of the satellite soundings in this case. This latter bogus LFM set is labelled INTERP LFM to emphasize the spatial interpolation. A comparison between these two bogus LFM analysis sets given later in this report provides an estimate of how much information is lost in the analysis process.

The satellite-derived analyses can at best be expected to reproduce the INTERP LFM bogus analyses. Therefore, those fields serve as the standard of comparison in the visual and gridded statistical evaluations. In essence, the LFM analyses have been degraded to the same level as their satellite-derived counterparts to provide equivalent comparisons.

A final point to consider in this discussion of the case study design is that the Nimbus-6 soundings provided only temperature data at 21 levels between 1000 mb and 100 mb inclusive, and thickness values derived from these temperatures for layers between 1000 mb and each remaining mandatory level

(1000-850 mb, 1000-700 mb, etc.). Reference level information was needed to determine heights on mandatory pressure levels used in the evaluations. Heights of the 1000 mb level derived from surface observations taken at 1800 GMT from the surface synoptic stations and other sources provided the reference level information. These 1000 mb heights were derived using standard reduction methods described in Schüepp et al. (1964).

In constructing the bogus LFM data sets, thickness values relative to 1000 mb rather than heights were the fields interpolated in time. The same reference level values used in the satellite analysis were used to derive the heights in these bogus LFM sets. The reason for proceeding in this manner, rather than interpolating height values directly, was to remove any bias that may enter from the different 1000 mb height determination methods used in this study and at NMC.

4. Data screening and analysis methods

An important and time consuming segment of this study was the manual screening of the DST and 4x7 satellite soundings. This screening procedure involved a careful examination of both vertical and horizontal sections of the atmosphere to detect inconsistent soundings removed to create the screened data sets. Before proceeding with this screening, the original 4x7 data set was supplemented with selected DST soundings in data gaps such as Texas, the northeast U.S. and central Canada, where soundings available in the DST set were not available in the 4x7 set (see Figures 4A and 4B). Only 14 DST soundings derived from a single 4x7 block of HIRS measurements were added to the original set of 356 4x7 soundings. These additional soundings were either microwave only or those rejected due to more stringent 4x7 acceptance criteria. While such soundings may have been of lower quality than the original 4x7 set, they provided more information than no data in these regions, and still had to pass the consistency checks in the screening procedure. The positions of the amended 4x7 sounding set, hereafter called simply the 4x7 set, are shown in Figure 4C.

The first step in the screening procedure was to plot and hand analyze horizontal maps of mandatory level temperatures and thicknesses relative to 1000 mb from both the DST and 4x7 sounding sets. Inconsistent soundings were noted for each analysis. Cross-sectional analyses of potential temperature and isotachs of the thermal wind relative to 1000 mb were constructed from

the level temperature information using an objective method developed by Whittaker and Petersen (1977). Thermal wind analyses measure thermal gradients along the cross section and are valuable in detecting vertically integrated gradient errors. Six roughly north-south cross sections were constructed for each orbital path, one for each of the columns labelled A through F in Fig. 1. The 6 cross sections for each pass were displayed sequentially to aid in detecting inconsistencies from one section to the next.

Figure 7 illustrates how cross-sectional analysis can emphasize sounding errors. The westernmost column of soundings from the 4x7 data set were used in this figure. Often errors of one sign in the lower troposphere for a given sounding were accompanied by errors of the opposite sign in the upper troposphere. The two soundings labelled 5068 and 5090 show this typical problem, with 5068 being too warm in the lower troposphere and too cold near 300 mb, while the opposite is true of 5090. Note how the thermal wind analysis emphasizes a problem between 5084 and 5090.

Inconsistent soundings detected in the horizontal hand analyses were double-checked on the cross sections, with gross inconsistencies at any level causing removal of the entire sounding. The multidimensional view from both horizontal and vertical sections helped in making the decision of which were the poor soundings, a decision that was sometimes easy, but often difficult. In the example from Figure 7, the decision to remove 5068 and 5090 from the screened data set was fairly straightforward, but the decision to remove 5084 was more difficult because it required comparisons with other cross sections.

The soundings deemed inconsistent by this method are indicated by a in Figure 4. The yield of acceptable soundings is much higher for the DST set than for the 4x7 set. Only 16 of 300 (5.3%) of the DST soundings were removed to form the screened DST set, while 107 out of 370 (28.9%) were removed from the 4x7 set. This result is not surprising since as many as three 4x7 soundings were averaged together to form one DST sounding, smoothing errors found in the 4x7 set. Thus, while the yield of the DST soundings was higher than that of the 4x7 set, good data may have been averaged with poor data to give mediocre yet consistent soundings.

Unfortunately, cloud contamination is not the sole factor in producing inconsistent soundings. A distinct inconsistent-cloudy relationship is difficult to perceive from Figure 8, where the 4x7 sounding locations are superimposed upon a hand analysis of percent cloudiness reported for each satellite

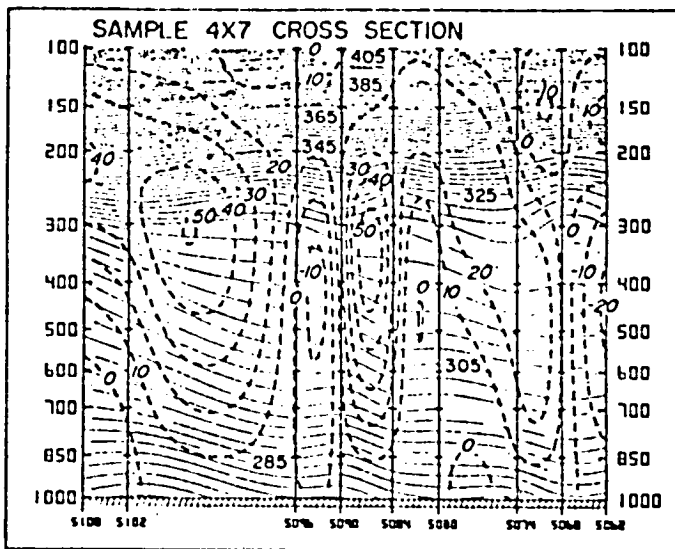


Figure 7. A sample cross section used in the screening procedure. Isentropes ($^{\circ}\text{K}$) are solid, and isotachs of the thermal wind component relative to 1000 mb and normal to the cross section (m s^{-1}) are dashed. Soundings 5090 and 5084 are 120 km apart.

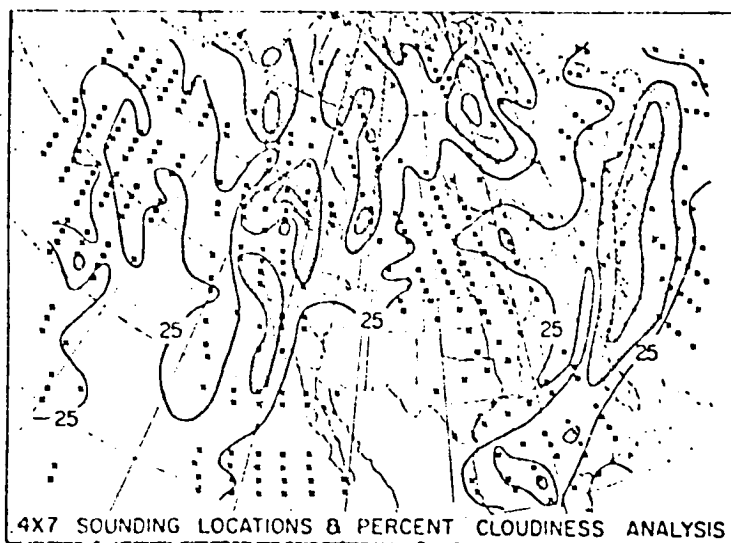


Figure 8. Satellite sounding percent cloudiness analysis superimposed upon the 4x7 sounding locations (Fig. 4C). Isopleths are drawn every 25%, with areas above 50% cloudiness shaded. \blacksquare again indicates unacceptable soundings.

sounding. (Comparisons against a cloud analysis from the surface synoptic network, satellite cloud photographs, radar maps and precipitation reports demonstrated that this analysis gives a reasonable representation of cloud cover.) The cloud band along the east coast was by far the most active in terms of precipitation, which may have degraded microwave only soundings in that region. Much of the cloud contamination problem already appeared in the form of missing data in the mostly cloudy regions.

The satellite data screening procedure took considerable time and effort. The decision to remove a given sounding often required a complete, three-dimensional view of the data structure. This fact, along with the lack of any systematic relation between clouds (and precipitation) and inconsistent soundings, would complicate attempts to computerize this screening procedure.

The next step in the study was to construct gridded height analyses for both the screened and unscreened 4x7 and DST sounding sets (4 satellite-derived sets total). The process of transforming data at observations into final analyses on the LFM grid involves several interpolation and filtering operations which form the analysis procedure. Several characteristics of the basic data (satellite soundings and surface observations) presented certain difficulties which required special consideration in the development of this procedure.

The wedge-shaped data gaps between satellite pass south of about 55°N create an abrupt transition in data coverage that can cause severe interpolation problems. Also, the satellite soundings provided only thickness information which was combined with base level information from surface observations to form the isobaric height data used in the analyses. The analysis procedure was designed taking these factors into account.

The analysis process employs two types of interpolation: interpolation from the unevenly spaced observations to the uniform set of grid points, and its inverse, interpolation from grid points to observations. The latter is needed to provide first guess and 1000 mb height values at observation locations. Several methods were tested for each type of interpolation, using a typical set of Nimbus-6 sounding locations to simulate the data gap problem. Data values at both LFM grid points and these observation locations were specified by analytic functions designed to approximate atmospheric height and temperature fields. The ability to specify values at both observation and grid point locations permitted an exact measure of accuracy for the different

interpolation methods tested.

The results from these interpolation experiments are presented in Koehler (1979). The grid to observation interpolation test results indicated that the optimum interpolation method developed by Gandin (1963) was among the most effective for this particular application. A modification of this method also discussed by Gandin, called optimum interpolation with normalized weights, was chosen for the observation to grid interpolations in this study. Normalization of the interpolation weights was incorporated to counter the variability in the sum of the interpolation weights that appeared in the satellite data gaps.

Excellent discussion on the theoretical basis for optimum interpolation methods and their development are presented by Gandin (1963), Schlatter (1975) and Bergman (1978). A detailed description of the interpolation method used in this study is presented in Koehler (1979). Only certain features of this method will be discussed here.

The method is designed to incorporate the statistical structure of the field being analyzed (isobaric height). The observational error structure is also included in the analysis method, such as the correlated nature of the satellite soundings. The specification of these statistical properties is fully described in Koehler (1979).

The eight closest observations are used for a given grid point, and only one set of interpolation weights are determined for each data set. These weights are used to construct analyses at all mandatory levels. The analyses for most variables used persistence first guess fields taken from the LFM analysis 18 hours previous to the satellite analyses. Analyses of variables with no first guess field (such as the time analysis in Figure 6) could still be performed due to normalization of the interpolation weights.

As mentioned before, a grid to observation interpolation method was needed to transfer the gridded first guess values and 1000 mb heights to the satellite observation locations. A method introduced by Bleck and Haagenson (1968) that employs overlapping quadratic polynomials proved to be both accurate and efficient for this type of interpolation.

A step-by-step description of the analysis procedure follows. Since all four satellite sounding sets and the bogus LFM fields used the same 1000 mb base level information, the 1800 GMT 1000 mb analysis was completed first. First guess values were interpolated to the surface synoptic station

and ship report locations. Interpolation weights were then derived for the 8 closest observations to each grid point, with only those observations within 2000 km eligible for use at that point. Thus, it is possible that fewer than 8 observations were used in the interpolation to certain grid points in data sparse regions. After the analysis values were determined by applying these weights, a filter consisting of a smoother-desmoother was passed over the 1000 mb analysis to remove small scale noise from the initial analysis. This filter is the same as one applied in the postprocessing of LFM initial hour and forecast fields. (See Gerrity and Newell, 1976.) The spectral response of this filter, and another called the combined filter are depicted in Figure 9, the latter being used to filter the upper level, satellite-derived height analyses. Note that the effect of these filters is to remove all $2\Delta x$ noise from the analysis, while synoptic scale features at longer wavelengths are retained.

The next series of steps was repeated for each of the four satellite sounding sets. The 1000 mb height values at each satellite sounding location were obtained by a grid to observation interpolation from the 1000 mb analysis. These 1000 mb heights were added to the satellite-derived thicknesses, yielding isobaric heights at each of the nine mandatory levels between 850 and 100 mb. First guess values were also estimated at each sounding location by grid to observation interpolation.

Analysis weights were then calculated for each of the four sounding location distributions. The raw height analyses at all mandatory levels for a given sounding distribution were then calculated with one set of interpolation weights. The combined smoother from Gerrity and Newell (1976) was applied to these raw height analyses to produce the final satellite height analyses studied extensively in the following sections.

One facet of the experiment was to determine the effect of model initialization on the mass field variables described by satellite soundings. The LFM model initialization program at NMC, described by Gerrity (1977), was run with the satellite data sets. While this initialization consists of several operations, the vertical interpolation of height and temperature values from the 10 mandatory pressure levels between 1000 mb and 100 mb to the model's σ -coordinate layers is of primary importance here. Also, while values on σ surfaces serve as model initialization fields, researchers using LFM save tapes are normally restricted to studying postprocessed initial hour data on

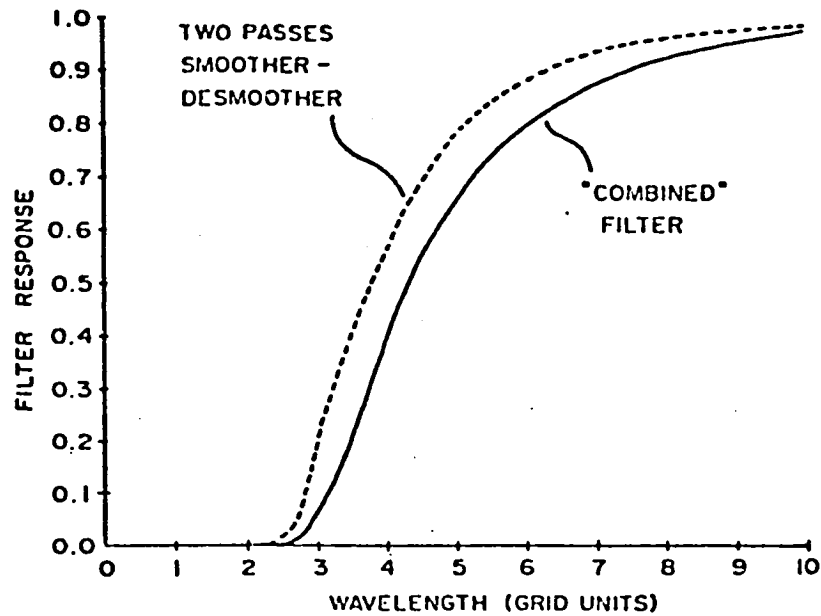


Figure 9. Filter response versus wavelength. (See Gerrity and Newell, 1976.)

Table 1. Statistics for the second bogus LFM minus first bogus LFM height field differences. Bias and RMS values are in meters while SI values are dimensionless. These statistics provide a measure of the information lost in the analysis process due mainly to systematic data gaps between satellite passes.

LEVEL (MB)	BIAS	RMS	SI
850	0.5	8.2	22.9
700	0.7	9.2	19.7
500	1.4	12.2	16.4
400	2.0	14.2	15.3
300	2.9	16.4	14.8
250	1.8	14.6	13.4
200	1.4	12.1	12.9
150	1.4	11.3	13.9
100	0.8	11.1	17.9

isobaric surfaces. Another vertical interpolation from σ to p is involved in the postprocessing, which has the effect of further smoothing the height and temperature field (Hyde, 1977). This should be kept in mind when considering the effects of the initialization presented in subsequent sections.

5. Results

The degree to which satellite soundings can provide either magnitude or gradient information for atmospheric mass field variables is an important consideration in their future application. Several methods were employed to evaluate both magnitudes and gradients from the satellite-derived analyses. These methods include visual comparisons of the basic fields, statistical measures commonly used in forecast verifications and comparisons of dynamic quantities derived from the basic fields, such as geostrophic wind, geostrophic temperature advection and available potential energy.

As mentioned earlier two LFM verification data sets were constructed from a time interpolation of the bracketing LFM fields to the times of the satellite observations. One of these sets (the INTERP LFM) included an application of the horizontal analysis procedure, while the other did not. This section begins with a comparison between these two bogus LFM data sets, which can be used to estimate the effect that data gaps between satellite passes have upon the satellite analyses. This comparison is followed by the evaluations of the satellite soundings described above.

A complete and detailed discussion of the results using data from 4 satellite sounding sets at 10 mandatory levels for both analysis and initialization fields could become quite laborious. Many results are given in tabular form for all mandatory levels. However, the text devoted to these tables will usually be brief and will concentrate on points of greatest relevance and interest.

In many of these presentations, labels for the 4 satellite sounding sets have been abbreviated. The unscreened DST and 4x7 sets are termed ALL DST and ALL 4x7 respectively. Similarly, their screened counterparts are labelled SCR DST and SCR 4x7.

a. A comparison between the two bogus LFM data sets

The first bogus LFM analysis set derived only from time interpolation provides an estimate of the LFM fields valid at the times of the satellite observations. This is illustrated in Figure 10 which includes heights,

ORIGINAL PAGES
OF BOOK COPY

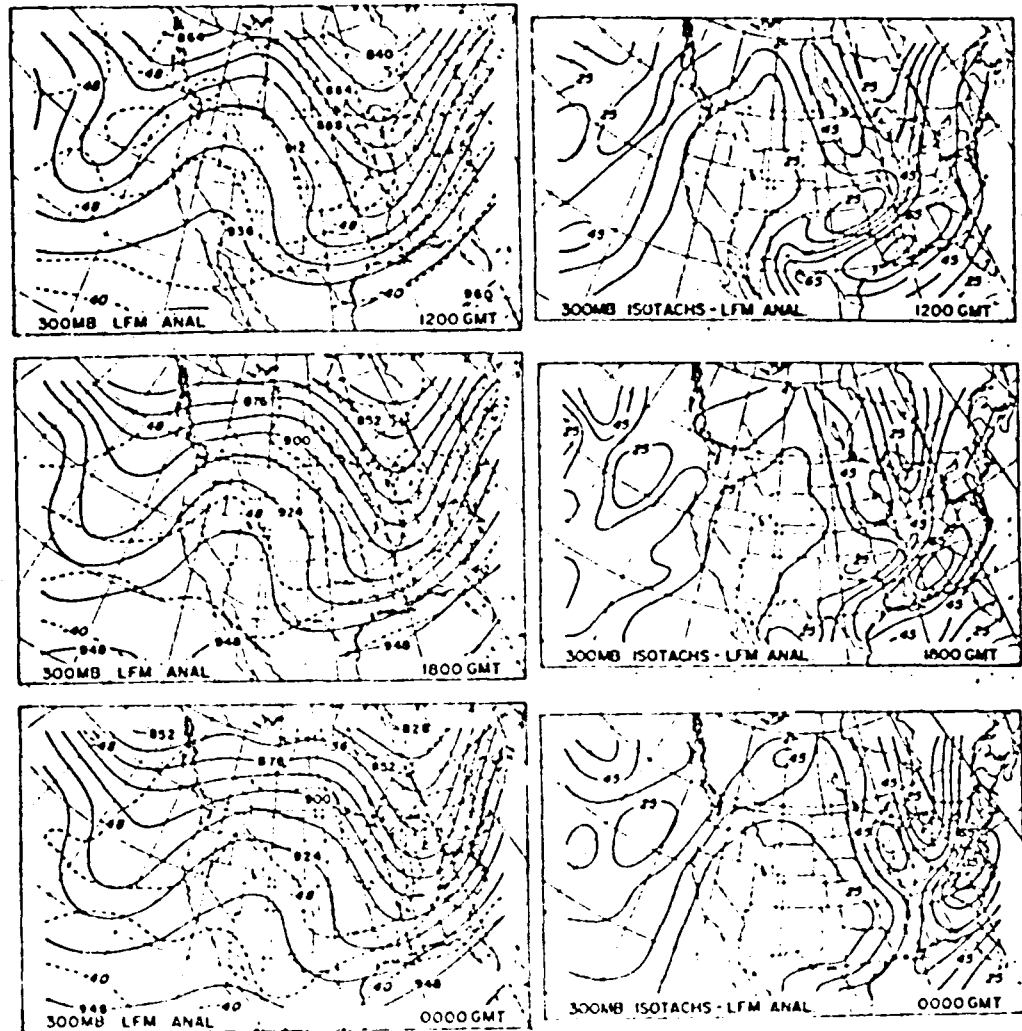


Figure 10. Analysis comparisons between the first bogus LFM set (1800 GMT) and the bracketing (1200 GMT and 0000 GMT) LFM analyses. Panels to the left depict height (solid, dam) and temperature (dashed, °C), while panels to the right show geostrophic isotachs ($m s^{-1}$).

temperatures, and isotachs of the geostrophic wind at 300 mb for the first bogus LFM and bracketing 1200 GMT and 0000 GMT LFM data sets. (Diagrams in this and subsequent figures valid at satellite observation times, are labeled 1800 GMT.) As indicated in Figure 10, the general propagation of features such as troughs, ridges and jet streak patterns, are well represented by the time interpolation. A slight degradation of the height gradients can be detected in a comparison of the maximum speeds for the jet streak in the southeast United States. The speed decreased from the bracketing values of 85.8 and 89.8 m s^{-1} to a value of 83.5 m s^{-1} .

In the second bogus LFM set, both time and space interpolations were employed to further simulate inherent spatial limitations of the satellite soundings. A comparison between the first and second bogus LFM analyses is offered in Figure 11. The second bogus LFM set is labeled INTERP LFM to emphasize the space interpolation. Gaps between satellite passes are shaded.

The largest height differences of over 40 m are found in these data gaps. Unfortunately, part of the jet streak in the southeast is also located in one of the data gaps and suffers a further decrease to 71.1 m s^{-1} , due to space interpolation and smoothing of the height field. Bias and RMS differences, and S1 scores for the second bogus LFM set versus the first are presented in Table 1. While the bias and RMS differences increase with elevation up to the tropopause, the S1 score which is designed to measure gradient difference decreases. The S1 score of 14.8 at 300 mb corresponds well with the 14.9% decrease in the jet max value, which suggests that gradient losses are distributed over the entire analysis region. Such a comparison provides an important measure of the loss of information due to systematic data gaps between satellite passes and the analysis procedure. Remember, satellite analyses can at best be expected to reproduce this second LFM bogus set. These fields will then serve as the standard of comparison for the visual and statistical evaluation methods.

b. Layer mean temperature comparisons at observation locations

Following an approach used by Hayden (1977), mean temperatures for layers between consecutive mandatory pressures were calculated at observation sites, and compared to similar values interpolated from gridded analyses to the observation locations. Comparisons with the four satellite sounding sets were made against both bogus LFM and satellite-derived analysis values interpolated back to the sounding locations. The former comparisons against LFM

ORIGINAL PAGE IS
OF POOR QUALITY

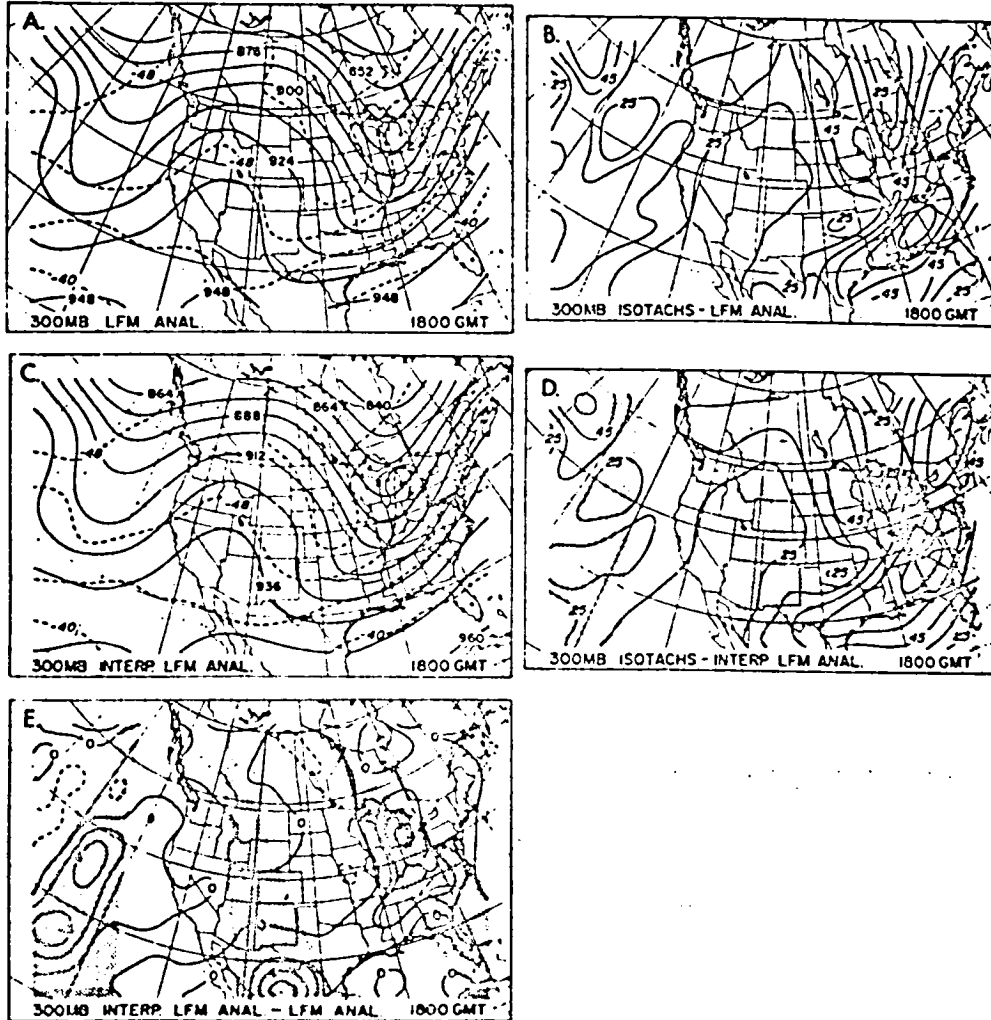


Figure 11. Bogus LFM 300 mb comparisons. Panel A - height (solid, dam) and temperature (dashed, °C) analyses for the first bogus LFM set (time interpolation at grid points only). Panel C - same as A except for the final bogus LFM set (time interpolation at sounding locations and subsequent space interpolation to grid points). Panels B and D are the corresponding geostrophic isotach analyses ($m s^{-1}$). Panel E shows the height difference fields (dam) between A and C.

analysis values measure the accuracy of the soundings, while the latter comparisons against satellite-derived analyses measure the noise removed from the original data by the analysis process. Included in the discussion are Hayden's comparisons of radiosonde and Nimbus-6 soundings against NMC's Northern Hemispheric analyses for the period from 15 February to 20 February during DST-6. While Hayden's comparisons were hemispheric, comparisons for the DST and 4x7 data sets used in this study were restricted to sounding locations within the satellite analysis subset of the LFM grid. Bias and standard deviation statistics for the observation minus analysis temperature differences are given in Table 2.

Values from Hayden's RAOB vs. analysis and Nimbus-6 vs. analysis comparisons are shown first. The hemispheric analyses used in his comparisons are based primarily on radiosonde measurements and are independent of Nimbus-6 satellite observations. This explains the relatively small bias differences in the RAOB vs. analysis comparisons in Table 2. The standard deviation results were larger for the Nimbus-6 satellite soundings than for the radiosonde measurements, especially near the surface and tropopause. Bias differences in the Nimbus-6 set are smaller below 700 mb than those from the radiosonde set, which may indicate a problem in hemispheric analyses at lower elevations.

The ALL DST set from this study is equivalent to Hayden's Nimbus-6 sounding set in terms of the sounding retrieval and averaging techniques described earlier. Standard deviations for the ALL DST vs. LFM analysis differences are larger than those from the Nimbus-6 comparison, again at lower levels and the tropopause. The ALL DST bias differences are also larger than the Nimbus-6 biases at lower levels, and the maximum bias of 2.44°C for the ALL DST set is in the 250-200 mb layer. Several factors contribute to differences in these ALL DST and Nimbus-6 comparisons (Table 2). The ALL DST results are only for a limited portion of the LFM grid over North America on February 22, while Hayden's Nimbus-6 comparison was hemispheric for five days during an earlier period. Also, the verifying analyses for the two comparisons (LFM vs. hemispheric) were constructed with different analysis methods on grids of different resolution.

The major difference in the comparisons of the DST and 4x7 sounding sets against analysis values in Table 2, is that bias differences for the DST sets are larger near the surface and smaller near the tropopause than bias

Table 2. Layer mean temperature comparisons (°C) between observed values and analysis values interpolated to the observation locations. The RAOB vs. Analysis and Nimbus-6 vs. Analysis comparisons are from Hayden (1977).

BIAS

DATA SETS	LAYER (MB)								
	1000 TO 850	850 TO 700	700 TO 500	500 TO 400	400 TO 300	300 TO 250	250 TO 200	200 TO 150	150 TO 100
RAOB VS ANAL	08	-02	02	00	00	08	-02	05	09
NIMBUS-6 VS ANAL	03	-01	03	05	05	14	08	08	03
ALL DST VS LFM ANAL	111	160	096	121	031	106	244	071	009
SCR DST VS LFM ANAL	120	162	096	121	033	109	242	073	006
ALL 4X7 VS LFM ANAL	074	110	020	053	003	136	305	102	002
SCR 4X7 VS LFM ANAL	101	128	038	051	008	124	286	085	006
ALL DST VS SAT ANAL	001	009	005	-001	-003	001	001	002	002
SCR DST VS SAT ANAL	005	007	004	-001	-002	002	001	000	000
ALL 4X7 VS SAT ANAL	020	033	023	012	-004	-016	-022	-013	-002
SCR 4X7 VS SAT ANAL	014	012	008	002	-006	-002	-006	-002	001

STANDARD DEVIATION

DATA SETS	LAYER (MB)								
	1000 TO 850	850 TO 700	700 TO 500	500 TO 400	400 TO 300	300 TO 250	250 TO 200	200 TO 150	150 TO 100
RAOB VS ANAL	16	15	15	15	17	20	17	16	19
NIMBUS-6 VS ANAL	26	20	17	17	19	25	31	25	20
ALL DST VS LFM ANAL	387	297	183	169	166	310	419	249	173
SCR DST VS LFM ANAL	389	299	181	167	166	313	426	250	172
ALL 4X7 VS LFM ANAL	370	287	184	173	164	294	401	251	170
SCR 4X7 VS LFM ANAL	380	286	186	169	167	298	396	247	159
ALL DST VS SAT ANAL	143	074	076	083	072	074	073	065	078
SCR DST VS SAT ANAL	139	068	066	068	057	063	069	062	073
ALL 4X7 VS SAT ANAL	192	190	159	154	107	143	156	118	121
SCR 4X7 VS SAT ANAL	152	077	074	075	066	079	084	065	068

NUMBER OF SOUNDINGS

ALL DST - 189 ALL 4X7 - 222
 SCR DST - 179 SCR 4X7 - 155

from the 4x7 sets. Little or no improvement from screening the satellite data sets can be detected in these comparisons against LFM analysis values.

Comparisons of satellite observations versus satellite-derived analysis values provide more information. While a general label of SAT ANAL is used in Table 2, a given satellite sounding set was only compared to analyses constructed from that set. For example, the screened 4x7 soundings (SCR 4x7) were only compared with SCR 4x7 analysis values. The small bias differences indicate that the analysis procedure does preserve the means of the data fields. Standard deviation values for the ALL 4x7 case are almost twice those for the ALL DST case, indicating more frequent inconsistencies in the raw 4x7 data set. The screening procedure succeeds in removing inconsistent soundings as shown by smaller standard deviations in the screened cases. The effect of screening the ALL 4x7 set is substantial, although the standard deviations for the SCR 4x7 vs. SAT ANAL comparisons are still slightly higher than those from the SCR DST vs. SAT ANAL comparisons.

c. Height and temperature analysis comparisons

The effect of a high noise level in the raw data on resulting analyses is illustrated in Figure 12 for the ALL 4x7 sounding set. Anomalous troughing in Colorado, Florida and the extreme west central portion of the grid stands out in the 500 mb analysis. All three problem areas are in data gaps and result from noisy soundings. The detrimental effect of a noisy sounding near the center of a satellite pass will be moderated by surrounding observations during the analysis. However, the analysis method tends to extrapolate gradient information into data gaps. Any noise near the edges of a satellite pass will create anomalous gradients which are extended into the data gaps. For example, heights for the ALL 4x7 sounding in central Colorado (Figure 4C) were too low, which caused an anomalous gradient between this sounding and the one just to the east on the Kansas-Nebraska border. The extrapolation of this gradient into the data gap formed the anomalous trough in Colorado. Because of these unsatisfactory results the ALL 4x7 data was not used in preparing model initializations or in performing more statistical evaluations.

Height and temperature analyses for the three remaining satellite data sets are presented in Figures 13 through 16 at 850 mb, 500 mb, 300 mb and 200 mb respectively. The final bogus LFM analyses are included for comparison. Trough and ridge positions are generally well represented in the

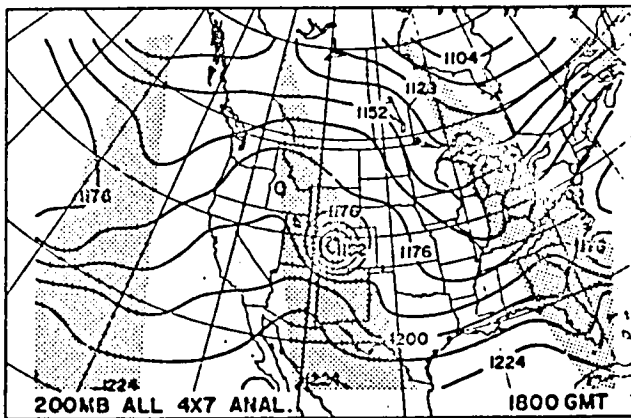
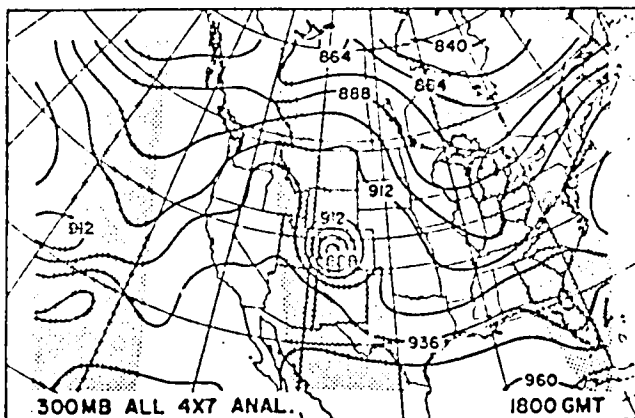
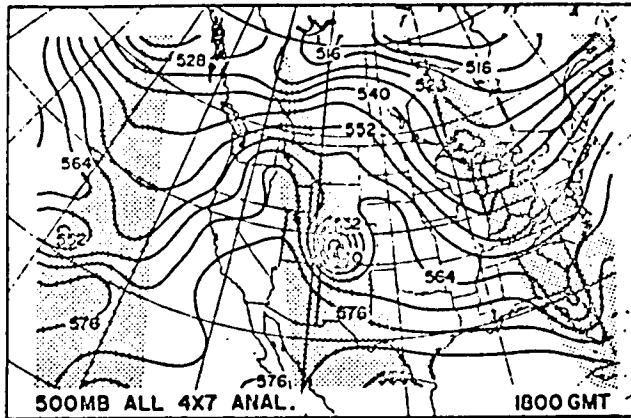
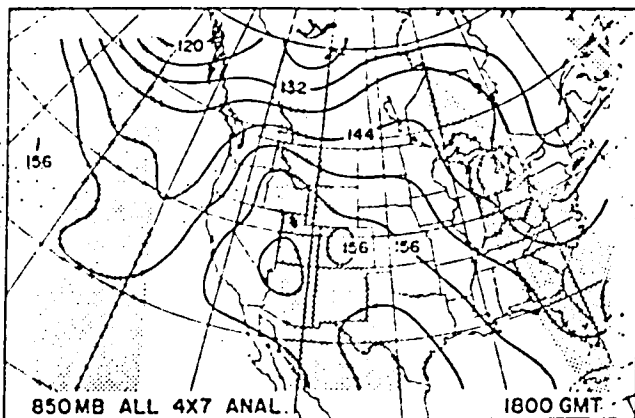


Figure 12. Selected ALL 4x7 height analyses (dam).

ORIGINAL PAGE IS
OF POOR QUALITY

satellite-derived analyses, however, as might be expected, the three satellite sets resemble each other more than they resemble the bogus LFM data. This is not surprising since all three satellite sounding sets were derived from the same HIRS and SCAMS measurements. In fact, the subtle differences between the ALL DST and SCR DST analyses are almost imperceptible in these figures.

At 850 mb (Figure 13), thermal gradients in the northeast corner of the grid are much weaker for the satellite cases than for the LFM. This is due to the inability of the satellite measurements to capture the colder temperatures north of the Great Lakes. Assuming that the LFM's temperature values over that portion of Canada to be correct, the satellite-derived temperatures are almost 7°C too warm. (The strength of this 850 mb cold dome in the LFM analysis is supported in the Canadian radiosonde reports in that region at both 1200 GMT February 22 and 0000 GMT February 23.) Note also that the warm region indicated by the 4°C line in Wyoming and Montana in the bogus LFM analysis is not well defined in the satellite-derived analyses, indicating a slight cold bias in that region.

The temperature field at 500 mb (Figure 14) is well represented in the satellite analyses. However, the overestimation of 850 mb temperatures is reflected by higher satellite heights in the 500 mb trough. A short wave trough not found in the LFM analysis is indicated in the satellite data in association with an Alberta low present in the conventional surface analysis (not shown). It is possible that the widely spaced Canadian radiosonde network was unable to define this feature. If so, the ability of satellite soundings to better define such shortwave features over Canada would be a definite advantage. On the other hand, in another data-sparse area, the trough south of California in the satellite analyses is not supported in the available conventional data.

The inability of satellite soundings to define the 300 mb cold pool over the Great Plains (see Figure 15) is an indication of their known difficulties in defining the temperature structure near the tropopause. This is further accentuated at 200 mb (Figure 16) where satellite soundings were able to locate a cold pool over the western United States, as indicated by the -56°C line. However, the intensity of this cold pool is underestimated, and subsequently, the strong reversal of the temperature gradient evident at this level in the LFM data is greatly underestimated.

A set of height difference fields (satellite minus LFM) at 300 mb is

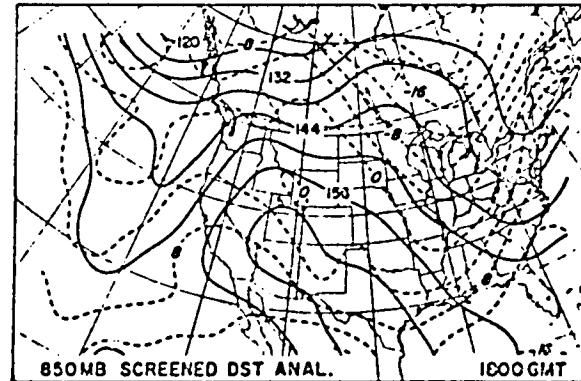
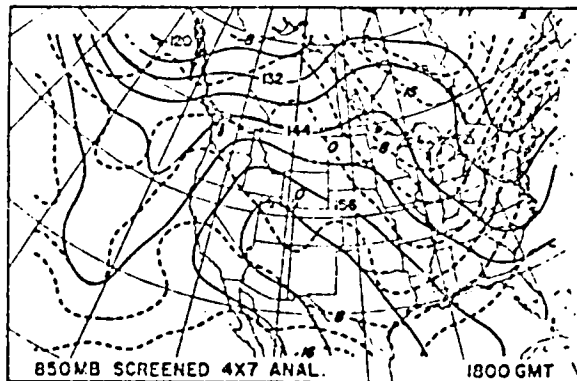
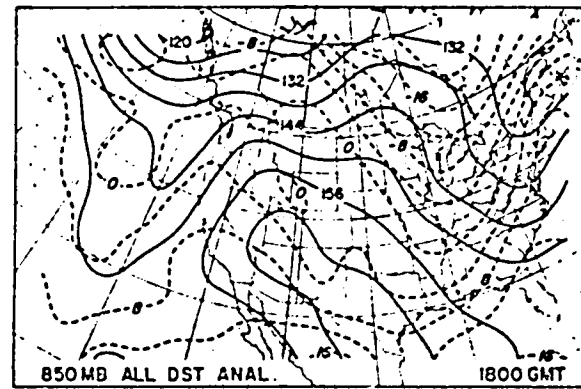
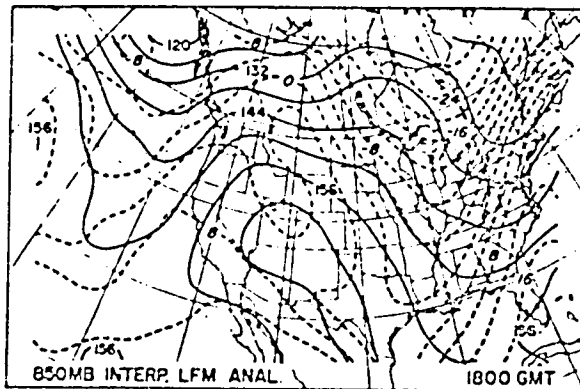


Figure 13. Height analyses (dam) in solid and temperature analyses ($^{\circ}\text{C}$) in dashed for the three satellite sounding sets and the verifying final bogus LFM field at 850 mb (upper left).

ORIGINAL PAGE IS
OF POOR QUALITY

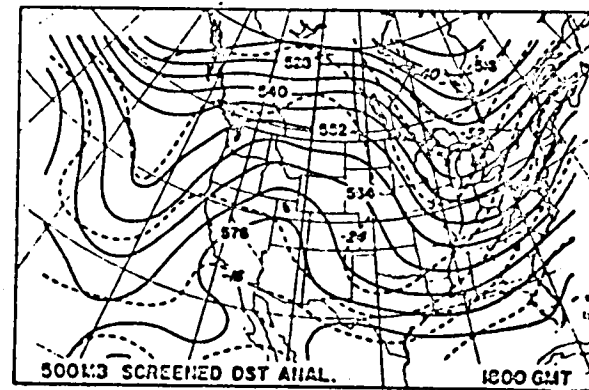
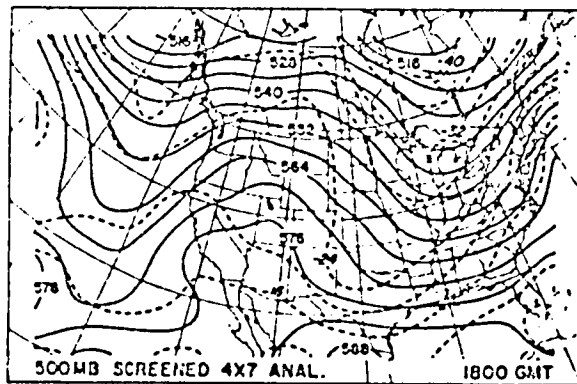
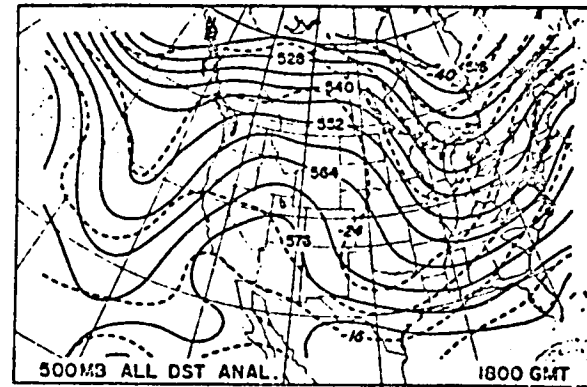
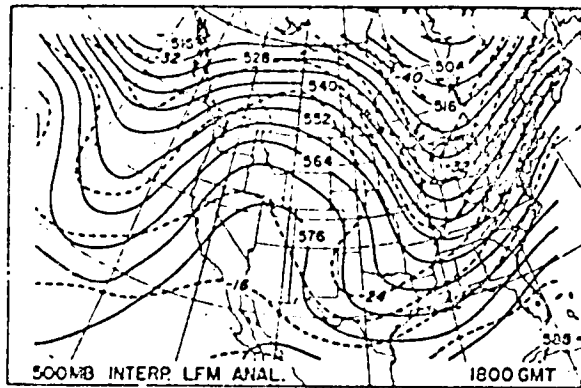


Figure 14. Same as Fig. 13 except at 500 mb.

ORIGINAL PAGE IS
OF POOR QUALITY

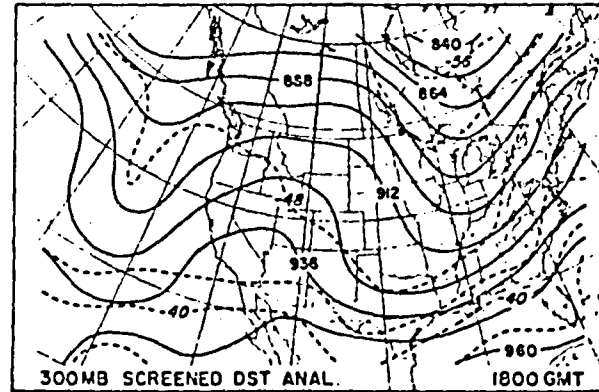
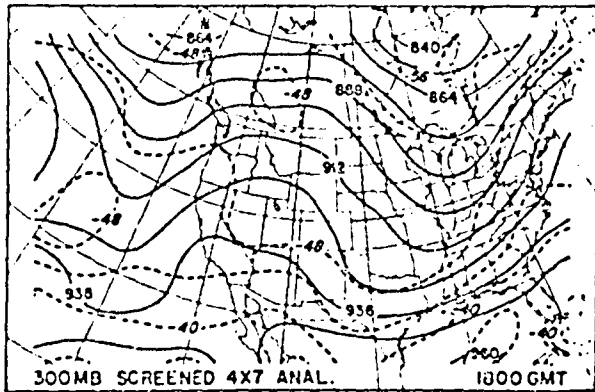
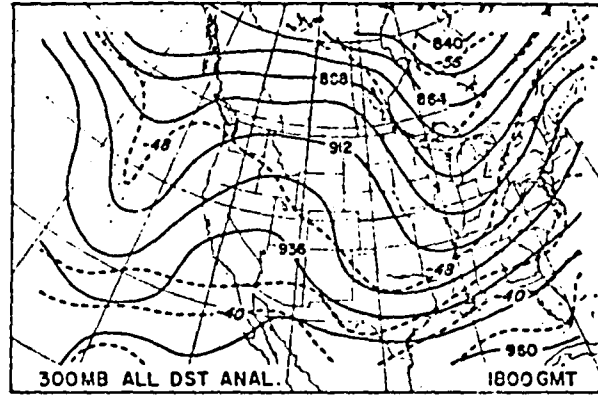
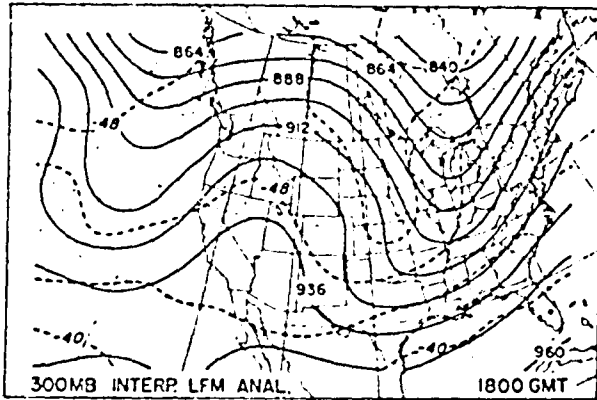


Figure 15. Same as Fig. 13 except at 300 mb.

ORIGINAL PAGE IS
OF POOR QUALITY

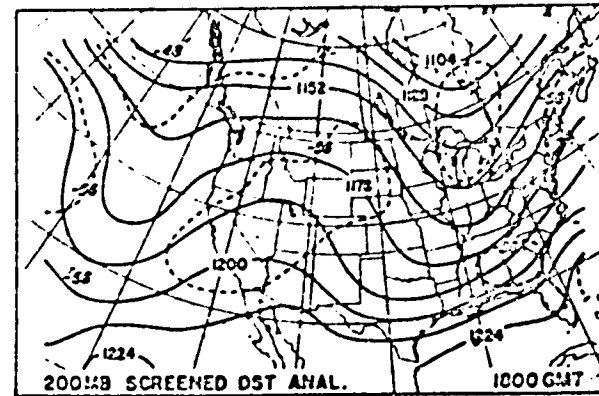
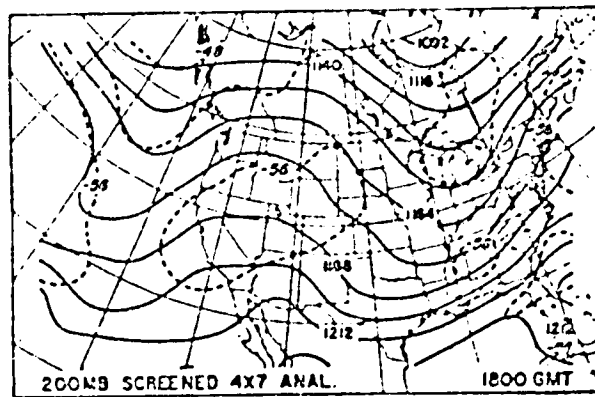
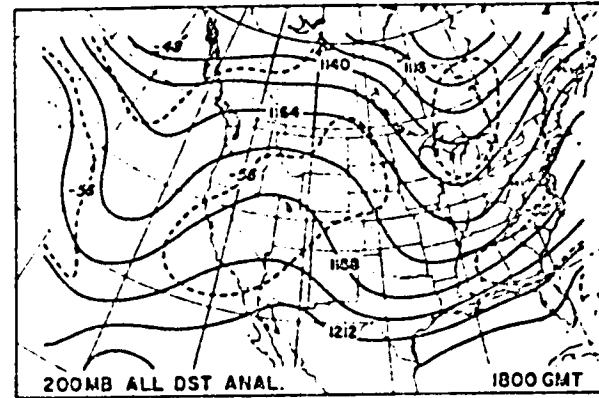
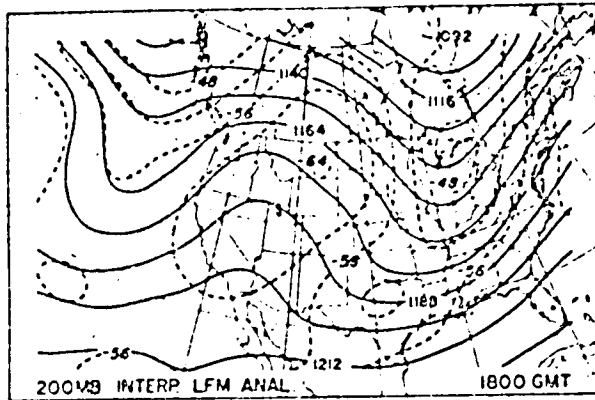


Figure 16. Same as Fig. 13 except at 200 mb.

ORIGINAL PAGE IS
OF POOR QUALITY

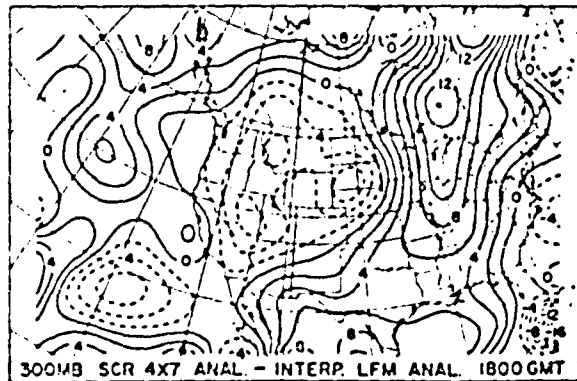
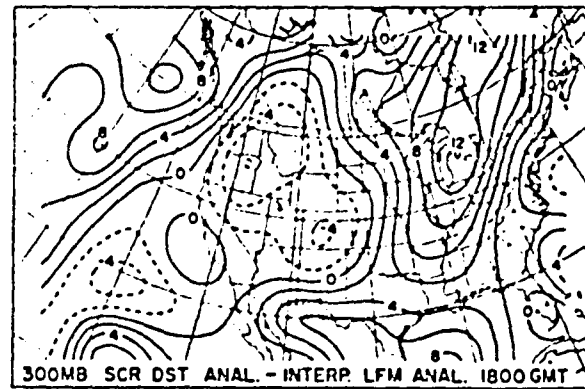
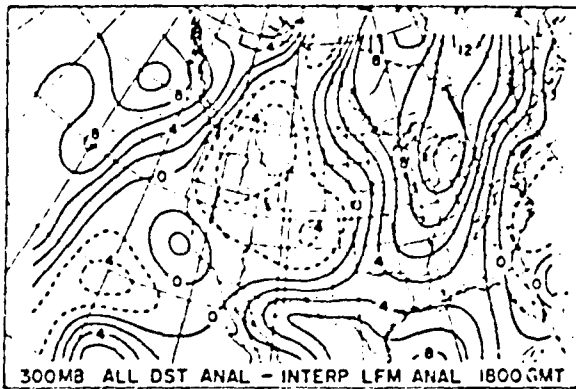


Figure 17. Height difference fields (dam) between the satellite-derived analyses and the bogus LFM analysis at 300 mb. Negative differences are dashed.

shown in Figure 17. Positive values in this figure indicate areas where satellite-derived heights were higher than the LFM heights. The general patterns for the three satellite sounding sets are similar, with the greatest overestimations in troughs and smaller underestimations in ridges. Positive 120 m differences in the eastern trough correspond to 1000 mb to 300 mb layer mean temperature differences being 3.4°C too warm, due mainly to low level temperature overestimates such as the 7°C error at 850 mb mentioned earlier. An anomalous trough in the SCR 4x7 set is evident from the large negative differences south of Florida, which will affect several of the statistical measures of accuracy.

The lack of conventional data in the Pacific region of the analyses makes verification there less reliable. To focus more attention on the land areas, the analysis region was divided into Pacific, western North American and eastern North American subregions, as shown in Figure 18. This also separates the flow pattern regimes, with the Eastern and Pacific regions dominated by troughs, and the Western dominated by a ridge.

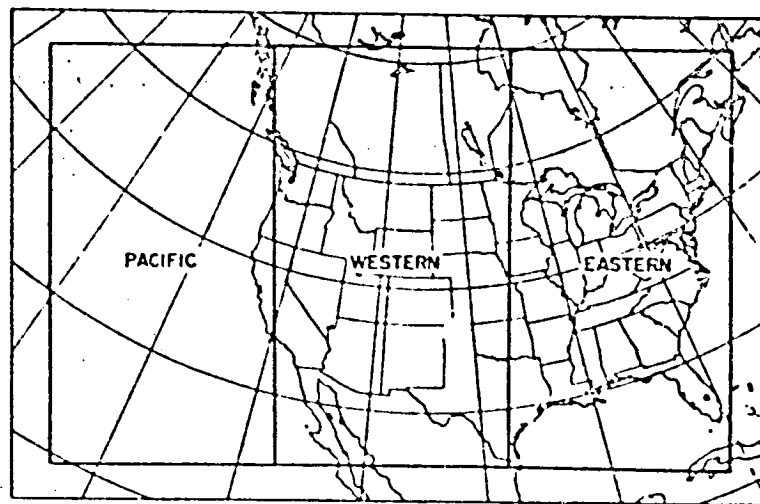


Figure 18. Subdivision of the analysis region for the calculation of evaluation statistics.

Height statistics for the three subregions, and the entire region, are given in Table 3. Positive bias differences predominate except in the troposphere of the Western region, where small negative values appear in the ridge regime. Both bias and RMS differences increase with altitude in all regions, while S1 scores decrease from 700 mb up to 300 mb in all except the Pacific

Table 3. Height analysis comparison statistics over the whole region and the three subset regions. The satellite-derived analysis values are compared against those from the second bogus LFM set. Bias and RMS values are in meters while the SI scores are dimensionless.

WHOLE REGION

LEVEL (MB)	BIAS			RMS			SI		
	SCR	ALL	SCR	SCR	ALL	SCR	SCR	ALL	SCR
	DST	DST	487	DST	DST	487	DST	DST	487
850	28	28	28	166	166	172	230	227	272
700	98	103	89	317	320	318	325	328	350
500	198	192	140	455	462	441	505	510	544
400	257	262	175	521	530	501	589	594	644
300	288	289	178	521	530	507	581	585	628
250	348	345	225	518	528	498	552	560	622
200	550	519	410	621	621	556	644	676	753
150	607	583	487	703	698	617	711	720	805
100	641	635	555	715	711	658	747	750	829

WESTERN REGION

LEVEL (MB)	BIAS			RMS			SI		
	SCR	ALL	SCR	SCR	ALL	SCR	SCR	ALL	SCR
	DST	DST	487	DST	DST	487	DST	DST	487
850	-20	-17	-17	129	128	129	236	237	245
700	-20	-17	-24	253	254	252	386	389	361
500	-17	-16	-53	339	346	356	370	386	367
400	18	4	-48	357	367	390	336	353	357
300	59	53	-28	369	382	421	290	307	337
250	178	169	82	414	419	444	287	304	339
200	-73	461	380	389	582	539	310	354	355
150	588	377	501	489	680	603	357	378	400
100	617	617	546	493	692	627	388	403	407

PACIFIC REGION

LEVEL (MB)	BIAS			RMS			SI		
	SCR	ALL	SCR	SCR	ALL	SCR	SCR	ALL	SCR
	DST	DST	487	DST	DST	487	DST	DST	487
850	-49	-48	-46	102	101	115	165	162	222
700	27	31	15	216	215	186	251	253	281
500	169	180	97	383	394	283	297	291	350
400	281	294	148	506	510	354	304	311	358
300	323	335	130	527	531	347	290	294	355
250	418	424	196	552	557	359	287	288	351
200	605	608	382	673	677	456	294	294	359
150	715	714	475	776	776	555	350	349	391
100	707	708	511	752	749	619	457	448	377

EASTERN REGION

LEVEL (MB)	BIAS			RMS			SI		
	SCR	ALL	SCR	SCR	ALL	SCR	SCR	ALL	SCR
	DST	DST	487	DST	DST	487	DST	DST	487
850	145	148	148	236	237	244	295	291	360
700	294	298	270	437	443	449	330	330	402
500	419	424	383	596	607	613	284	281	358
400	488	493	458	660	673	689	241	236	324
300	494	492	440	638	650	647	217	213	299
250	484	454	411	579	597	640	201	206	289
200	518	486	487	602	604	651	207	218	298
150	523	494	514	642	634	683	251	257	358
100	602	580	608	700	692	725	255	256	357

ORIGINAL PAGE IS
OF POOR QUALITY

region. A closer examination of how the SI score is formulated will help explain the decrease in this score with altitude, up to the 300 mb level. The SI score is defined as the sum of the magnitudes of satellite gradient minus verification (LFM) gradient vector differences, divided by the sum of the verification (LFM) gradient magnitudes. As altitude increases in the troposphere, LFM height gradients generally increase in magnitude, while gradient differences between the satellite and LFM fields also increase, but at a slower rate than the LFM height gradients. In terms of the SI formulation, the denominator is increasing faster than the numerator, yielding decreasing SI scores.

The anomalous trough in the southeast corner of the SCR 4x7 analyses produces smaller biases than the DST sets in the Eastern region. However, this erroneous trough is characterized by larger RMS and SI scores which accompany the smaller biases. In fact, the SCR 4x7 heights exhibit higher SI scores everywhere except at 700 and 500 mb in the Western region. In both the Western and Eastern subregions, smaller biases accompany larger RMS differences for the SCR 4x7 jet compared to the DST sets. Only in the Pacific do both smaller SCR 4x7 bias and RMS differences appear together. Unfortunately, verification is questionable in that region.

Layer mean temperature comparisons are presented in Table 4. Throughout the troposphere, satellite estimates are too warm, as indicated by the positive biases. Biases of one sign at lower levels are not being compensated by biases of the opposite sign at higher levels, as found in studies with other satellite data sets such as Horn et al. (1976). If such compensating biases exist, an advantage can be found in using height and thickness variables in which temperature information is integrated vertically. This allows biases of opposite sign to counterbalance each other. This compensation is not present in DST-6 soundings, and thus, the advantage in using vertically-integrated variables is lost.

While RMS values for mid and upper tropospheric layers (700 mb to 300 mb) are reasonable, values near the surface and tropopause are unreasonably large. The strong positive biases and related large RMS values at lower levels in the Eastern trough region have already been alluded to in the 850 mb analysis and 300 mb height difference field discussions. Very large SI scores of over 100 are found in the tropopause layers and are indicative of the temperature gradient reversal problem also described earlier.

Generally, the satellite data's deficiencies in defining the thermal

Table 4. Layer mean temperature statistics in the same format as Table 3. In this case the bias and RMS values are in °C.

WHOLE REGION

LAYER (MB)	BIAS			RMS			SI		
	SCR	ALL	SCR	SCR	ALL	SCR	SCR	ALL	SCR
	DST	DST	4X7	DST	DST	4X7	DST	DST	4X7
1000-850	0.54	0.59	0.60	3.49	3.49	3.62	23.0	22.7	27.2
850-700	1.29	1.31	1.07	3.03	3.07	2.91	44.7	45.4	48.4
700-500	0.90	0.91	0.51	1.79	1.81	1.68	31.5	31.7	41.0
500-400	1.07	1.07	0.55	1.76	1.73	1.82	39.1	38.7	50.0
400-300	0.38	0.31	0.03	1.52	1.43	1.55	58.2	57.4	68.8
300-250	1.14	1.04	0.81	2.91	2.90	2.78	102.2	104.2	119.6
250-200	2.78	2.67	2.83	4.66	4.56	4.57	83.7	83.6	90.8
200-150	0.91	0.88	1.03	2.41	2.40	2.56	57.1	57.8	65.6
150-100	0.29	0.34	0.49	1.42	1.41	1.53	49.7	50.9	60.3

WESTERN REGION

LAYER (MB)	BIAS			RMS			SI		
	SCR	ALL	SCR	SCR	ALL	SCR	SCR	ALL	SCR
	DST	DST	4X7	DST	DST	4X7	DST	DST	4X7
1000-850	-0.41	-0.56	-0.37	2.72	2.69	2.71	23.6	23.2	24.5
850-700	-0.01	0.00	-0.12	2.40	2.44	2.43	53.6	57.4	53.2
700-500	0.03	0.00	-0.29	1.21	1.23	1.44	35.9	37.8	43.7
500-400	0.51	0.47	0.07	1.09	0.98	1.16	39.7	38.3	48.7
400-300	0.50	0.46	0.24	1.56	1.50	1.66	57.7	57.1	69.4
300-250	2.20	2.15	2.07	3.10	3.03	3.12	114.4	113.9	130.8
250-200	4.53	4.49	4.56	5.59	5.54	5.59	85.7	85.5	91.8
200-150	1.36	1.38	1.44	2.86	2.90	3.07	68.8	70.0	73.1
150-100	0.25	0.33	0.37	1.56	1.58	1.37	40.7	43.1	46.8

PACIFIC REGION

LAYER (MB)	BIAS			RMS			SI		
	SCR	ALL	SCR	SCR	ALL	SCR	SCR	ALL	SCR
	DST	DST	4X7	DST	DST	4X7	DST	DST	4X7
1000-850	-1.03	-1.00	-0.97	2.15	2.12	2.37	16.5	16.2	22.2
850-700	1.33	1.19	1.08	2.85	2.87	2.27	55.2	53.8	61.7
700-500	1.45	1.51	0.83	2.15	2.17	1.57	42.1	43.4	58.5
500-400	1.70	1.73	0.78	2.28	2.31	1.72	53.7	54.5	63.7
400-300	0.51	0.49	-0.21	1.29	1.28	1.31	72.1	72.4	80.2
300-250	1.73	1.68	1.06	2.89	2.86	2.40	77.3	79.9	89.1
250-200	2.89	2.79	2.69	4.29	4.18	3.63	71.6	72.7	67.7
200-150	1.31	1.27	1.32	2.27	2.24	2.14	50.4	51.6	60.3
150-100	-0.07	-0.07	0.32	1.22	1.21	1.59	48.1	48.1	63.8

EASTERN REGION

LAYER (MB)	BIAS			RMS			SI		
	SCR	ALL	SCR	SCR	ALL	SCR	SCR	ALL	SCR
	DST	DST	4X7	DST	DST	4X7	DST	DST	4X7
1000-850	3.05	3.12	3.11	4.95	4.98	5.13	28.5	29.1	36.0
850-700	2.61	2.63	2.30	3.71	3.78	3.78	31.1	31.0	38.2
700-500	1.27	1.28	1.05	1.91	1.93	2.06	23.0	21.7	30.4
500-400	1.05	1.05	0.79	1.75	1.70	1.90	30.4	29.9	42.1
400-300	0.07	0.00	0.06	1.87	1.48	1.64	50.3	48.6	61.4
300-250	-0.56	-0.79	0.53	2.74	2.80	2.89	113.6	117.9	137.3
250-200	0.83	0.65	1.18	3.98	3.69	4.17	82.9	91.1	110.3
200-150	0.05	-0.63	0.32	1.97	1.91	2.32	49.6	49.6	61.6
150-100	0.67	0.73	0.78	1.42	1.40	1.63	42.2	43.4	52.3

ORIGINAL PAGE IS
OF POOR QUALITY

structure in the cold dome account to a large degree for problems in defining the tropospheric height fields. As expected, bias and RMS mean temperature values for the whole region analysis comparisons are similar to those from the raw data comparisons at observation points presented earlier. Only slight improvements can be detected in the RMS differences due to screening the DST data set.

d. Energetic and dynamic parameters

Parameters related to atmospheric energetics and dynamics derived directly from mass field variables (height, temperature and pressure) can assist in the satellite data evaluations. The first parameter to be discussed is available potential energy (APE), a quantity that provides a one number measure of the integrated baroclinity over a region, and has been used in other satellite data evaluations (Desmarais et al., 1978). A technique described by Kochler (1979) was employed in the APE calculations. It uses an exact formulation of APE in isentropic coordinates rather than an approximate formulation in isobaric coordinates used in previous studies.

The available potential energy values presented in Table 5 are in the form of specific (per unit mass) values. The mass in the computation volume can vary for different data sets, so effects of the total mass in the APE values have been removed. The calculations were made with an upper boundary at the 370K isentropic level, which corresponds roughly to the 150 mb isobaric surface.

Table 5. Values for the specific available potential energy ($m^2 s^{-2}$) for the whole region and the three subset regions.

WHOLE REGION	Interp. LFM	164.4
	All DST	135.2
	Screened DST	135.7
	Screened 4x7	140.9
EAST REGION	Interp. LFM	318.6
	All DST	284.4
	Screened DST	287.5
	Screened 4x7	288.7
WESTERN REGION	Interp. LFM	74.6
	All DST	70.1
	Screened DST	69.2
	Screened 4x7	72.5
PACIFIC REGION	Interp. LFM	88.1
	All DST	51.1
	Screened DST	50.2
	Screened 4x7	65.6

The strong baroclinity associated with the east coast trough is reflected by the large APE values for the Eastern subregion. Satellite estimates show about a 10% weaker APE in calculations for the Eastern region compared to LFM values. Over the entire region, APE is 18% weaker for both DST analysis sets than for the LFM set. APE values calculated from the SCR 4x7 analyses are slightly larger than those from the DST analyses, and are thus closer to the LFM value. This normally implies higher baroclinity in that set than in the DST data sets. Without other gradient measures such as the S1 score, it would be difficult to say whether this increased baroclinity is real, or a measure of noise in the data set. (In this case it is the latter.)

The next set of comparisons involve visual inspections. Analyses of the 300-mb geostrophic wind speed are provided in Figure 19. In all three satellite data sets, the major jet maximum in the southeast U.S. is placed too far south and west, with an extension back into New Mexico. Also, geostrophic wind calculations in the southwest grid corner are unreliable due to a small Coriolis parameter and, more importantly, problems with interpolation into the wide data gap.

Differences between the three satellite sounding sets are accentuated in these isotach analyses. The SCR 4x7 set failed to define the jet maximum propagating down the west side of the east coast trough, although it did show stronger winds over the St. Lawrence River Valley. Overall, the SCR DST isotach analysis was probably best. It indicated another jet maximum over the Carolinas, and produced a better isotach configuration on the west side of the trough. In fact, the 45 m s^{-1} geostrophic wind maximum west of Hudson Bay in this analysis may be a feature not resolved in Canadian radiosonde height measurements. A jet maximum was present in NMC's 0000 GMT 300 mb wind analysis over Trout Lake, Ontario (54°N , 90°W), which was due mainly to a 68 m s^{-1} wind reported at that station. Considering the general underestimation of gradients in the satellite-derived analyses, the actual geostrophic speeds of this feature may have been even stronger.

Geostrophic temperature advections at 850 mb are fairly well represented in the satellite-derived analyses (Figure 20). In the Eastern region, the strong cold advection in northern Georgia and adjoining states is captured in all three satellite sounding sets. The SCR 4x7 set provides a better indication of the maximum south of Lake Ontario than the DST sets, although the central value is still weaker than that from the LFM analysis.

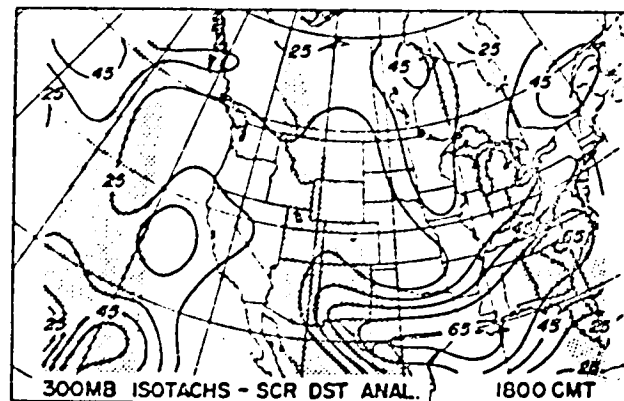
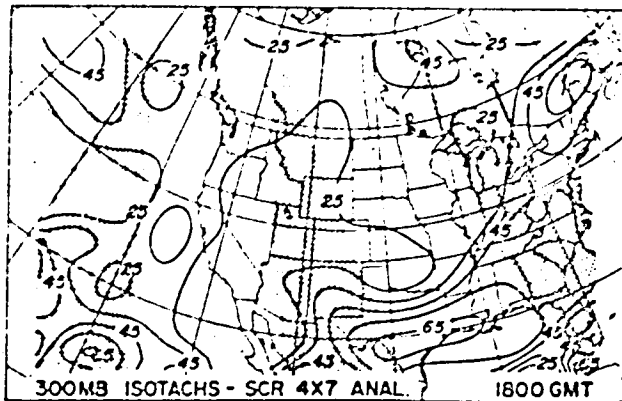
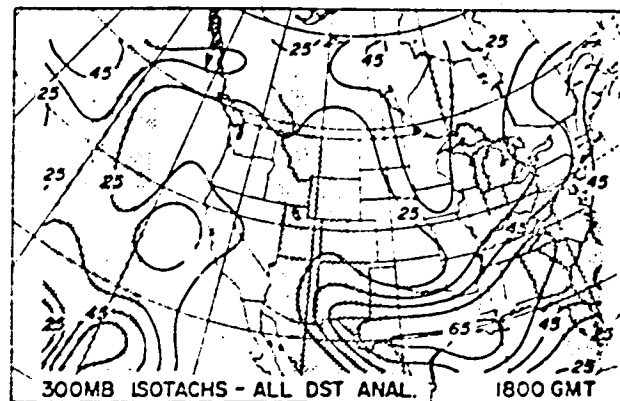
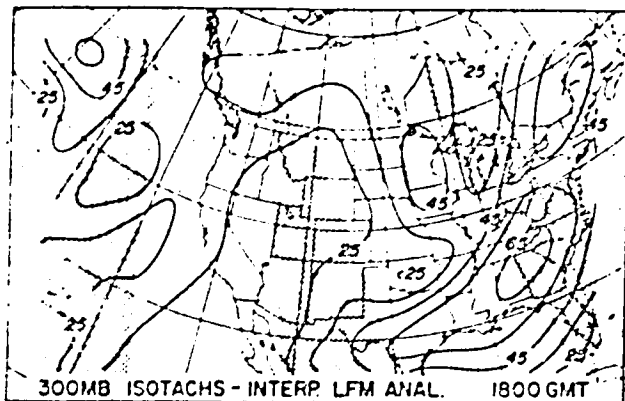


Figure 19. Geostrophic 300 mb isotachs ($m s^{-1}$) for the three satellite-derived analyses and the bogus LFM analysis.

ORIGINAL PAGE IS
OF POOR QUALITY

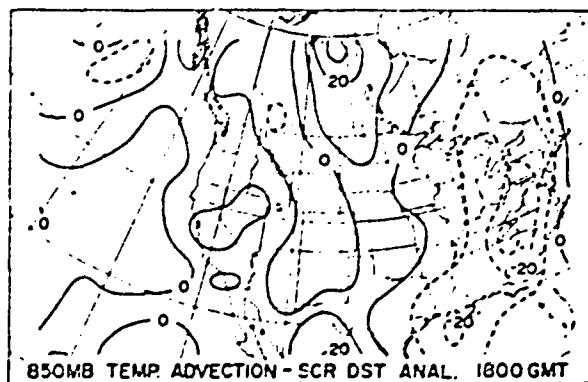
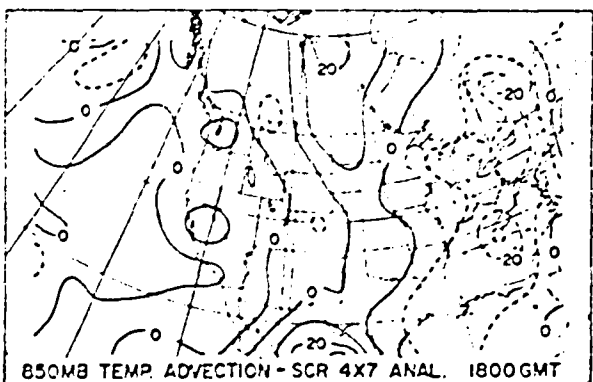
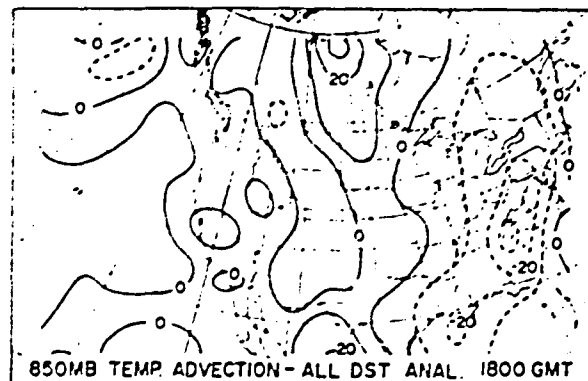
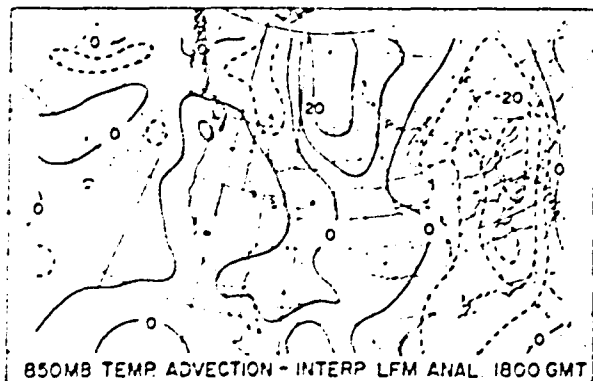


Figure 20. Geostrophic temperature advection ($^{\circ}\text{C day}^{-1}$) at 850 mb. Cold advections are dashed.

The 200 mb geostrophic temperature advection (Figure 21) further illustrates the general problem satellite soundings have in resolving the tropopause. The temperature gradient at this level has reversed in direction from that in the mid-troposphere. While some general agreement may be found in the southeast, the strength of the warm advection in the northeast ($40^{\circ}\text{C day}^{-1}$) and the large area of cold advection in the central United States have been grossly underestimated in the satellite sounding data.

For the final analysis comparison, isentropic cross sections were constructed across the frontal zone situated along the east coast, as illustrated in Figure 22A. Analysis values were interpolated from the LFM grid points to the radiosonde locations shown. Panel B is from the SCR DST analysis and panels C and D are from the bracketing 1200 GMT and 0000 GMT LFM analyses, respectively. (The satellite analysis grid did not extend far enough east to include the Bermuda station, so values at the intersection of the path of the cross section with the last row of the analysis grid were plotted for the SCR DST analysis set.) Also shown are analyses of the thermal wind component normal to the cross section, built up from a value of zero at 850 mb. Positive values point into the page. While the wind maxima in the SCR DST cross section are well positioned horizontally, they are about 50 mb higher than those in the LFM cross section. Also, the eastern maximum is about 35% too weak in the SCR DST set. The cold dome is much weaker in the satellite analysis, and its isentropes show almost no slope near the tropopause, a good visualization of the deficiencies of the satellite-derived tropopause data. With such poor results near the tropopause appearing in almost every evaluation parameter, there may be some question in using satellite sounding height data above about 300 mb.

c. LFM initialization with satellite-derived analysis fields

In the process of defining model initial fields from observations, several operations affecting the temperature gradient information are performed. Consider, for example, the steps taken in preparing the LFM initial hour fields. Rawinsonde measurements of temperature, pressure, moisture and wind are made at significant levels. However, only values at the ten mandatory pressure levels from the surface to 100 mb and tropopause data, enter the LFM analysis. Finally, the resulting analysis fields are used as input for the initialization procedure.

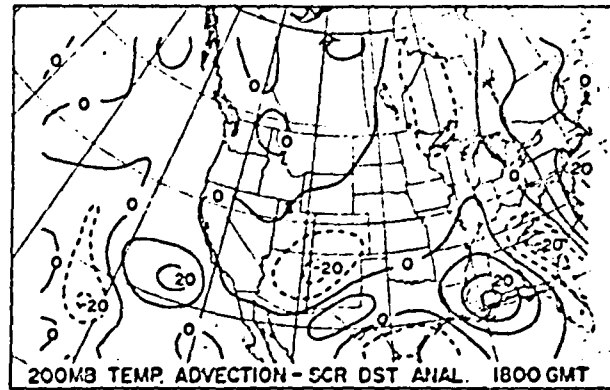
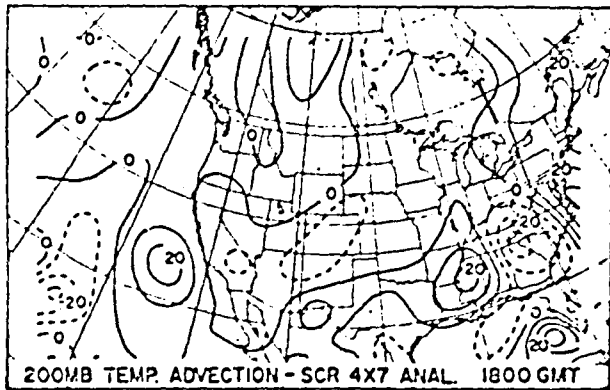
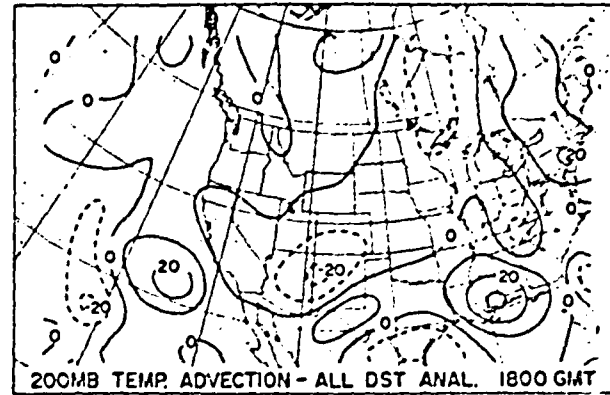
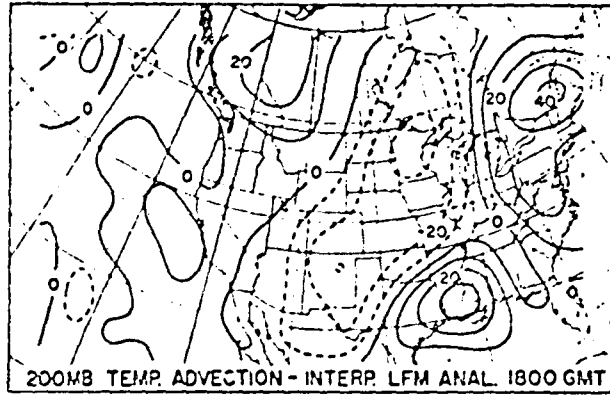


Figure 21. Geostrophic temperature advection ($^{\circ}\text{C day}^{-1}$) at 200 mb.

ORIGINAL PAGE IS
OF POOR QUALITY

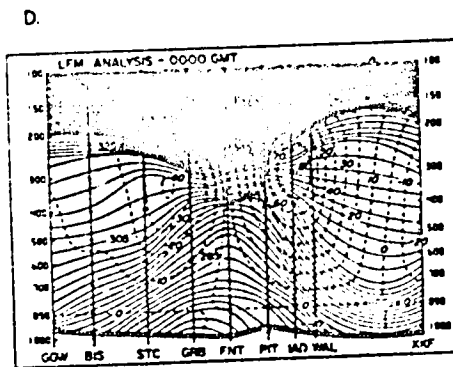
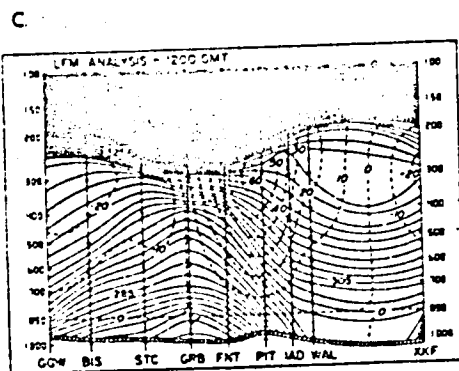
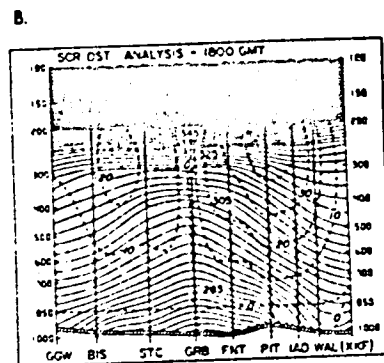
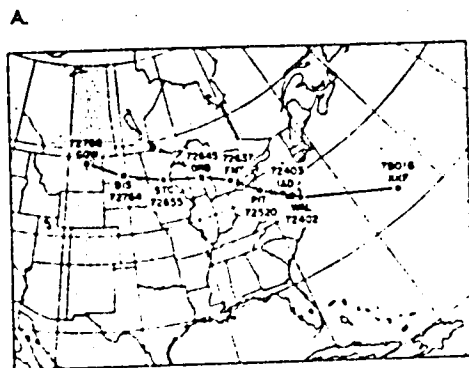


Figure 22. Analysis cross section comparisons. Isentropes ($^{\circ}\text{K}$), solid and thermal wind component (m s^{-1}) normal to the cross section relative to 850 mb, dashed (positive into the page). Panel A - cross section station locations. Panel B - SCR DST analysis cross section at roughly 1800 GMT. Panels C and D - bracketing 1200 GMT and 0000 GMT LFM analysis cross sections.

ORIGINAL PAGE IS
OF POOR QUALITY

The various steps in this process are illustrated with cross sections from 1200 GMT 22 February 1976 in Figure 23. (This is the same cross section employed in Figure 22.) Only subtle differences can be found between the significant level and mandatory level analyses. A 13% loss of gradient information is indicated by a decrease in the maximum thermal winds in the step from mandatory level data to LFM analyses. Model initialization has only a slight effect on the analyzed temperature gradients. The dramatic losses shown by Horn et al. (1976) also probably occurred in the analysis step, not in the initialization step.

The differences between the satellite-derived analysis fields and their corresponding initial hour fields were quite small, with only a 2% loss in height gradient information. The available potential energy decreased 4% for the LFM fields and only 2% for the satellite fields due to initialization. In both the satellite and conventional data cases, mass field changes due to the initialization process were small. The smooth vertical nature of the satellite-derived data provides little benefit to the initialization procedure.

6. Summary and conclusions

Detailed comparisons between analyses constructed from satellite soundings and surface data only with conventional analyses from the LFM model, have been presented for one period from DST-6. The grid mesh employed in this study has a higher resolution (190.5 km) than those used in most of the previous DST-6 impact studies (400 km). As stated earlier in the description of the experiment, these satellite sounding evaluations addressed questions related to the following topics: defining the strengths and weaknesses in satellite soundings, investigating the effect of increasing the horizontal resolution of satellite soundings, assessing the impact of careful data screening on the final satellite-derived analyses, and evaluating the effect of model initialization on the analyses. The results of this study in regard to these topics are summarized in the following discussion.

Many of this study's findings parallel those from the coarser resolution DST-6 impact tests of Desmarais et al. (1978) and Halem et al. (1977), and tests with data from earlier satellites, such as Bonner et al. (1976). The satellite soundings are able to define the major trough and ridge positions quite well, but are "conservative", with temperatures too warm in

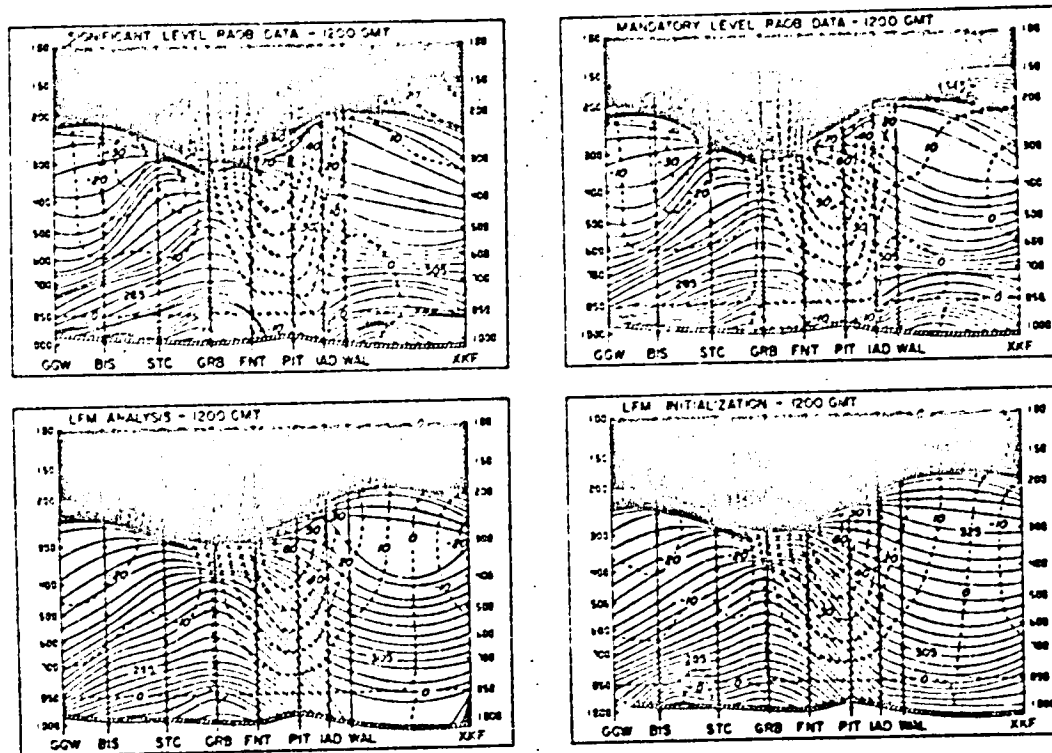


Figure 23. A cross-sectional representation of thermal gradient changes during the LFM analysis - initialization process at 1200 GMT 22 February 1976. The parameters and station locations are the same as those in Fig. 21. The upper panels used significant and mandatory pressure level radiosonde reports. The lower panels are for the LFM analysis and initialization fields.

ORIGINAL PAGE IS
OF POOR QUALITY

troughs and too cold in ridges. In fact, the results presented here indicate that the inability of Nimbus-6 satellite soundings to define cold domes outweighs problems in the ridge regimes during DST-6.

The 4x7 data set presented here has a higher horizontal resolution (about a 150 km spacing) than the sounding sets provided for the DST impact studies (about 300 km). The higher noise level and resulting higher removal rate in the screening procedure of 29% for the ALL 4x7 set compared to 5% for the ALL DST set, suggest that both good and poor information from 4x7 data blocks were averaged together to yield mediocre yet consistent DST soundings. While the manual screening of the ALL 4x7 set produced pronounced improvements, the SCR 4x7 set still had a slightly higher noise level and a less uniform observation distribution than the SCR DST sounding set. These factors are probably responsible for the disappointing SCR 4x7 performance. However, the removal of poor 4x7 block data before the averaging to produce DST soundings may have yielded better results. Only minor improvements could be noted from screening the ALL DST data set. LFM initialization with these satellite data sets is feasible, and has only minor effects on thermal gradients in the step from analysis to initialization for both the satellite and conventional data sets.

The deterioration of the longwave infrared (15 μ m) channels of the HIRS instrument before the start of DST-6 had a detrimental effect on soundings used in this study and in the DST-6 impact studies. The seven channels lost comprise almost half of the temperature sounding channels available from Nimbus-6 and would provide additional tropopause and tropospheric information. Petersen and Horn (1977) showed promising results in tracking a closed 500 mb low and its associated wind maximum across eastern Canada from an August DST-5 sample of Nimbus-6 soundings before the HIRS instrument malfunction. The inability of the Nimbus-6 soundings in this DST-6 study to correctly position the jet streak in the southeastern United States could be attributed to a number of factors, including the unfortunate position of the data gap in the region of interest, and the loss of the 15 μ m channels.

More reliable soundings derived from a complete set of infrared and microwave radiance measurements have since become available. TIROS-N and NOAA-6 satellite soundings were incorporated into the FGGE year data sets, and the quality of the soundings has improved to the degree that they are now included in the NMC operational data base over oceanic regions. However,

results from Phillips et al. (1979), Schlatter (1981) and Schmidt et al. (1981) indicate that satellite versus conventional differences for these newer satellites exhibit much the same type of structure as the Nimbus-6 differences presented here, especially with large differences near the surface and tropopause. A recent study by Schmidt et al. (1981) demonstrates a conservative nature (too warm in troughs, too cold in ridges). The similarity in the structure of these differences suggests limitations in the basic approach of inferring temperatures from radiance measurements, in radiance measurement accuracy, and/or in the procedures used to estimate temperatures from radiances.

While the overall results from this DST-6 case study are somewhat disappointing, the soundings were able to define the major trough and ridge positions. Their ability to resolve smaller scale features was inconsistent. There was some indication that satellite soundings could define certain short wave features over Canada that were not evident in the LFM analyses. On the other hand other short wave features found in the satellite data were inconsistent with conventional data.

Satellite soundings are currently unable to define temperature features, particularly important inversions such as the tropopause, with a detail commensurate with the radiosonde. One should remember however, that a major purpose of satellite soundings is to supplement conventional data in data-sparse regions, not to replace the current rawinsonde networks. Considerable effort should be focused on further defining what satellite soundings can contribute, and how they can be mixed with data from other sources.

Acknowledgments

I would like to thank all those who had an active part in this study. Special thanks go to Mr. John Derber and Prof. Lyle Horn for their careful scrutiny and helpful suggestions concerning the text, and to Eva Singer for typing the final manuscript. This research was supported by NASA Grant NSG5252.

REFERENCES

- Blechman, A.G. and L.H. Horn, 1981: The influence of higher resolution Nimbus-6 soundings in locating jet maxima. Case Studies Employing Satellite Indirect Soundings. Dept. of Meteor., U. of Wis., Final Report for NOAA Grant 04-4-158-2, 1-30.
- Bleck, R., and P.L. Haagenson, 1968: Objective analysis on isentropic surfaces. NCAR Tech. Notes, NCAR-TN-39, Boulder, Colo., 27 pp.
- Bonner, W.D., R. Van Haaren and C.M. Hayden, 1976: Operational-type analyses derived without radiosonde data from Nimbus-5 and NOAA-2 temperature soundings. NOAA Tech. Memo. NWS NMC-58, Washington, D.C., 17 pp.
- Desmarais, A., S. Tracton, R. McPherson and R. Van Haaren, 1978: The NMC Report on the Data Systems Test (NASA Contract S-70252-AG. US Dept. of Commerce, NOAA, NWS.
- Gandin, L.S., 1963: Objective Analysis of Meteorological Fields. Gidrometeorologicheskoe Izdatel'stvo, Leningrad. Translated from Russian, Israel Program for Scientific Translations, Jerusalem, 1965, 242 pp.
- Gerrity, J.P., Jr., 1977: The LFM model - 1976: a documentation. NOAA Tech. Memo., NWS NMC 60, 68 pp.
- Gerrity, J.P., Jr., and J. Newell, 1976: Post processing the LFM forecasts. Technical Procedures Bulletin No. 174, NOAA, National Weather Service, Silver Spring, Md.
- Halem, M., M. Ghil, R. Atlas, J. Susskind and W.J. Quirks, 1978: The GISS sounding temperature impact test. NASA Tech. Memo. 78063.
- Hayden, C.M., 1977: A summary of Nimbus-6 temperature retrieval accuracy statistics for DST-5 and DST-6. Third National Aeronautics and Space Administration Weather and Climate Program Science Review. NASA Conference Publication 2029, Goddard Space Flight Center, Greenbelt, Md.
- Horn, L.H., R.A. Petersen and T.M. Whittaker, 1976: Intercomparisons of data derived from Nimbus-5 temperature profiles, rawinsonde observations and initialized LFM model fields. Mon. Wea. Rev., 104, 1362-1371.
- Hyde, R.A., 1977: Effects of post-processing on the National Meteorological Center's primitive equation prediction models. Meteorological Applications of Satellite Indirect Soundings II. Dept. of Meteor., U. of Wis., Project Report for NOAA Grant 04-4-158-2, 66-127.
- Koehler, T.L., 1979: A case study of height and temperature analyses derived from Nimbus-6 satellite soundings on a fine mesh model grid. Ph.D. Thesis, University of Wisconsin-Madison, 186 pp.

- Miyakoda, K., T. Bettge, W. Davis, R. Hovanec, R. Lusen, F. Pratte, J. Ryan and L. Umscheid, 1977: Preliminary report on satellite sounder impact test at GFDL. Report submitted to the Associate Director for Environmental Monitoring and Prediction of NOAA. 10 pp.
- Petersen, R.A., and L.H. Horn, 1977: An evaluation of 500 mb height and geostrophic wind fields derived from Nimbus-6 soundings. Bull. Amer. Meteor. Soc., 58, 1195-1201.
- Phillips, N., L. McMillin, A. Gruber and D. Wark, 1979: An evaluation of early operational temperature soundings from TIROS-N. Bull. Amer. Meteor. Soc., 60, 1188-1197.
- Schlatter, T.W., 1975: Some experiments with a multivariate statistical objective analysis scheme. Mon. Wea. Rev., 103, 246-257.
- Schlatter, T.W., 1981: An assessment of operational TIROS-N temperature retrievals over the United States. Mon. Wea. Rev., 109, 110-119.
- Schmidt, B.D., T.L. Koehler and L.H. Horn, 1981: Evaluation of TIROS-N and NOAA-6 satellite data: comparisons of colocated soundings and analyses for a January case. Evaluations of Satellite Temperature Soundings Using Analyses and Model Forecasts. Dept. of Meteor., U. of Wis., Final Report for NASA Grant NSG-5252, 51-81.
- Schuëpp, M., R.W. Burnett, K.N. Rao, and A. Rowland, 1964: Note on the standardization of pressure reduction methods in the international network of synoptic stations. WMO Tech. Note No. 61, WMO-No. 154. TP. 74.
- Smith, W.L., and H.M. Woolf, 1976: The use of eigenvectors of statistical covariance matrices for interpreting satellite sounding radiometer observations. J. Atmos. Sci., 33, 1127-1140.
- Whittaker, T.M. and R.A. Petersen, 1977: Objective cross-sectional analyses incorporating thermal enhancement of the observed winds. Mon. Wea. Rev., 105, 147-153.

N82

19770

UNCLAS

Evaluation of TIROS-N and NOAA-6 Satellite Data:

Comparisons of Colocated Soundings and Analyses for a January Case

Brian D. Schmidt, Thomas L. Koehler and Lyle R. Horn
Department of Meteorology
University of Wisconsin-Madison, WI 53706

Abstract

This study uses an early January 1980 synoptic situation in evaluating the performance of TIROS-N and NOAA-6 operational temperature soundings. Visual and statistical comparisons of temperature and thickness fields were employed to determine the effects of manual screening of the satellite soundings and measure the accuracy of both the satellite soundings and analyses derived from them. A companion study by Derber et al. (1981) used these satellite data as numerical weather prediction model input. In both studies, comparisons between the performance of TIROS-N and NOAA-6 were emphasized.

Although the manual screening did not improve the statistics, removal of the poorest soundings produced more consistent analyses. Both satellites were able to correctly position the major troughs and ridges. Gradients were underestimated though, with troughs markedly too warm and ridges slightly too cold. The poorest data occurred near the surface and tropopause as reflected by larger standard deviations in those layers. As indicated in both types of comparisons, the performance of TIROS-N was slightly superior to that of NOAA-6. The results of this study are encouraging, although more attention should be directed toward correcting the problems satellites exhibit near the surface and the tropopause.

1. Introduction

A major development in the meteorological community during the 1970's was the advent of satellite-derived vertical temperature soundings. These soundings promised to improve numerical weather prediction models by providing an adequate data base over the large data-sparse regions of the earth. However, the ability of satellite soundings to actually improve prediction models has been inconclusive. Studies conducted at the National Meteorological Center (NMC) indicated that the addition of satellite soundings did not improve numerical model forecasts (Tracton and McPherson, 1977 and Desmarais et al., 1978). Similar studies carried out by Hale et al. (1978) and Kelly et al. (1978) reported slightly improved model forecasts when satellite data were included. The satellite data in these studies were mixed with data from conventional sources complicating the evaluation of the satellite soundings.

A second approach in evaluating satellite soundings involves comparing them against independent verification data usually based on radiosonde observations. Such evaluations are far simpler and less expensive than the numerical model impact studies noted above. For example, Phillips et al. (1979) examined the nature of TIROS-N soundings under varying degrees of cloudiness through comparison with colocated radiosondes. Another example of this second approach examines the ability of satellite data to define synoptic features. Horn et al. (1976) found that Nimbus-5 soundings successfully located the thermal gradient beneath an upper tropospheric jet streak. TIROS-N data was used recently by Streit and Horn (1981) to track the polar and subtropical jets over the eastern Pacific preceding the Wichita Falls tornado outbreak. Other satellite sounding studies involve constructing height analyses. For example, Petersen and Horn (1977) tracked a closed 500mb low using Nimbus-6 data. More recently, Koehler (1981) was able to delineate atmospheric trough and ridge positions over North America from Nimbus-6 height analyses constructed on a fine mesh model grid.

This study continues the approach of not mixing satellite and radiosonde data. Both collocation comparisons similar to Phillips et al. (1979), and comparisons of synoptic features similar to Koehler (1981) are performed. Unlike previous studies, two satellite data sets (TIROS-N and NOAA-6) will be examined. A case study of an early January 1980 synoptic situation occurring in the United States (U.S.) will be used. The choice of this area allows the use of the familiar Limited-area Fine Mesh (LFM) model analysis fields for verification. Derived entirely from conventional observations, the LFM analysis fields provide an independent standard of comparison.

With TIROS-N and NOAA-6 in operation at that time, a unique opportunity was provided to evaluate and compare the performances of the two satellites. The evaluation is pursued in two distinct ways. This study examines the quality of both the actual satellite temperature soundings and analysis fields based on them. In a second study by Derber et al. (1981), the resulting TIROS-N and NOAA-6 analyses are used to initialize and run a numerical weather prediction model to further evaluate the satellite soundings. Thus these two studies employ some aspects of the two basic approaches for satellite sounding evaluation, independent satellite sounding comparisons against conventional data and assessment of satellite data as numerical model input. In both studies comparisons between TIROS-N and NOAA-6 will be emphasized.

2. The region and period of study

A subset of NMC's LFM model output grid was chosen as the region of study as shown in Figure 1. This polar stereographic grid located over North America has a grid spacing of 190.5 kilometers true at 60°N and is fine enough to delineate small scale synoptic features revealed by the satellite soundings. Reasonably reliable analyses derived entirely from conventional rawinsonde data are available on this grid from NMC. In this study they served two purposes: 1) they provided the verification data set against which satellite sounding data were compared and 2) they were used as a first guess in an interpolation scheme employed in the horizontal analyses of the satellite data. LFM analyses were extracted from the entire domain shown in Figure 1. However, the satellite-derived analyses were constructed only on the sub-region outlined. This analysis region was chosen to facilitate interpolation to the model grid used in the companion study by Derber et al. (1981).

In order to use and evaluate the satellite data, the period of study had to satisfy several requirements. The ability of satellite soundings to define strong temperature gradients could best be evaluated in a synoptic situation that exhibited intense baroclinity. A wintertime pattern satisfies this requirement. Furthermore, two synoptically active regions, e.g. well developed troughs, within the analysis region would allow for more meaningful evaluation of the horizontal error structure. Also, a sustained period of nearly complete data sets from TIROS-N and NOAA-6 was necessary for inter-satellite comparisons and interpolation to synoptic times.

ORIGINAL PAGE IS
OF POOR QUALITY

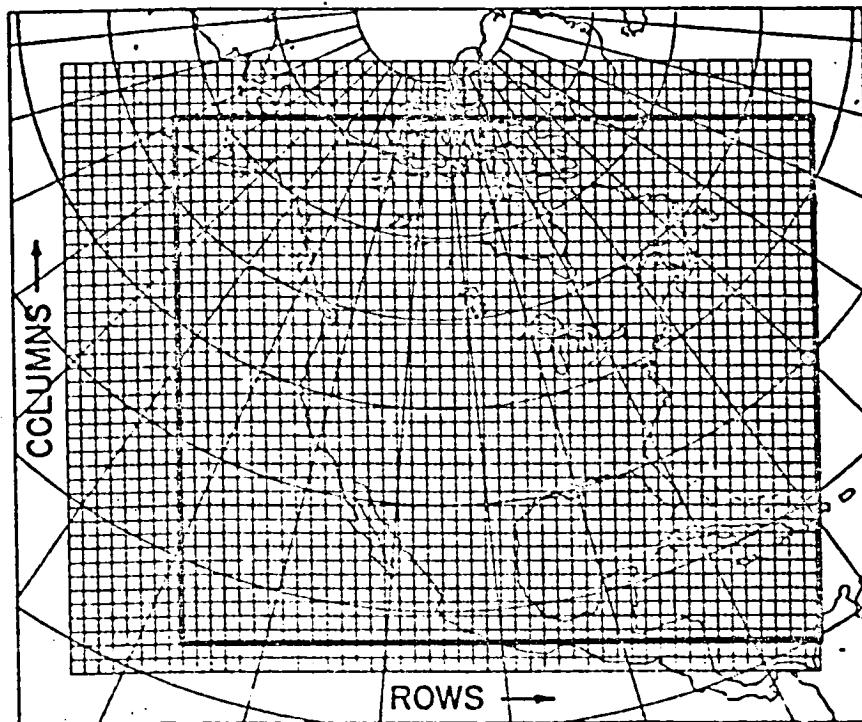


Figure 1. The LFM grid and the analysis subset grid (dark outline) for this study.

A period between 0000 GMT 5 January and 0000 GMT 8 January was found to satisfy these requirements. Figure 2 depicts the 500 mb and 1000 mb height fields for the period 0000 GMT 6 January through 0000 GMT 7 January 1980. At 0000 GMT 6 January, a long wave trough was located over the eastern portion of the U.S., while a short wave trough was located over the Pacific Northwest. An intense jet streak was associated with this vigorous short wave as it rapidly propagated eastward. Reasonably complete TIROS-N and NOAA-6 satellite data sets were available from the Environmental Data and Information Service (EDIS), and LFM

ORIGINAL PAGE IS
OF POOR QUALITY

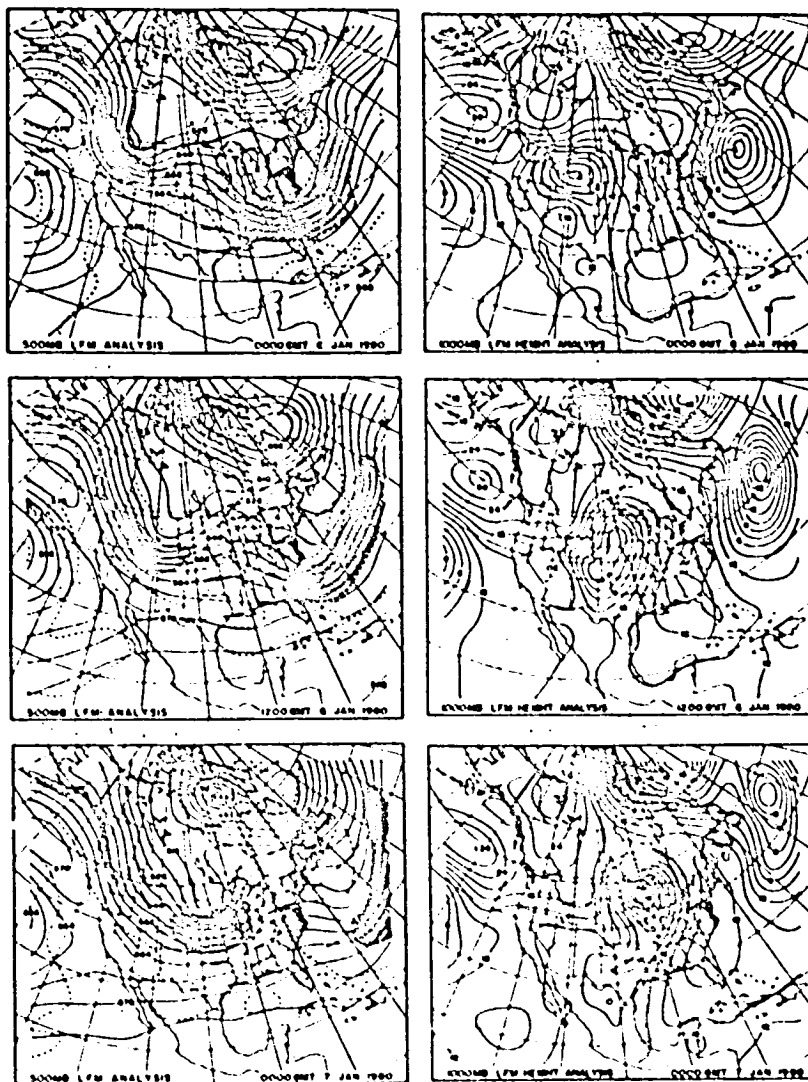


Figure 2. LFM 500mb height (solid) and geostrophic isotach (dashed) analyses, and 1000mb height analyses for 0000 GMT 6 January through 0000 GMT 7 January 1980.

save tapes were furnished by NMC for this period. These data sets allowed for interpolation of the asynoptic satellite data to the synoptic times, 0000 GMT and 1200 GMT 6 January and 0000 GMT 7 January.

3. The satellite sounding data

TIROS-N and NOAA-6 operational satellite soundings were used in this study. The character of the study was influenced by the satellite orbits, instrument design and retrieval procedures. Features pertinent to this study are provided in the following discussion. A more detailed description of the orbital and instrumental characteristics can be found in Kidwell (1979). The operational satellite soundings produced by the National Environmental Satellite Service (NESS) contained three major types of soundings, differing in both the raw data and the processing procedures. These soundings produced reasonably complete data coverage across the analysis region.

The TIROS-N and NOAA-6 satellites were launched on 13 October 1978 and 27 June 1979, respectively. They were placed in nearly sun-synchronous orbits with southbound equatorial crossings at approximately 0300 (TIROS-N) and 0730 (NOAA-6) Local Solar Time (LST). With northbound equatorial crossings occurring twelve hours later, the analysis region was covered twice each day by each satellite. For example, Figure 3 displays sounding locations obtained from TIROS-N on 6 January 1980. The orbital period of approximately 102 minutes resulted in an observation time variation of nearly ten hours from east to west across the analysis region. This asynoptic nature of the data made a time interpolation necessary to produce analyses at standard times to facilitate verification.

Both satellites carried similar versions of the TIROS Operational Vertical Sounder (TOVS). The TOVS consists of three instruments, the High resolution Infrared Radiation Sounder (HIRS-2), the Microwave Sounding Unit (MSU) and the Stratospheric Sounding Unit (SSU). Vertical temperature profiles produced by NESS were derived from the radiance measurements provided by these instruments. Clear, partly cloudy and cloudy soundings were produced using procedures described in Smith et al. (1979). Clear soundings were derived from a combination of all available HIRS and MSU channels. A special method described by Smith and Woolf (1976) which compensates to some degree for cloud contamination of the infrared (HIRS) channels was used for the partly cloudy soundings. Cloudy soundings were derived from all stratospheric channels, but only the microwave channels in the troposphere.

ORIGINAL PAGE IS
OF POOR QUALITY

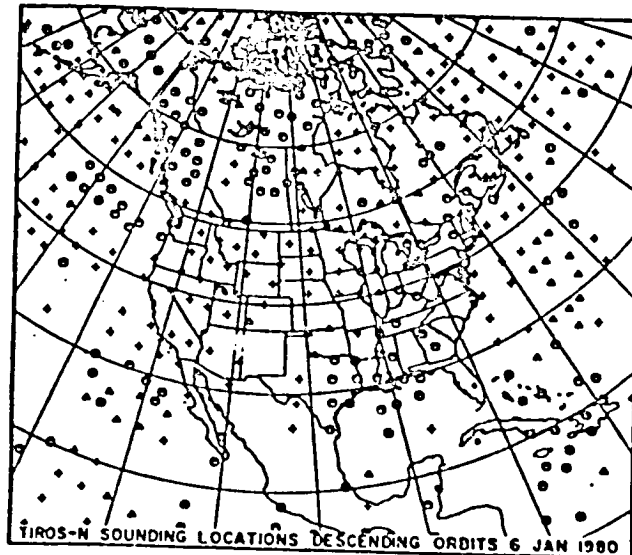


Fig. 3. TIROS-N sounding locations from descending orbits at approximately 0300 Local Solar Time (LST) on 6 January 1980. Soundings are divided into three types: clear (O), partly cloudy (Δ) and cloudy (+).

At the time of this case study (January 1980), the acceptance criteria for the partly cloudy retrieval technique was such that too few partly cloudy soundings were produced (Smith, 1981). Also, the automated quality control procedure used during the data processing was too liberal, making manual screening of the satellite soundings important. Previous work by Horn et al. (1976), Blechman and Horn (1981) and Paulson and Horn (1981) has shown that such manual screening can produce data sets superior to unscreened satellite data sets.

4. Data preparation and screening

The original format of the operational satellite soundings received from EDIS was in terms of layer mean temperatures, along with temperatures and pressures at the surface and tropopause. This study's screening and analysis procedure, required that the data be in terms of isobaric level temperatures and thicknesses relative to 1000mb. Using a method described by Polger (1978), the

level temperatures were determined by a linear interpolation between the layer mean temperatures, surface temperature and tropopause data. Level temperatures below the reported surface were estimated assuming a lapse rate of one-half the dry adiabatic lapse rate. Thicknesses relative to 1000mb were hydrostatically calculated using the original layer mean temperatures where possible, and the layer temperatures estimated from the level values below the surface and near the tropopause.

For screening and analysis purposes, the data were divided into five sets per satellite, each set consisting of soundings from either ascending or descending orbits at the same subsatellite LST. A sample of one of these data sets is given in Figure 3. The arduous process of manually screening the ten data sets was undertaken by intercomparing horizontal hand analyses, vertical cross sections, cloudiness and type of sounding. Initially, questionable soundings were flagged in hand analyses of temperatures at seven mandatory levels up to 100mb and also for cumulative thicknesses (i.e. 1000-850mb, 1000-700mb, etc.). Vertical cross sections of potential temperatures and thermal winds relative to 850mb were constructed through the flagged data points using a technique developed by Whittaker and Petersen (1977). When the horizontal analyses and vertical cross sections failed to clearly identify inconsistent soundings, other factors such as cloudiness and type of sounding were considered. When this occurs, the cloudy (microwave) soundings and soundings with higher percentages of cloudiness were deemed inconsistent. To reduce the effect of personal bias, agreement between the two people involved in the screening procedure was necessary. During this process, direct comparisons between satellite and conventional analyses were avoided to insure independent judgements. It was found in the screening procedure that inconsistent soundings which were too cold (warm) in the lower layers were too warm (cold) in the upper layers. In regions of overlapping passes, sounding pairs less than sixty kilometers apart could produce instabilities in the analysis routine. Special attention was given these pairs with the less consistent sounding being removed from all data sets.

From these screening procedures, ten data sets for each satellite emerged, five screened (i.e. obviously inconsistent soundings removed) and five unscreened (i.e. obviously inconsistent soundings retained). For TIROS-N, the unscreened data sets contained a total of 2095 soundings. Of these, 6.4 percent were removed to create the screened data sets consisting of 1962 soundings. Likewise, the NOAA-6 unscreened data sets contained 2257 soundings with 6.4 percent removed to form screened data sets consisting of 2113 soundings.

5. The asynoptic problem

A major difficulty encountered in studies comparing satellite soundings with conventional data is the time variation between the two types of data. Conventional observations and the analyses based on them are synoptic in nature. However, satellite soundings are made in continuous orbital swaths at the same LST, resulting in time differences of 102 minutes between consecutive passes. To cover the North American region, at least six passes are required, which leads to time differences of nearly ten hours between the easternmost and westernmost soundings. Since this type of study requires comparisons of the asynoptic satellite data with an independent verification set, both fields must be valid at the same time to produce truly meaningful comparisons. To place both data sets in the same time frame for comparison, one or the other must be modified. If the comparisons are performed at the satellite observations, a series of bracketing conventional standards of comparison should be interpolated to the satellite times. This allows statistical comparisons which identify actual sounding error characteristics. On the other hand, if the comparisons are performed at the synoptic times of conventional analyses, a series of bracketing satellite fields should be interpolated to synoptic time. This provides an opportunity to evaluate the performance of satellite data in defining the structure of weather patterns. However, time interpolations may provide an inadequate representation of the actual temporal changes in the atmosphere.

To facilitate an understanding of this complex topic, a detailed description of the time-related aspects of this study will be presented. An appreciation of this topic is essential to better understand the results given in later sections.

Conventional NMC analyses on the LFM grid based on synoptic radiosonde observations provide the standard of comparison for the satellite sounding evaluations. Assessment of satellite data is performed using both types of comparisons noted earlier: 1) statistical comparisons done at satellite sounding locations by interpolating the gridded LFM data in time and space to the sounding locations (colocated comparisons) and 2) comparisons of synoptic features based on satellite and LFM analyses at synoptic times.

Figure 4 illustrates the time dependency of the data sets employed. Both the discrete synoptic times of the LFM analyses and the continuous periods of the satellite soundings are presented. For the colocated comparisons, the seven LFM analysis periods shown schematically in Figure 4 produce verification values for the four shaded TIROS-N and NOAA-6 data sets. Both morning and afternoon colocated comparisons were performed to prevent a diurnal bias.

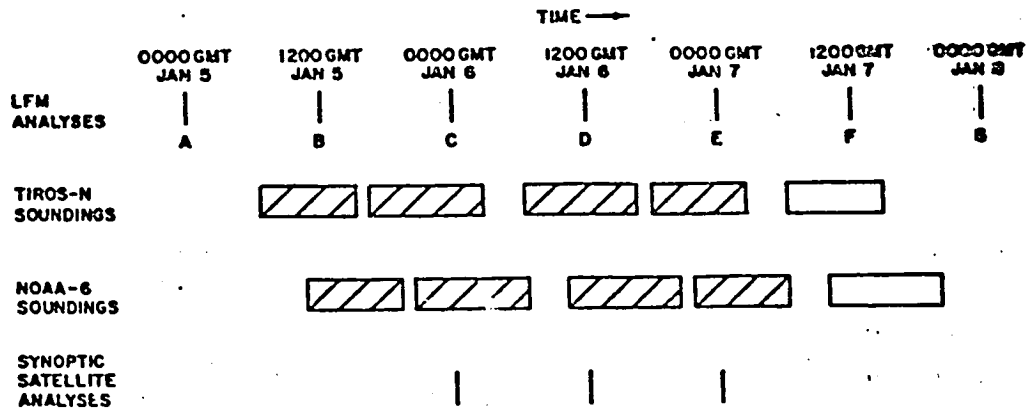


Figure 4. The satellite data sets and LFM analyses used in this study. Comparisons at sounding locations were made for the shaded satellite sets. Satellite-derived analyses were interpolated to the times shown at the bottom for synoptic feature comparisons.

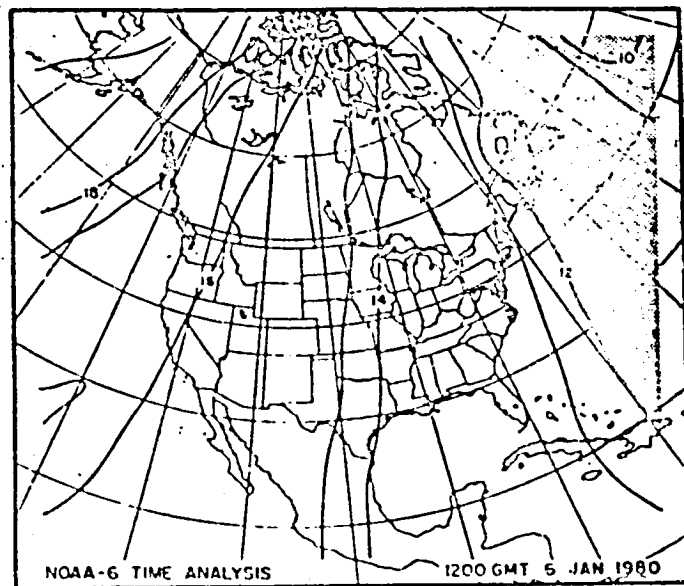


Figure 5. Satellite sounding time analysis for the 6 January 1980 NOAA-6 morning soundings, with observations before 1200 GMT shaded.

Verification values for each level at every satellite sounding location were determined as follows. First, the satellite sounding time was used to identify four bracketing LFM times. A spatial interpolation for each of these four analyses was then performed to the satellite sounding location using overlapping quadratic polynomials in two dimensions. This was followed by an overlapping quadratic polynomial interpolation in time to the sounding time, producing the collocated value. This process is clarified by considering a complete satellite period as shown in Figure 5, which presents a time analysis of the 6 January 1980 NOAA-6 morning soundings. LFM periods B, C, D and E (Figure 4) were used in interpolations for all observations in the shaded area (i.e. before 1200 GMT), while LFM periods C, D, E and F were employed in interpolations in the unshaded area (i.e. after 1200 GMT). Thus, the production of collocated verification values for all four TIROS-N and NOAA-6 periods required seven LFM analysis sets.

Conversely, for comparisons at synoptic times, five satellite periods were employed to construct the three satellite synoptic analyses shown in Figure 4. First, satellite analyses at LFM grid points were constructed for each of the five TIROS-N and NOAA-6 data sets, ignoring time variations in the observations. Separate time analyses were also constructed, such as that shown in Figure 5. To determine the "synoptic" satellite value at an LFM grid point, the synoptic time was compared to the values of the five time analyses, the bracketing times for the polynomial interpolation identified, and the value calculated. This process was repeated at each level for every grid point, yielding the final satellite synoptic fields for the three times shown in Figure 4. In any event, more data sets were involved in generating compatible comparisons than were actually evaluated in the result sections.

6. Thickness analysis procedure

Satellite thickness analyses were produced on the LFM grid using an optimum interpolation method with normalized weights. This method, developed by Koehler (1979) based on Gandin (1963), was specifically designed to handle the abrupt changes in coverage, such as gaps between satellite passes. Since the interpolation weights are normalized, the analysis can be performed either with or without first guess fields. Persistence first guess fields provided by the LFM thickness analyses approximately twelve hours preceding the average sounding time were used in the satellite thickness analyses. Thickness analyses were produced at nine vertical levels with identical weights used at each level. The satellite time

analyses, required for the interpolation to synoptic times, were constructed without a first guess using the same weights employed in the thickness analyses. The combined filter described by Gerrity and Newell (1976) was applied to the final, time interpolated, synoptic satellite thickness analyses.

7. Results

The discussion of the results is divided into two sections: 1) colocated comparisons and 2) the synoptic pattern analyses. Because this study examines the performance of two satellites over a two day period, a thorough discussion of the results could become tedious. Thus, while detailed results are presented, only those features deemed most significant will be discussed.

a) Colocated comparisons

As previously mentioned, this approach compares satellite layer mean temperatures with conventional gridded data interpolated to the satellite observation locations. This comparison provides an estimate of the accuracy of the soundings.

Table 1 shows TIROS-N and NOAA-6 sounding statistics for the screened and unscreened data sets. Since there are only very minor differences between the two sets of data, it is apparent that manual screening did not improve the overall statistical results. However, it must be emphasized that the screening procedure does remove the poorest soundings, thus providing more consistent satellite sounding sets for analysis purposes. For this reason, all future comparisons will use only the screened satellite data sets.

Figure 6 shows a comparison of TIROS-N and NOAA-6 soundings over both the whole region of study and the U.S. subregion. The data in this figure are a composite of all four time periods and all three soundings types. Excluding the lower two layers, the graphs exhibit strikingly similar patterns for both satellites. The larger bias and standard deviation values in the 200-300mb region reflects the difficulty in defining the tropopause using satellite soundings. The U.S. region exhibits a much more pronounced pattern, with larger negative biases in the upper troposphere. Several factors may contribute to this pattern. The U.S. region with its dense radiosonde network, provides a more stringent verification standard than that available in the entire region. Additionally, the U.S. region is primarily in mid-latitudes where January baroclinity is strong, while the whole region includes areas north and south of this strongly baroclinic region. In these weaker baroclinic areas there is less likelihood of

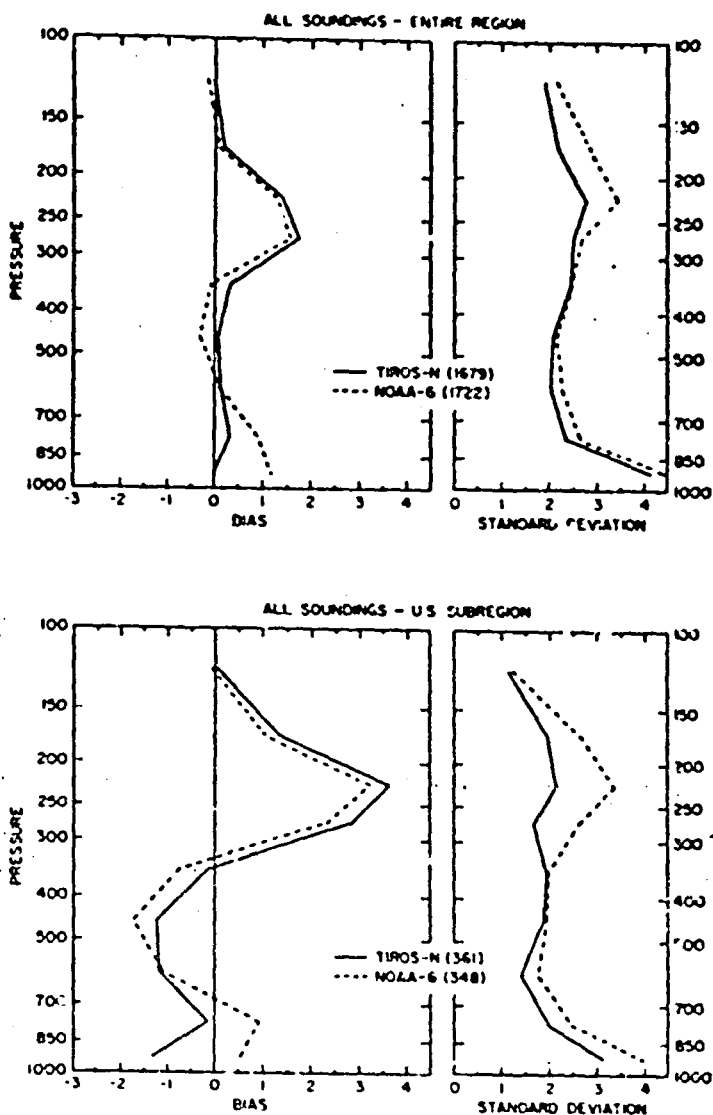


Figure 6. Colocated layer mean temperature comparisons ($^{\circ}\text{C}$) between TIROS-N/NOAA-6 values and LFM analysis values (interpolated in space and time to the satellite sounding locations).

Table 1: Layer mean temperature comparisons ($^{\circ}\text{C}$) between screened (SCR) and unscreened (ALL) satellite soundings and analysis values interpolated to observation locations.

	LAYER (MB)								
	1000- 850	850- 700	700- 500	500- 400	400- 300	300- 250	250- 200	200- 150	150- 100
BIAS									
ALL NOAA-6	1.08	.83	.04	-.36	-.10	1.59	1.35	.13	-.14
SCR NOAA-6	1.17	.89	.08	-.34	-.09	1.58	1.29	.09	-.15
ALL TIROS-N	-.12	.24	.08	.06	.32	1.74	1.42	.21	.02
SCR TIROS-N	-.01	.30	.12	.07	.32	1.74	1.41	.20	.03
ST. DEV.									
ALL NOAA-6	4.51	2.68	2.29	2.20	2.46	2.69	3.45	2.89	2.17
SCR NOAA-6	4.47	2.64	2.28	2.18	2.48	2.70	3.45	2.88	2.17
ALL TIROS-N	4.16	2.40	2.04	2.08	2.45	2.51	2.81	2.22	1.94
SCR TIROS-N	4.12	2.33	2.02	2.09	2.46	2.52	2.79	2.20	1.92

large differences between the satellite soundings and radiosonde based verification data. Thus with the larger sample, the differences should be reduced. Finally, within the larger north-south extent of the whole region, there is a greater variation in the height of the tropopause. Thus the distribution of differences is spread over several layers, which reduces the magnitude of the differences in the upper troposphere.

Figure 7 presents the TIROS-N and NOAA-6 soundings subdivided into the three sounding types: clear (CLR), partly cloudy (P CLDY) and cloudy (CLDY). This type of figure, similar to one used in Phillips et al. (1979), reveals the characteristics of the various sounding types.

In the Phillips study, TIROS-N soundings from various regions of the globe during April 1979 were compared with colocated radiosondes. Bias and RMS values were calculated. In this study, the standard deviation is used, rather than the RMS. The standard deviation provides a better measure of the "noise" since the bias has been removed.

A comparison between the bias values obtained for TIROS-N in this study (based on the entire region) with those obtained by Phillips et al. (1979) for the North American region shows similar values with largest biases amounting to about 2°C . While the largest biases in this January study occur at about 200-300mb, the largest values in the Phillips et al. study occur between 150-250mb. This probably reflects the higher altitude of the tropopause in April. Overall, the bias values obtained by Phillips et al. for North America are not greatly different from those in this study based on the entire region. However, biases

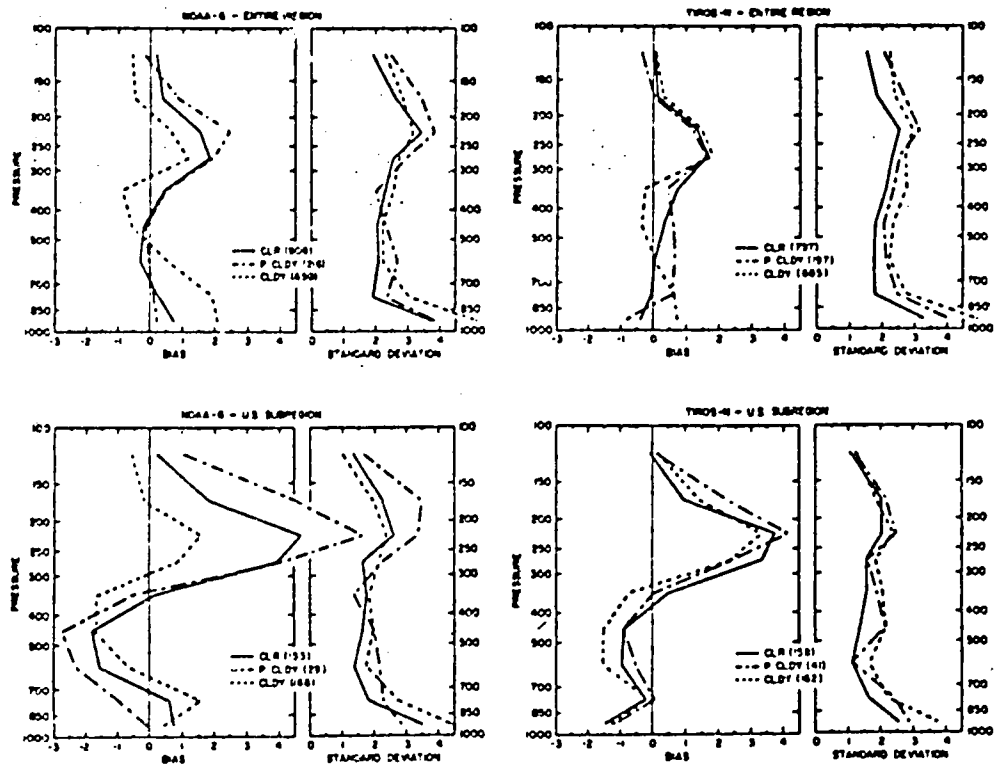


Figure 7. Same as Fig. 6 except soundings subdivided into clear (CLR), partly cloudy (P CLDY) and cloudy (CLDY) sounding types.

based on the U.S. subregion show considerably larger values than obtained by Phillips et al.. The largest standard deviation near the tropopause obtained in this study (based on the entire region) of 2.95°C yields an RMS of 3.3°C when combined with the bias. This compares well with an RMS value near the tropopause of about 3.4°C in the Phillips et al. study. On the other hand, an RMS of 4.8°C is reached for the U.S. subregion of this study. However, the standard deviations for both TIROS-N and NOAA-6 in the U.S. subregion tend to be somewhat smaller than those in the whole region. This stands in contrast to the larger bias values in the U.S. subregion.

As noted in the introduction, the major aspect of this study is the comparison of the relative performance of two satellites, TIROS-N and NOAA-6. Figure 8 provides a direct comparison of TIROS-N and NOAA-6 for the clear and cloudy soundings over both the entire region and the U.S. subregion. The partly cloudy soundings are not presented since they comprise such a small percentage of the sample. As shown in Figure 8, the TIROS-N and NOAA-6 bias and standard deviation curves are quite similar above the lowest layers. This similarity is not surprising since nearly identical instruments are aboard both satellites. However, the standard deviations show NOAA-6 to be slightly noisier throughout the soundings.

The most significant difference in the curves occurs in the bias for the 1000-850mb layer where TIROS-N soundings are noticeably colder. In an attempt to isolate the reason for these low level differences, histograms were prepared showing the distribution of the TIROS-N and NOAA-6 colocated temperature differences over the eastern U.S. (Figure 9). This region of the U.S. was used to lessen the problems of topography. The NOAA-6 clear cases (Figure 9a) shows a distinct shift toward warmer values (i.e. NOAA-6 warmer than the radiosonde). In contrast, the TIROS-N clear cases (Figure 9b) are skewed toward values colder than the radiosonde. The cloudy comparisons provided in Figures 9c and 9d show a strong skewness toward warmer temperatures at low levels for NOAA-6 while the TIROS-N data are more normally distributed. Attempts were made to explain differing distributions shown in Figure 9 without success. Perhaps future studies should further investigate this tendency.

b) Height and thickness synoptic analysis comparisons

Figures 10 and 11 depict the TIROS-N, NOAA-6 and LFM 500mb height and geostrophic isotach analyses for all three time periods. Both satellites

ORIGINAL PAGE IS
OF POOR QUALITY

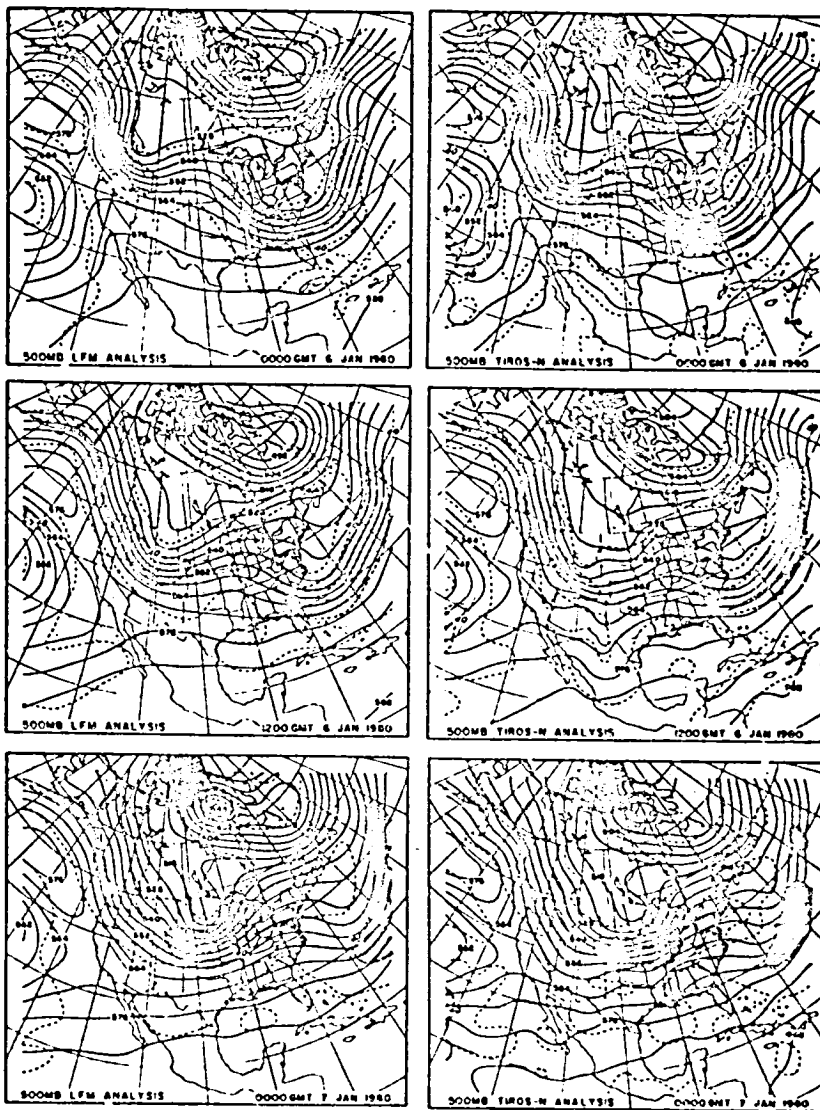


Figure 10. TIROS-N and LFM 500mb height (solid, dam) and geostrophic isotach (dashed, $m s^{-1}$) analyses for 0000 GMT 6 to 0000 GMT 7 January 1980.

PRECEDING PAGE BLANK NOT FILMED

67-68

ORIGINAL PAGE IS
OF POOR QUALITY

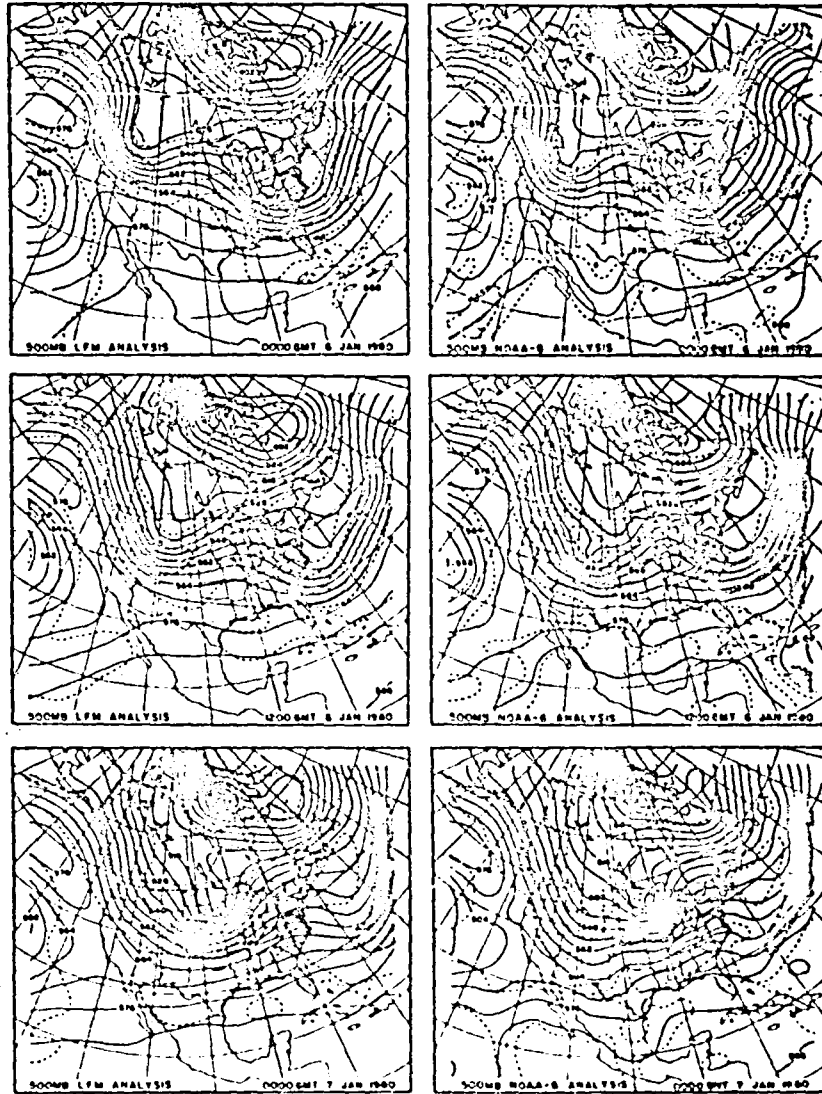


Figure 11. Same as Fig. 10 except for NOAA and LFM.

define the trough and ridge positions relatively well, although some of the gradients are weaker than in the LFM analyses. This is particularly evident at 0000 GMT 7 January, when both satellites fail to capture the 60 m s^{-1} jet maximum associated with the trough located in the Northern Plains states. Weaker satellite gradients have been noted in early studies (e.g. see Koehler, 1981 or Desmarais et al., 1978). Also, at 1200 GMT 6 January both satellites show a tendency toward a double wave in the western trough. This tendency is not present in the LFM analysis. A further discrepancy occurs over Mexico, where apparently anomalous troughs are found in several of the satellite analyses. These troughs are located in data gaps between satellite passes and can probably be attributed to the extrapolation of gradients into the data gaps by the analysis method.

In summary, an examination of the 500mb heights and geostrophic winds shown in Figures 10 and 11 are relatively encouraging despite the discrepancies noted above. The quality of these satellite analyses will be further revealed in numerical forecast experiments conducted by Derber et al. (1981).

Since the collocation results showed relatively poor values at low levels and near the tropopause, an attempt was made to decrease the effects of these layers in further evaluations. This was done by calculating thicknesses over three tropospheric layers (1000-700mb, 700-300mb, 300-100mb). The discussion that follows pertains to these three layers.

The satellite minus LFM 1000-700mb thickness differences shown in Figure 12 illustrate satellite sounding problems near the surface. Both positive and negative centers are present. Over southern Canada and the U.S., both satellites show positive centers (i.e. satellite thicknesses too high) propagating eastward and southward with the major trough. This is consistent with the 500mb trough (Figures 10 and 11) being too weak. On the other hand, the negative anomaly (i.e. satellite thicknesses too low) remains more stationary, primarily over the mountainous western region of the U.S. This may indicate a recognized difficulty in the retrieval procedures over high terrain, or it may reflect inadequacies in the extrapolation to 1000mb in this study.

Two other large anomalies exist in northern Canada. One is a large positive anomaly located over the North Atlantic coastal region near Labrador. Since it is located near the center of the North American branch of the polar vortex and occurs in both satellites it may simply represent another example of troughs being too warm in satellite analysis fields. However, since this area is nearly devoid of conventional data, it is possible that the anomaly reflects a deficiency in the verification data. The other anomaly exists over mountainous western Canada and

ORIGINAL PAGE IS
OF POOR QUALITY



Figure 12. Satellite-derived minus LFM thickness differences (dam) for the 1000-700mb layer from the 0000 GMT 6 to 0000 GMT 7 January 1980 periods.

is also positive. This feature could be another example of satellite sounding problems over high terrain. However, since it weakens with time it may also reflect the propagation of the trough from this region.

The largest departures are in the NOAA-6 data, as compared to the TIROS-N data. Since both data sets are interpolated to the same time, the greater NOAA-6 anomalies may reflect problems with either its instrumentation or sounding retrieval procedure. This is also supported by the slightly better performance of TIROS-N in the colocation comparisons.

Results for the 700-300mb layer should be more promising, considering the smaller collocated differences found in that layer. Figures 13 and 14 show the TIROS-N, NOAA-6 and LFM 700-300mb thickness analyses for the three time periods. Also shown are isotachs (dashed lines) of the 700-300mb thermal wind. The troughs in the thickness field are located west and north of their position in the 500mb analyses, which would be expected in a developing baroclinic wave. Many of the variations present in the 500mb fields are removed by isolating this layer from the lower levels. For example, both the TIROS-N and NOAA-6 700-300mb thickness patterns give little or no indication of the tendency toward a "double wave" pattern in the 1200 GMT 6 January 500mb field. Also, the eastern Pacific closed high and low in the 500mb field apparent in all three periods is weakened in the 700-300mb thickness field.

Both satellites show general agreement with the LFM analysis trough and ridge positions, although the satellite features are shifted 3-5° to the west. The intensity of the troughs and ridges are underestimated with the troughs also showing less curvature. As usual, there is a loss of gradient information in both sets of satellite data.

However, TIROS-N does a better job in defining the 700-300mb gradients than NOAA-6. This is particularly evident in the western trough at 1200 GMT 6 January and 0000 GMT 7 January when TIROS-N better defines the 40 m s^{-1} thermal wind jet and related thickness gradient apparent in the LFM analyses. Neither satellite does very well in delineating the thermal wind jet associated with the eastern trough, although it is unclear whether this is totally a satellite problem or simply a lack of conventional data over the Atlantic.

Examination of the statistics in Table 2, which includes S1 scores, also reveals NOAA-6's deficiency in defining gradients.¹ The NOAA-6 S1 scores are consistently larger than those for TIROS-N for both the entire region and the U.S.

¹The S1 score measures the accuracy of the intensity and positioning of gradients in a given field; with smaller S1 scores indicating more accurate gradient representation.

ORIGINAL PAGE IS
OF POOR QUALITY

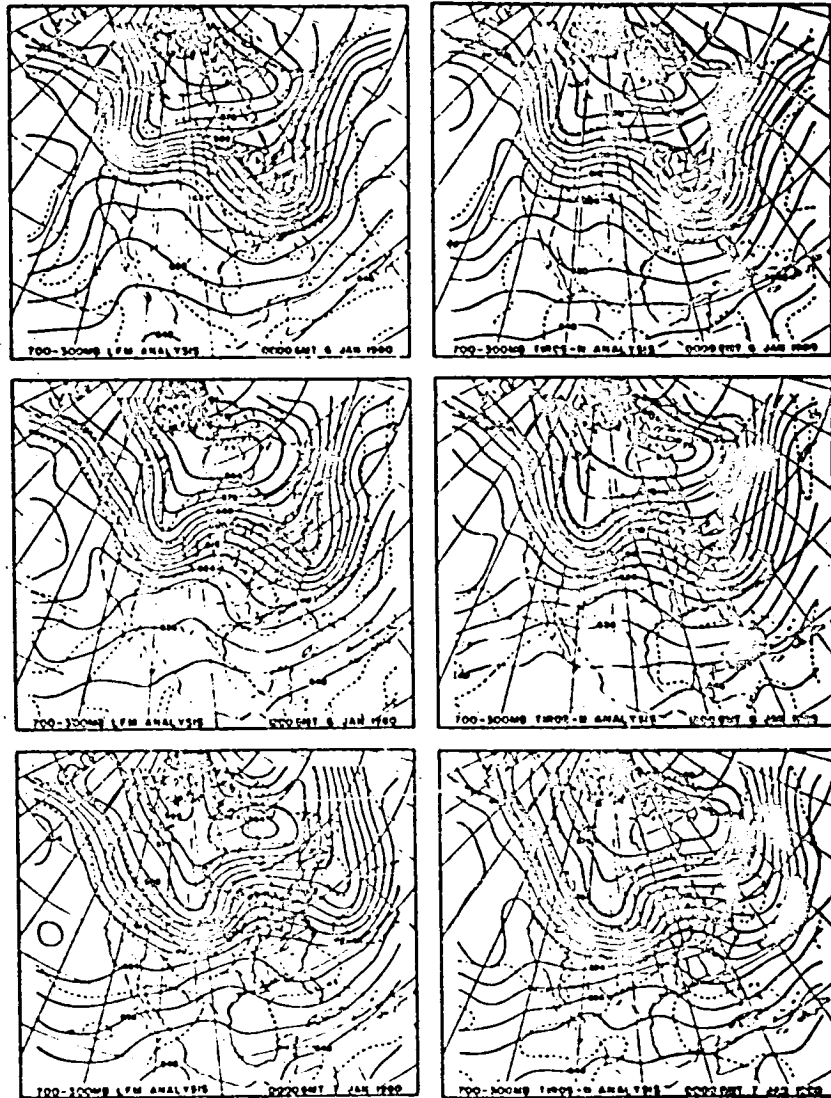


Figure 13. TIROS-N and LFM 700-300mb thickness (solid, dam) and thermal wind isotach analyses (dashed, $m s^{-1}$) for 0000 GMT 6 to 0000 GMT 7 January 1980.

ORIGINAL PAGE IS
OF POOR QUALITY

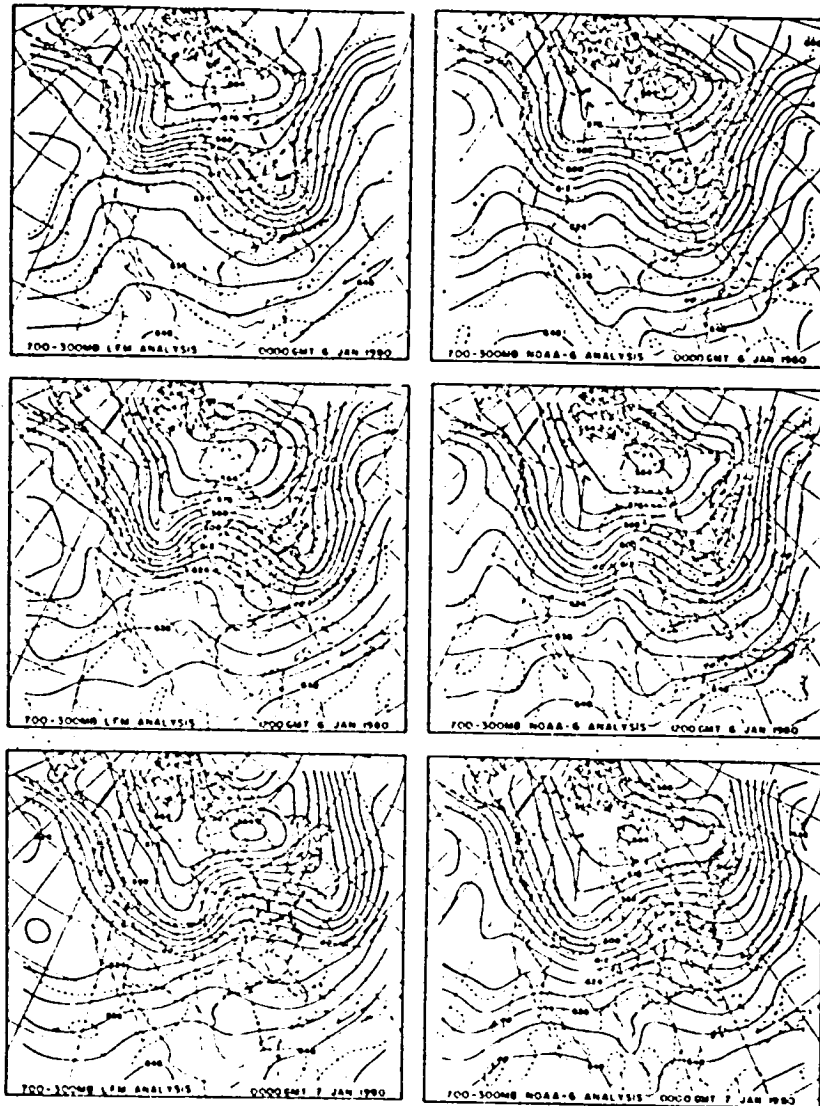


Figure 14. Same as Fig. 13 except for NOAA and LFM.

Table 2: TIROS-N (T) and NOAA-6 (N) vs. LFM layer mean temperature analysis statistics. Bias and standard deviation values are in Celsius degrees, while the S1 scores are dimensionless.

	0000 GMT 6 JANUARY				1200 GMT 6 JANUARY				0000 GMT 7 JANUARY			
	ENTIRE REGION		U.S. SUBREGION		ENTIRE REGION		U.S. SUBREGION		ENTIRE REGION		U.S. SUBREGION	
	T	N	T	N	T	N	T	N	T	N	T	N
BIAS												
1000-700MB	-.20	.83	-.41	.81	-.08	.29	-.87	.45	-.29	.74	-.50	1.17
700-300MB	.09	.17	-.77	-.86	.15	-.15	.92	-1.38	.12	.10	-.66	-.84
300-100MB	.77	.47	1.38	1.54	.65	.35	1.74	1.31	.77	.37	1.52	.87
ST. DEV.												
1000-700MB	2.20	2.82	1.70	2.41	2.59	2.59	2.59	2.50	2.50	2.69	2.23	2.85
700-300MB	1.36	1.64	1.17	1.65	1.39	1.45	1.48	1.54	1.30	1.58	1.10	1.35
300-100MB	1.31	1.84	1.06	1.74	1.52	1.91	1.10	1.70	1.48	1.98	.91	1.47
S1												
1000-700MB	51.0	60.2	36.9	47.5	50.6	51.6	42.6	45.0	49.4	54.1	36.9	45.3
700-300MB	42.2	45.9	32.6	39.4	43.4	45.1	35.2	41.4	38.9	42.8	31.0	41.0
300-100MB	63.5	74.2	45.0	68.7	69.5	81.7	52.2	79.4	65.9	73.8	47.9	63.3

subregion. The SI scores for both satellites are smaller in the U.S. subregion than in the whole region. One possible explanation is that the lack of radiosonde data in the data sparse areas of the entire region prevents an accurate definition of the verification field gradients. The standard deviations in Table 2 indicate greater values for NOAA-6. This agrees with the collocation results.

Figure 15 shows the 700-300mb thickness difference fields (i.e. satellite minus LFM analysis). As in the 1000-700mb thickness differences, the positive anomalies, indicative of too high satellite thicknesses, follow the troughs throughout the period in both satellites. This is true for both the western and eastern troughs. However, unlike the 1000-700mb thickness difference fields, negative anomalies indicative of too low satellite thicknesses, are found in most of the ridges. This is apparent in the ridge between the eastern and western troughs throughout the three time periods. Negative anomalies also tend to remain stationary over the western U.S. mountains. This possibly reflects the effects at higher levels of sounding problems over high terrain. The 700-300mb thickness difference results support the premise that NOAA-6 is poorer in defining gradients. For example, NOAA-6 exhibits a large negative anomaly over Colorado at 1200 GMT 6 January and a large positive anomaly over the Northern Plains at 0000 GMT 7 January.

The 300-100mb analysis results are only given in statistical form. These results are poorer than those in the 700-300mb layer for both satellites with consistently larger SI scores and biases. This is not surprising, since the 300-100mb layer contains the large tropopause errors found in the collocated results.

8. Conclusions

Evaluation of TIROS-N and NOAA-6 soundings was performed using both collocated and analysis comparisons between satellite and conventional data for an early January 1980 synoptic situation. Although paralleling similar studies (Desmarais et al., 1978; Koehler, 1981; Schlatter, 1981), this study is unique in that it simultaneously evaluates the performance of two satellites.

Extensive manual screening was performed on the original soundings sets. Although the collocated statistics showed little or no improvement, removal of the poorest soundings provided more consistent analyses.

The TIROS-N and NOAA-6 collocated statistics exhibit similar characteristics above the lower layers (i.e. 1000-700mb), with the best results in the middle troposphere. The large differences near the tropopause are indicative of poor vertical resolution in satellites, while those near the surface are probably due to

ORIGINAL PAGE IS
OF POOR QUALITY

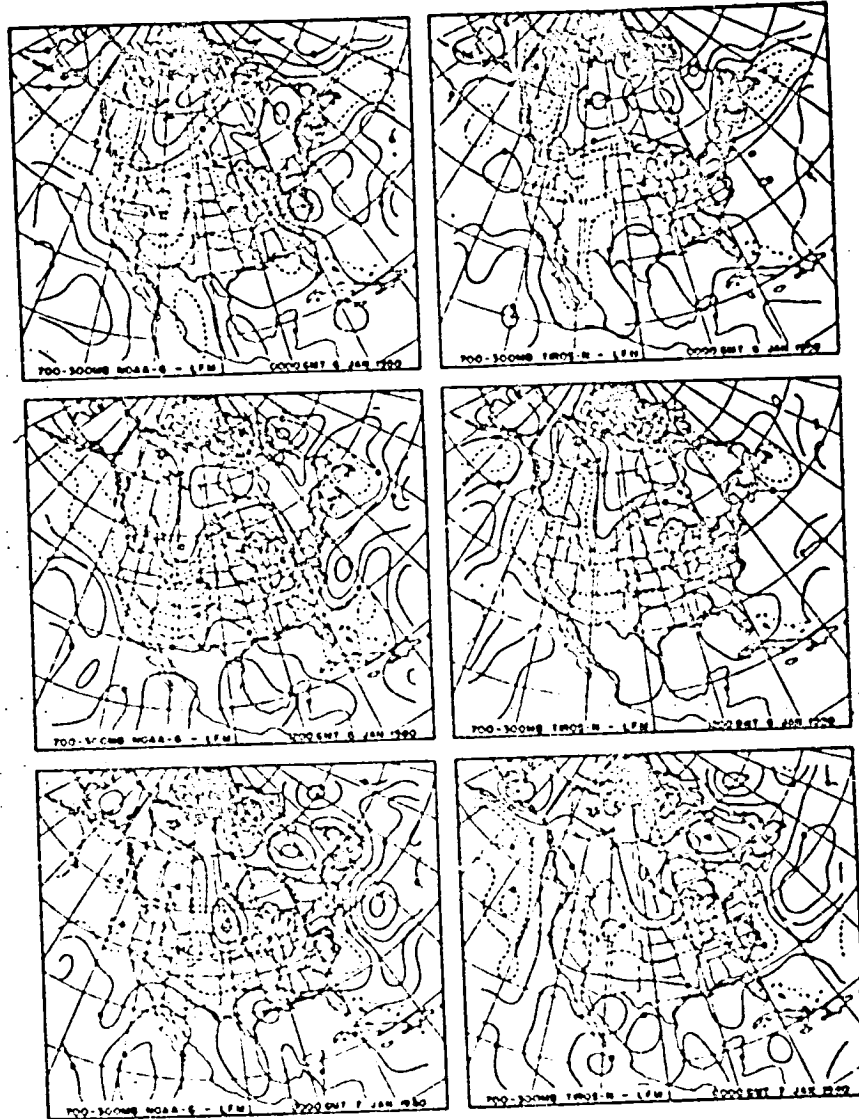


Figure 15. Same as Fig. 12 except for the 700-300mb layer.

retrieval problems over high terrain and poor vertical resolution. The TIROS-N statistics for the entire region are similar with those obtained by Phillips et al. (1979). However, the TIROS-N and NOAA-6 biases in the U.S. subregion are larger than those of the entire region.

TIROS-N and NOAA-6 analyses show general agreement with the LFM 500mb height and 700-300mb thickness analyses, especially in locating trough and ridge positions. However, some differences were noted. For example, several of the variations found in the 500mb satellite fields were not present in the 700-300mb thickness fields. The large differences found in the layers below 700mb help explain the improvement. The 700-300mb thickness differences exhibited positive anomalies (too warm) in troughs and negative anomalies (too cold) in ridges with the positive anomalies especially moving with the synoptic situation. These anomalies indicate that satellites underestimate gradients and that the underestimation is correlated to the synoptic pattern.

Overall, TIROS-N performs slightly better than NOAA-6 in this study. The smaller TIROS-N colocated standard deviations indicate less noise in the soundings. Visual comparisons of the 500mb height and 700-300mb thickness analyses reveal more accurate TIROS-N gradients. This is supported by the smaller TIROS-N anomalies in both 1000-700mb and 700-300mb thickness difference fields. Additionally, smaller TIROS-N SI scores quantitatively show more accurate gradient intensity and positioning.

In summary, the rather accurate description of synoptic features by TIROS-N and NOAA-6 is encouraging, although it is evident that the problems near the surface and tropopause have not been corrected. Improvement in these areas should be given greater priority. This study's results show TIROS-N soundings to be of slightly better quality than NOAA-6 soundings. Whether this result is true in general or is simply an anomaly in this one case study remains to be seen.

Acknowledgements

We wish to thank all those who had an active part in this study. Special thanks go to John Derber, who completed a companion study and helped write the introductory sections, to Linda Whittaker who proofread the manuscript, and to Eva Singer who typed the final version. This research was supported by NASA Grant NSG-5252.

REFERENCES

- Blechman, A.G., and L.H. Horn, 1981: The influence of higher resolution Nimbus-6 soundings in locating jet maxima. Case Studies Employing Satellite Indirect Soundings. Dept. of Meteor., U. of Wis., Final Report for NOAA Grant 04-4-158-2, 1-30.
- Derber, J.C., T.L. Koehler and L.H. Horn, 1981: A numerical evaluation of TIROS-N and NOAA-6 analyses in a high resolution limited area model. Evaluations of Satellite Temperature Soundings Using Analyses and Model Forecasts. Dept. of Meteor., U. of Wis., Final Report for NASA Grant NSG-5252, 82-108.
- Desmarais, A., S. Tracton, R. McPherson and R. van Haaren, 1978: The NMC Report on the Data Systems Test (NASA Contract S-70252-AG). U.S. Dept. of Commerce, NOAA, NWS.
- Gerrity, J.P., Jr., and J. Newell, 1976: Post-processing the LFM forecasts. Technical Procedures Bulletin No. 174, NOAA, National Weather Service, Silver Spring, Md.
- Halem, M., M. Ghil, R. Atlas, J. Susskind and W.J. Quirks, 1978: The GISS sounding temperature impact test. NASA Tech. Memo. 78063.
- Horn, L.H., R.A. Petersen and T.M. Whittaker, 1976: Intercomparisons of data derived from Nimbus-5 temperature profiles, rawinsonde observations and initialized LFM model fields. Mon. Wea. Rev., 104, 1362-1371.
- Kelly, G.A.M., G.A. Mills, and W.L. Smith, 1978: Impact of Nimbus-6 temperature soundings on Australian region forecasts. Bull. Amer. Meteor. Soc., 59, 1225-1240.
- Kidwell, K.B., 1979: NOAA Polar Orbiter Data (TIROS-N and NOAA-6) Users Guide Preliminary Version. Satellite Data Services Division, National Climatic Center.
- Koehler, T.L., 1979: A case study of height and temperature analyses derived from Nimbus-6 satellite soundings on a fine mesh model grid. Ph.D. Thesis, Univ. of Wisc., 186 pp.
- Koehler T.L., 1981: A case study of height and temperature analyses derived from Nimbus-6 satellite soundings. Evaluations of Satellite Temperature Soundings Using Analyses and Model Forecasts. Dept. of Meteor., U. of Wis., Final Report for NASA Grant NSG-5252, 1-50.
- Paulson, B.A., and L.H. Horn, 1981: Nimbus-6 temperature soundings obtained using interactive video-graphics computer techniques. Bull. Amer. Meteor. Soc., 62, 31-36.
- Petersen, R.A. and L.H. Horn, 1977: An evaluation of 500mb height and geostrophic wind fields derived from Nimbus-6 soundings. Bull. Amer. Meteor. Soc., 58, 1195-1201.

Phillips, N., L. McMillin, A. Gruber, D. Wark, 1979: An evaluation of early operational temperature soundings from TIROS-N. Bull. Am. Meteor. Soc. 60, 1188-1197.

Polger, P., 1978: Conversion of TIROS-N data to O.N. 29 format. Office Note 186, NOAA, NMC 5 pp.

Schlatter, T.W., 1981: An assessment of operational TIROS-N temperature retrievals over the United States. Mon. Wea. Rev., 109, 110-119.

Smith, W.L., 1981: Personal communication, Univ. of Wisc.

Smith, W.L., H.B. Howell and H.M. Woolf, 1979: The use of interferometric radiance measurements for sounding the atmosphere. J. Atmos. Sci., 36, 566-575.

Smith, W.L., and H.M. Woolf, 1976: The use of eigenvectors of statistical covariance matrices for interpreting satellite sounding radiometer observations. J. Atmos. Sci., 33, 1127-1140.

Streit, D.F., and L.H. Horn, 1981: Intercomparisons of TIROS-N satellite soundings, radiosonde data and NMC analyses in tracking jet streaks. Synoptic-Dynamic Applications of Meteorological Satellite Data. Dept. of Meteor., U. of Wis., Final Report for NOAA Grant NA79AA-H-00011.

Tracton, M.S., and R.D. McPherson, 1977: On the impact of radiometric sounding data upon operational numerical weather prediction at NMC. Office Note 136, NOAA, NMC, 11 pp.

Whittaker, T.M. and R.A. Petersen, 1977: Objective cross-sectional analyses incorporating thermal enhancement of the observed winds. Mon. Wea. Rev., 105, 147-153.

N82

19771

UNCLAS

D3 1 N82 1977I

A Numerical Evaluation of TIROS-N and NOAA-6

Analyses in a High Resolution Limited Area Model

John C. Derber, Thomas L. Koehler and Lyle H. Horn
Department of Meteorology
University of Wisconsin-Madison, WI 53706

Abstract

Vertical temperature profiles derived from TIROS-N and NOAA-6 radiance measurements are used to create separate analyses for the period 0000 GMT 6 January to 0000 GMT 7 January 1980. The 0000 GMT 6 January satellite analyses and a conventional analysis are used to initialize and run the University of Wisconsin's version of the Australian Region Primitive Equations model. Forecasts based on conventional analyses are used to evaluate the forecasts based only on satellite upper air data.

The forecasts based only on TIROS-N or NOAA-6 data did reasonably well in locating the main trough and ridge positions. The satellite initial analyses and forecasts revealed errors correlated to the synoptic situation. The trough in both TIROS-N and NOAA-6 forecasts which was initially too warm remained too warm as it propagated eastward during the forecast period. Thus, it is unlikely that the operational satellite data will improve forecasts in a data dense region. However, in regions of poor data coverage, the satellite data should have a beneficial effect on numerical forecasts.

1. Introduction

Since the advent of numerical weather prediction, the development and use of numerical models have been hampered by the lack of complete and accurate data sets, especially in oceanic regions. Recent advances in remote sensing have established the possibility of using satellite derived temperature profiles to improve the data base. However, in several recent numerical experiments, the results have failed to show any consistent positive impact when satellite temperature profiles were included in the model initial fields. These results have raised questions concerning the usefulness of the satellite data in numerical weather prediction. Since many other factors can influence forecast quality, this conclusion may be faulty. This study, along with a companion study by Schmidt et al. (1981), attempts to determine whether vertical temperature profiles derived from TIROS-N and NOAA-6 radiance measurements contain useful meteorological information. In this paper, the evaluation is performed by comparing numerical forecasts made using only sounding data from each satellite with a control forecast based on only conventional data.

In previous studies the quality of satellite data has been analyzed using two distinct methods: direct comparisons of satellite data with conventional data and numerical model forecasts. The direct comparison can either be done using colocated soundings or analysis comparisons. Both direct comparison methods are used by Schmidt et al. (1981) on the same data set employed in this study. The colocated sounding technique compares individual satellite profiles to nearby radiosonde profiles or analyses interpolated to the sounding locations. Phillips (1979) and Schlatter (1981) have recently compiled colocated statistics for the TIROS-N satellite. In addition, Schlatter (1981) also employed analysis comparisons. Halem et al. (1978) and Tracton et al. (1980) combined Nimbus-6 satellite data with conventional data to produce horizontal analyses for use in their impact studies. However, the combination of the satellite data with conventional data makes satellite data evaluation difficult. Peterson and Horn (1977) used only Nimbus-6 data to track a 500mb low. Koehler (1981) was able to define major synoptic features using only Nimbus-6 data. Using cross-sectional analyses created from Nimbus-5 data, Horn et al. (1976) were able to describe the thermal gradient beneath an intense upper tropospheric jet streak. Blechman and Horn (1981) used higher resolution Nimbus-6 data to better locate a jet streak in a summertime situation. Recently, using both horizontal and cross-sectional TIROS-N analyses, Streit and Horn (1981) were able to track the polar and subtropical jets, which later influenced the Wichita Falls tornado outbreak.

The inclusion of satellite data in numerical weather prediction models provides another method of satellite data evaluation. Nearly all of the recent studies of this type have concentrated on employing a combination of temperature data derived from radiance measurements from Nimbus-6 and conventional upper air data. Ghil et al. (1979) found a slight positive impact with inclusion of satellite data, while Tracton et al. (1980) found no consistent positive impact with the inclusion of satellite data. Kelly et al. (1978) did find a consistent positive impact in a Southern Hemisphere study. This result may have been due to the more extensive data poor regions in the Southern Hemisphere. A good summary of recent model impact studies is presented by Ohring (1979).

The improvement or degradation of numerical model forecasts when satellite data are combined with conventional data is often used to imply the quality of the satellite data. However, as pointed out by Tracton et al. (1981), the impact of satellite soundings is a function not only of the satellite data quality, but also the analysis and forecast system. Analysis errors may result from incompatibility between satellite and conventional data. Consequently, analyses based separately on satellite and conventional data may be superior to an analysis based on a combined data set. Also, the combination of data sets makes the evaluation of the satellite soundings difficult. Analysis techniques which take into account the unique characteristics of the satellite data may produce superior analyses. The model may also influence the effect of satellite temperature data on numerical model forecasts. If the resolution of the model is too coarse, the model may be insensitive to small differences in the initial field. Also, inadequate model physics may overwhelm the effects of the changes in the initial field.

Unlike most previous impact studies, this study involves comparisons of numerical model forecasts based either entirely on conventional data or entirely on satellite data. This approach circumvents problems arising from the mixing of data sets. It appears that the only previous study using this approach was by Bonner et al. (1976), which produced hemispheric forecasts from analyses based only on Nimbus-5 and NOAA-2 temperature soundings. Furthermore, separate analyses were produced from TIROS-N and NOAA-6 data allowing intercomparisons between two satellite data sets. These analyses were inserted into a limited area primitive equation model with high horizontal resolution. The resulting forecasts are verified against those produced from conventional initial fields. From these comparisons, a better understanding of the characteristics and limitations of satellite data in a forecast situation can be developed.

2. The experiment

In this study, TIROS-N and NOAA-6 operational satellite soundings were used in a numerical forecast model to evaluate the data's quality and usefulness in numerical weather prediction. As noted in the introduction, this and a companion study apply the same data sets. In the first, Schmidt et al. (1981) examines the satellite sounding quality and the improvement achieved through manual screening of the data. In this second portion of the experiment only the analyses derived from the 0000 GMT 6 January 1980 TIROS-N and NOAA-6 screened data sets are used in a numerical forecast experiment. The data and procedures used to construct these satellite-derived analyses are described fully in Schmidt et al. (1981).

To evaluate the model forecast results achieved using TIROS-N and NOAA-6 analyses, a control forecast was necessary. For this purpose the thickness fields obtained from the Limited-area Fine Mesh (LFM) model of the National Meteorological Center (NMC) were used. Upper air temperature and geostrophic wind fields were derived using the LFM 1000 mb height analyses and TIROS-N, NOAA-6 and LFM thickness analyses. The mean sea level pressure data required by the initialization procedure, were also taken from the 0000 GMT 6 January 1980 LFM analysis fields. Since the same surface data was used in each case, differences between the satellite and conventional initial fields were limited to the upper air temperature and wind fields. Forecasts out to twenty-four hours were produced from the TIROS-N, NOAA-6 and control initial fields. The control run was verified against conventional analyses to evaluate model performance, while the forecasts derived from the TIROS-N and NOAA-6 data were compared to the control forecasts in order to evaluate the satellite data. This evaluation may provide insights into the ability of the satellite temperature data to describe synoptic fields in a numerical forecast situation. It should be emphasized that the satellite data forecasts were not necessarily expected to be superior to the control forecasts, particularly since the experiment was conducted over an area rich in conventional data. Rather, the comparisons were intended to provide indications of the information content of satellite data.

3. Forecast model description

The Australian Region Primitive Equations model was adapted by the Australian Numerical Meteorology Research Centre for use by the University of Wisconsin and the National Environmental Satellite Service (NESS). (Hereafter,

this model will be referred to as the ANMRC model.) The operational version upon which the ANMRC model is based is described in McGregor et al. (1978). The ANMRC model is a semi-implicit primitive equation model with second order truncation errors in space and time. In the version of the ANMRC model used in this experiment, only adiabatic processes were allowed. Additional information on this model can be found in Mills et al. (1981). In the vertical, the ANMRC model had ten sigma levels while it uses a staggered spatial grid in the horizontal.

The ANMRC model grid shown in Figure 1 is on a Lambert conformal projection with a grid spacing of 67.56km at 50° and 20°N. This high resolution not only reduces the truncation error, but also is small enough to resolve the information contained in the satellite data. Computer memory limitations encountered with such a high horizontal resolution restricts the model domain to a limited area. Boundary conditions which must then be specified, presented a major difficulty in this study. To simplify the experiments, fixed boundary conditions were used. As can be expected, the fixed boundary conditions produced large forecast errors near the boundaries. Not only are time variations of the atmospheric structure along the boundary neglected by the use of fixed boundary conditions, but also an incorrect specification of the initial condition may continuously produce larger errors as the forecast progresses. Thus, only the inner region shown in Figure 1 was used to verify the forecasts.

4. The ANMRC model forecasts

The ANMRC model initialization procedures required temperature and wind analyses at 1000, 850, 700, 500, 300, 250, 200, and 100mb, moisture data below 300mb and a sea level pressure field on the ANMRC grid. Since the data were only in terms of thickness analyses on the LFM subset grid, the following procedure was applied identically to the screened TIROS-N, screened NOAA-6 and LFM thickness analysis. The thickness fields derived from LFM analyses were included to serve as a control forecast in satellite data and model performance evaluations. The procedure used to produce the required fields was designed to ensure consistency between data sets and to minimize the influence of outside data sources.

First, the 1000mb height, dew point temperature and sea level pressure analyses were extracted from the LFM analysis and 00hr forecast data sets. From the TIROS-N, NOAA-6 and LFM thickness analyses, temperature fields were derived

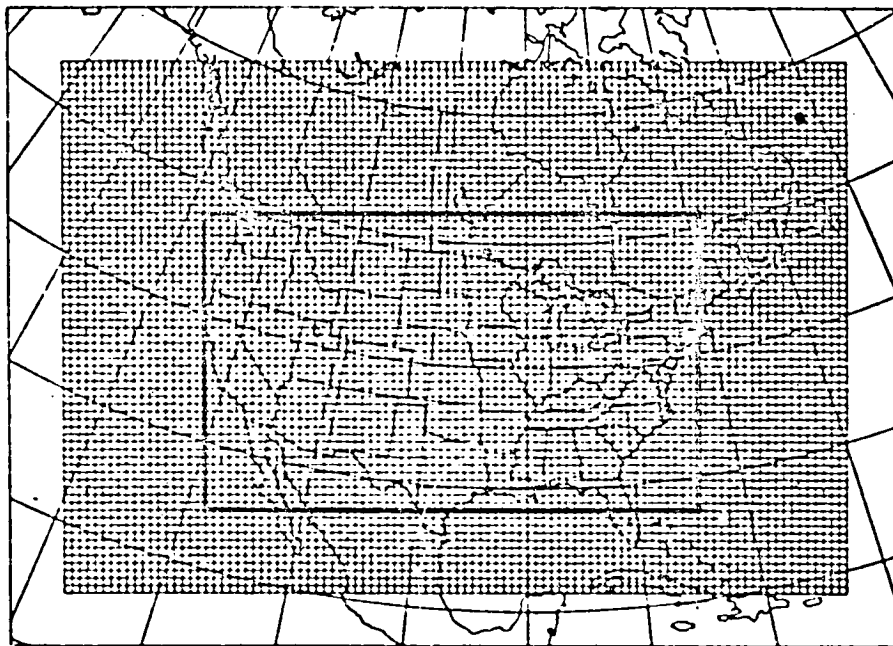


Figure 1: The ANMRC model grid. Verification statistics were calculated for only the outlined inner region.

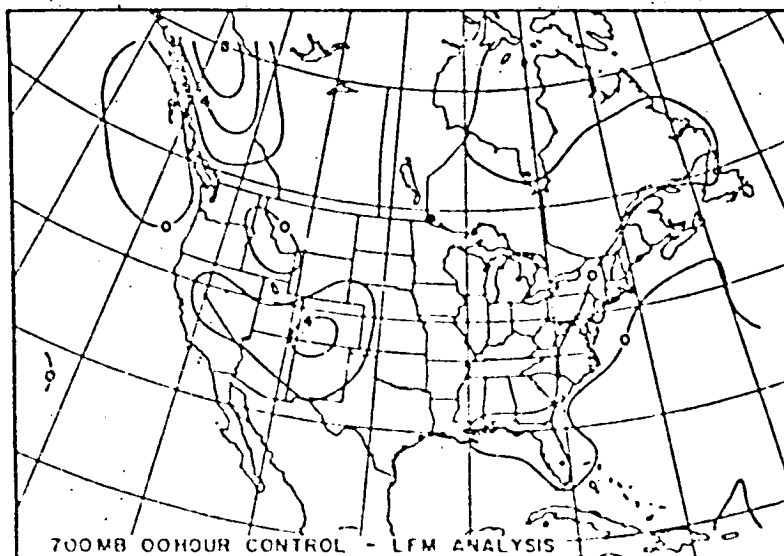


Figure 2: Differences between the control 00hr and LFM analysis 700mb height fields (dam) for 0000 GMT 6 January 1930.

hydrostatically and height fields created using the LFM 1000mb analyses. The sea level pressure, temperature, height and dew point temperature analyses were interpolated to the ANMRC model grid using overlapping quadratic polynomials in two dimensions. Since a small area in the southeast corner of the ANMRC model grid is located outside the LFM model grid, an extrapolation to these grid points was required. However, in this region any errors introduced by the extrapolation are unlikely to significantly effect the forecasts in the verification region.

On the ANMRC model grid, geostrophic winds were calculated from the height fields. The approximations of geostrophic winds, adiabatic processes, and fixed boundary conditions were applied consistently between model runs. Thus, comparisons with the control case should minimize the effects of these approximations on the final results.

The LFM (control), NOAA-6 and TIROS-N data sets produced using the preceding procedure were used to initialize and run the ANMRC model on the CRAY-1 computer at the National Center for Atmospheric Research (NCAR). The model was run out to twenty-four hours with a timestep of six minutes. In order to ensure consistency between the LFM verifying analyses and the ANMRC model forecasts, the filtering in the post processing was altered to simulate NMC's combined filter described in Gerrity and Newell (1976). Each forecast was produced consistently under the simplified conditions of fixed boundary conditions, geostrophic winds, and a minimum of parameterization. Thus, comparisons between ANMRC model runs (i.e. the TIROS-N, NOAA-6 and the control run) are more meaningful in data evaluations than comparisons against operational LFM analyses. Model performance under these simplified conditions can be evaluated through comparisons between the control forecast (the ANMRC model forecast initialized using the LFM analyses) and the operational NMC LFM analyses and forecast.

5. Results

The TIROS-N, NOAA-6, and control model runs each produced forecasts of four different variables at ten levels of the atmosphere for five time periods (00, 06, 12, 18, and 24 hours). Since a complete presentation of all these results is unmanageable, the evaluation will concentrate on the 00, 12, and 24 hour forecasts of the 500mb heights and 700-300mb thicknesses. The 500mb height field was chosen for evaluation because of the importance of this level to forecasters. The 700-300mb layer was chosen for several reasons. Figure 2 shows the effect of the ANMRC initialization and post-processing procedures on the 700mb control height

field. Obviously the errors arising from these procedures are related to the surface topography, which lies below 700mb. The 700-300mb layer is also above and below the layers in which the satellite temperatures display maximum differences from conventional data sources. (See Schmidt et al., 1981.) However, data from the levels above 700mb and below 300mb may still significantly influence the 700-300mb layer forecasts. Also, an inconsistency was found in the model initialization procedure after these forecasts were run. The result was a large height bias in the top sigma level ($\sigma = .05$) in the forecasts. However, the results suggest that the levels below 300mb were not greatly affected. The forecast verification will concentrate on the trough initially located over the Pacific Northwest, since the eastern trough is severely affected by the boundary conditions.

a. The 500mb level

The control forecasts are first evaluated against the LFM 500mb analyses to give an indication of the ANMRC model performance under the simplified conditions of initial geostrophic winds, fixed boundaries and a minimum of parameterization. The 00, 12, and 24hr control forecasts along with verifying analyses are shown in Figure 3. In this and subsequent 500mb figures both height and geostrophic isotach analyses are shown. The geostrophic winds are used to indicate the strength of the gradient in the height field.

Since the control forecast was initialized using the LFM analyses for 0000 GMT 6 January, the difference between this analysis (Figure 3a) and the 00hr forecast (Figure 3b) indicates the effects of the initialization and post-processing. A slight decrease in the areas of geostrophic wind maxima is apparent, indicating a decrease in the 500mb height gradient. This effect, which is at least partially due to the filtering done in the post-processing, should be present in all the model forecasts.

As the trough over the Pacific Northwest intensifies and propagates eastward, the 12hr control forecast moves the trough somewhat too quickly and overintensifies the height gradient in the base of the trough. (Compare Figures 3c and 3d.) However, more apparent differences in the 12hr forecasts are the closed center and the nearly north-south trough axis in the control forecast compared to the open wave and the positive tilt in the LFM analysis. As shown in Figures 3e and 3f, the location of the trough in the 24hr forecast is only slightly too far to the east. However, the control forecast does not intensify the trough enough. This lack of intensification is reflected in the weaker geostrophic jet maximum over the central states.

ORIGINAL PAGE IS
OF POOR QUALITY

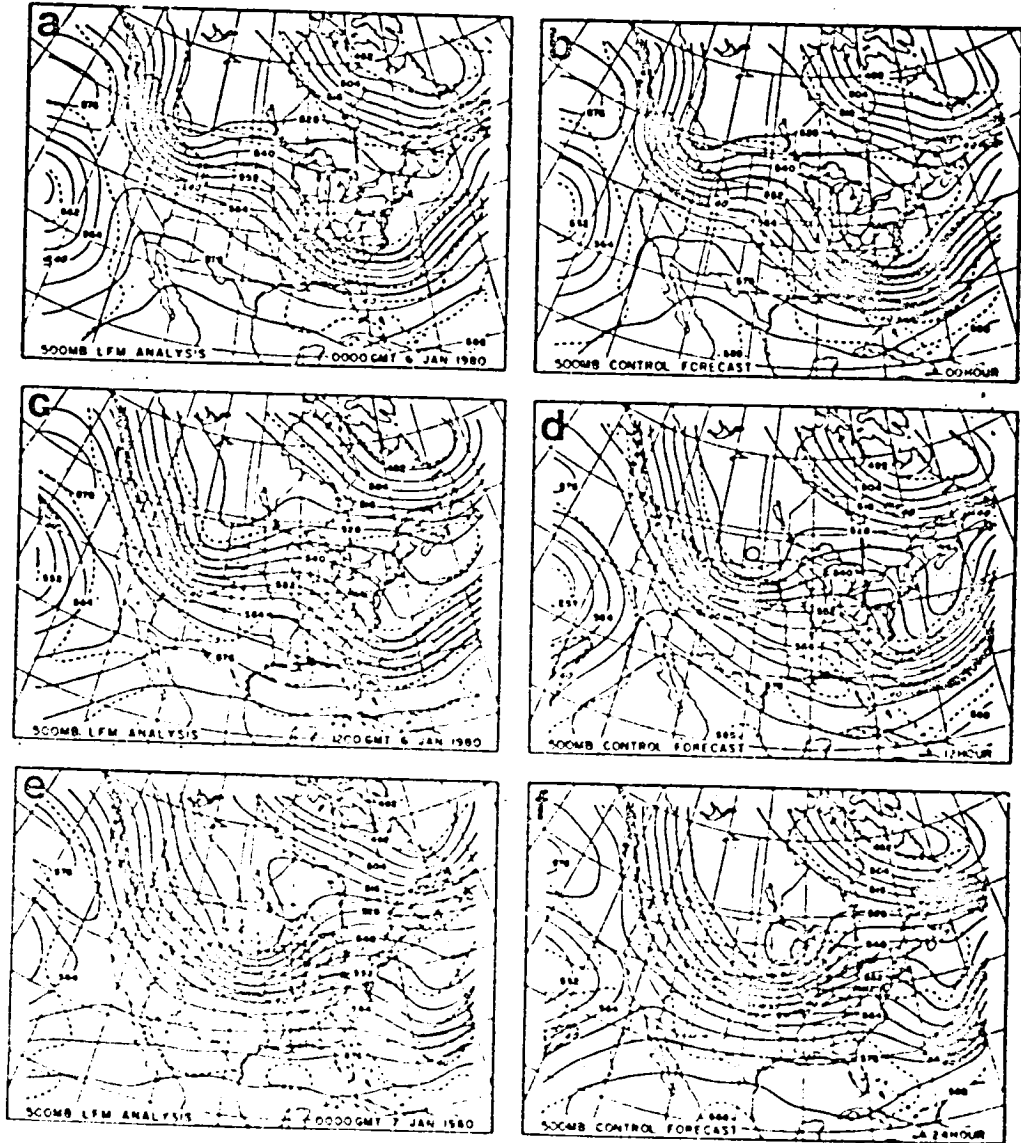


Figure 2: 500mb height (solid, dam) and geostrophic isotach (dashed, 20 m s⁻¹ interval) analyses from the LFM analyses (a,c,e) and the control forecast (b,d,f). Isotach values greater than 40 m s⁻¹ are shaded.

In order to partially assess the effect of the simplifications employed in obtaining the control forecast, the NMC LFM forecasts are compared with the control forecasts in Figure 4. Also, since the control initial fields were taken from the LFM analyses, deficiencies in the initial fields should be reflected in both model forecasts.

Away from the boundaries, two major differences are noted. In the 12hr forecasts, the center of the 500mb low over North Dakota is shifted further south in the control forecast, thus increasing the gradient in the base of the trough (Figures 4c and 4d). Also, in the 24hr forecasts the LFM model correctly forecasts the center of the 500mb low. Compare Figures 4f with 3e. The control forecast (Figure 4e) shows a center about sixty meters higher than the LFM forecast. In general, the NMC operational LFM forecast and the ANMRC control forecasts were in better agreement with each other than either was with the verifying LFM analyses. Considering the simplifications used in the control run, it was surprising that the control forecasts were in reasonably good agreement with the operational LFM forecast.

Since the satellite forecasts were produced under the same model limitations as the control forecasts, many of the same features found in the control forecasts can be expected to also be present in the satellite forecasts. Thus, differences between the control forecasts and the TIROS-N and NOAA-6 forecasts should reveal strengths and limitations of satellite data in a numerical model forecast. The companion study by Schmidt et al. (1981), which gives a more complete description of the satellite data and analyses used in the model initialization, found that the satellite data tended to be too warm in troughs and too cold in ridges. Thus, the gradients in the height and thickness fields were usually underestimated. In comparisons between TIROS-N and NOAA-6 analyses, Schmidt et al. found that the TIROS-N analyses tended to be slightly better than those from NOAA-6.

Because of the weaker gradients in the analysis fields, one may expect to find weaker gradients in the satellite forecasts, with TIROS-N possibly performing somewhat better than NOAA-6. The TIROS-N 00hr forecast shows weaker gradients with an accompanying underestimation of the geostrophic jet maxima in the base of both the eastern and western troughs as shown in Figure 5. Also at 00hr the western trough extended back further into central Canada. This feature, also found in the NOAA-6 data (Figure 6b), is synoptically realistic and may not have been resolved by the widely spaced Canadian radiosonde network. In the 12 and 24hr TIROS-N forecasts the main trough is in approximately the same position as the control forecast. However, at 12hrs a weak secondary wave is evident in south-central Canada.

ORIGINAL PAGE IS
OF POOR QUALITY

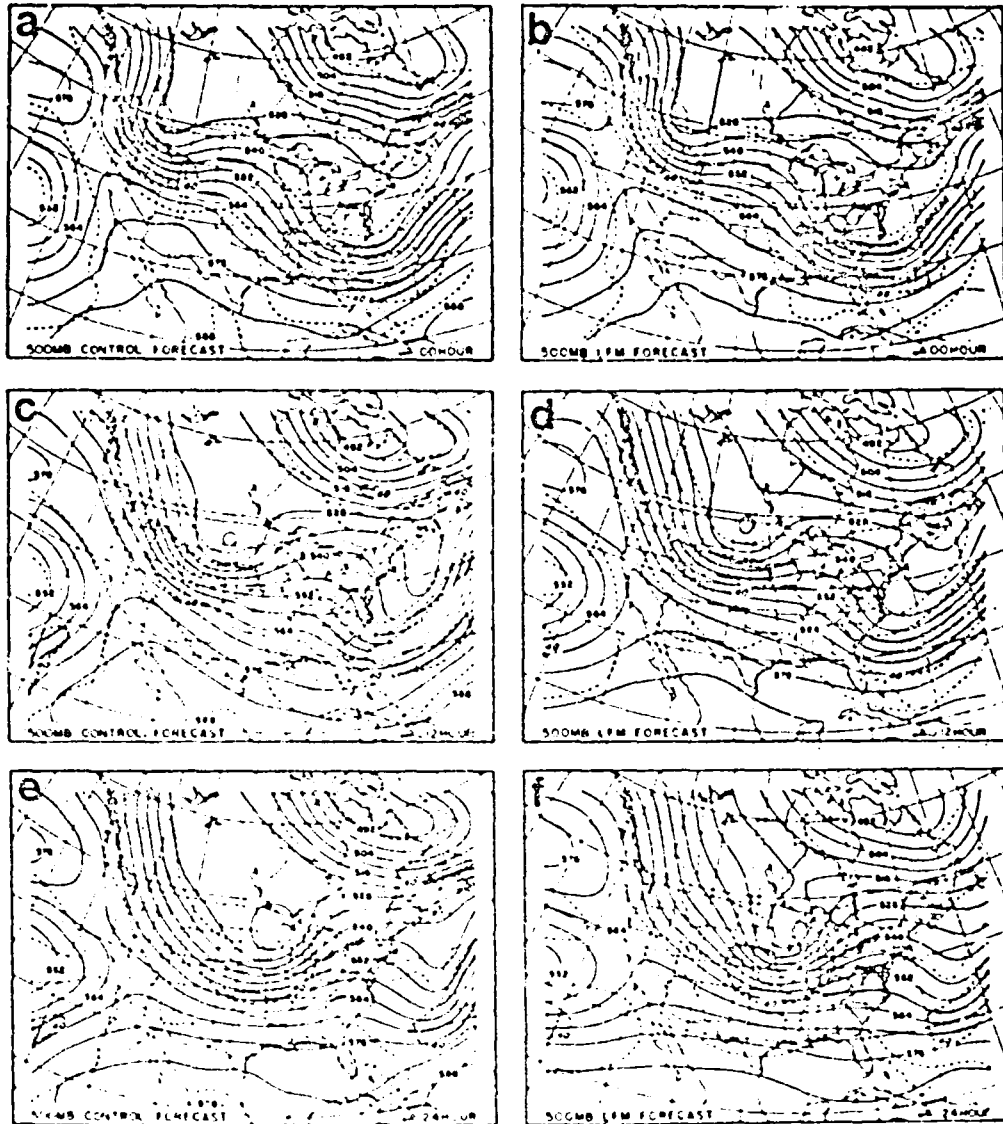


Figure 4: Same as Fig. 3 except from the control (a,c,e) and the 1FM (b,d,f) forecasts.

ORIGINAL PAGE IS
OF POOR QUALITY

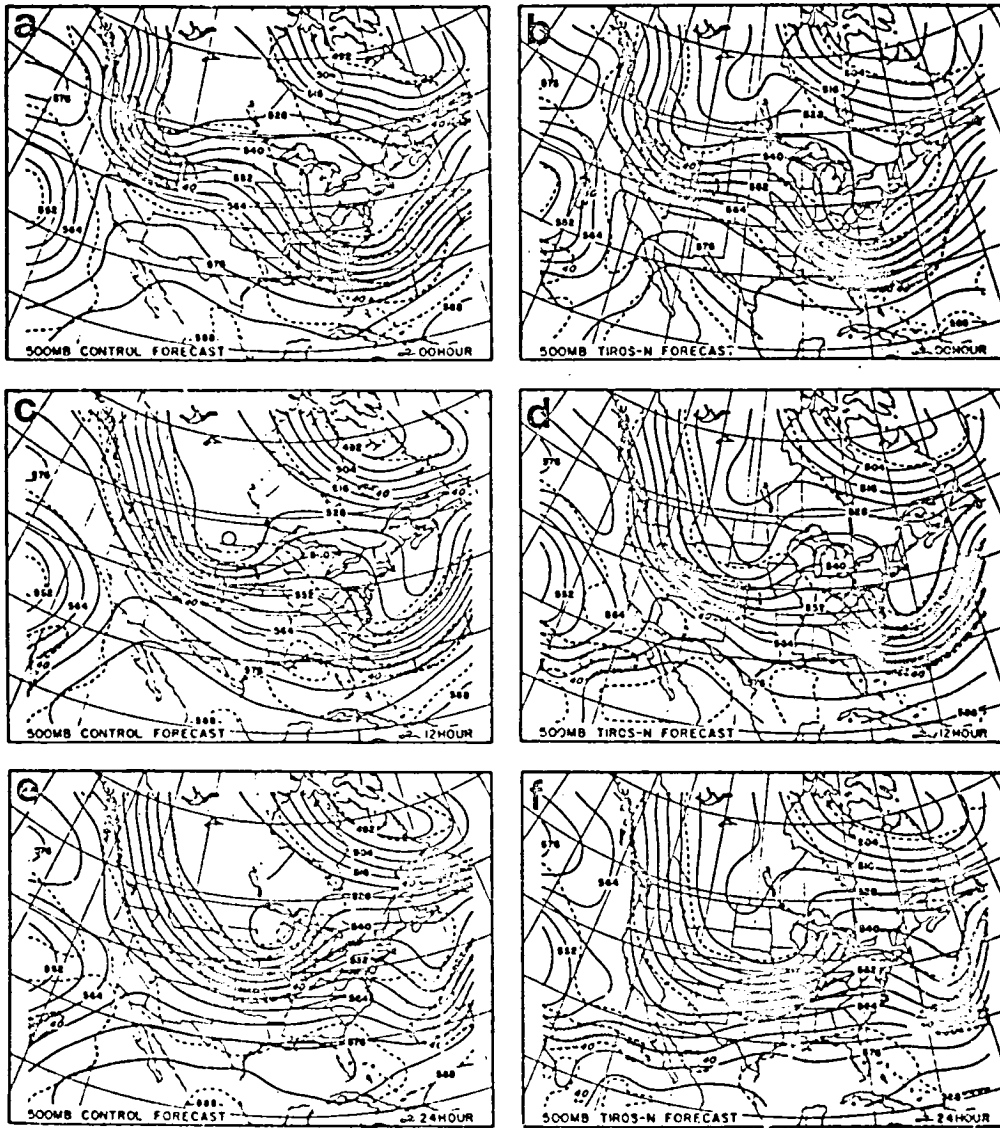


Figure 5: Same as Fig. 3 except from the control (a,c,e) and the TIROS-N (b,d,f) forecasts.

C-2

ORIGINAL PAGE IS
OF POOR QUALITY

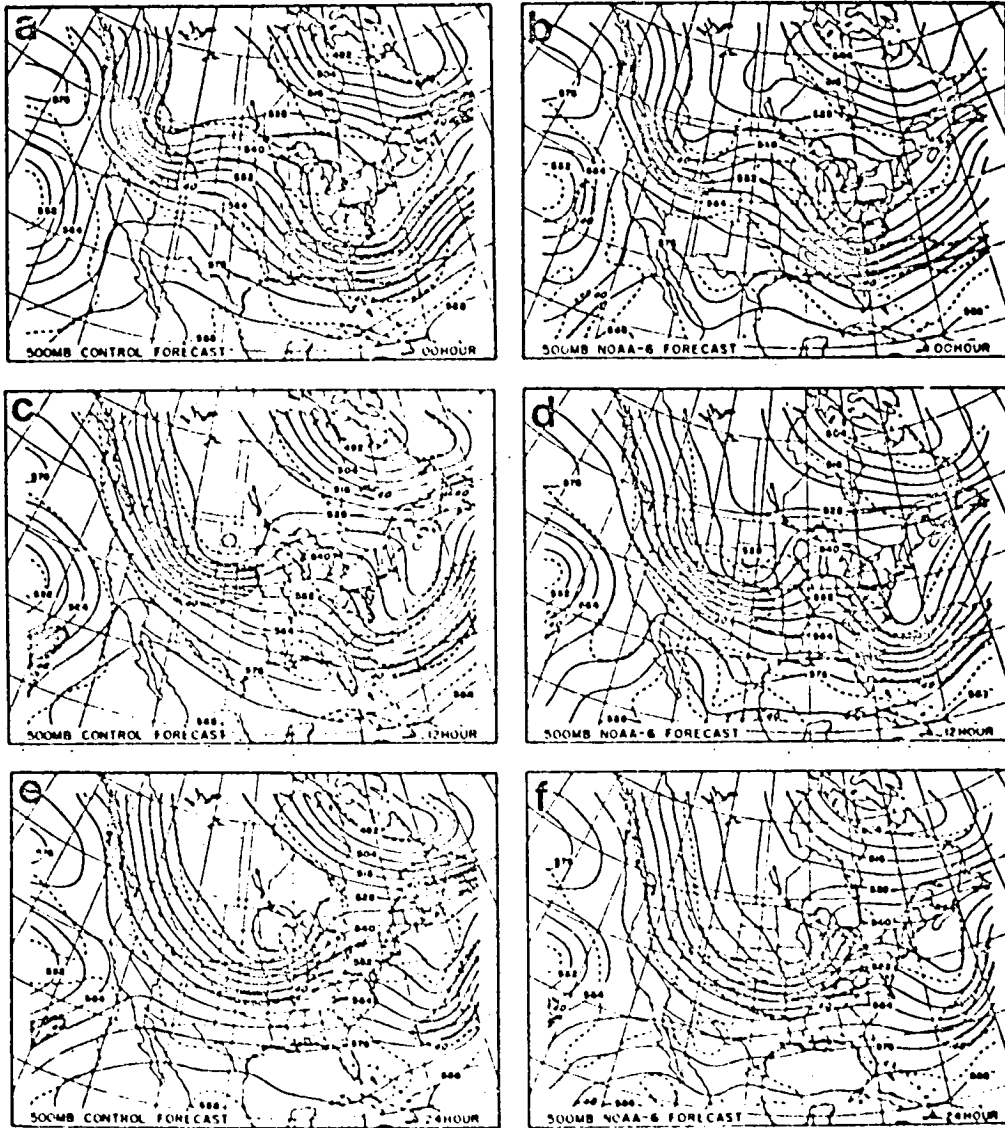


Figure 6: Same as Fig. 3 except from the control (a,c,e) and the NOAA-6 (b,d,f) forecasts.

This secondary trough deepens at 24hrs which along with the main trough created a very broad trough over the north-central United States. Inspection of the intermediate forecasts (not shown) reveals that this feature propagates in from the northern boundary. In both the 12 and 24hr forecasts, the maximum gradients as described by the geostrophic jet are slightly underestimated and too far to the south. Also, the overestimation of heights in the center of the 500mb trough seems to propagate through to the 24hr forecast.

Many features of the NOAA-6 and TIROS-N forecasts are similar: the initial gradients are too weak, the western trough extends back into Canada in the initial data, in the 12 and 24hr forecasts the geostrophic jet maximum was too far to the south, and the western trough was too shallow. However, a comparison between Figures 5 (TIROS-N) and Figure 6 (NOAA-6) demonstrates some major differences. In the initial data, the NOAA-6 analysis shows an anomalous trough located over Mexico (Figure 6b). The analysis scheme probably created this anomalous trough by interpolating the gradient created by slightly inferior data into a satellite data gap. Apparently, this trough did not greatly influence the forecast as it was nearly damped out by 24hr. In the Pacific Northwest, there was little tendency in the NOAA-6 forecasts for a secondary trough to form and intensify. (See Figures 6b, d and f.) Thus, the troughs in the 12 and 24hr forecasts are considerably more realistic than those in the TIROS-N forecasts. The NOAA-6 00hr fields also overestimated the heights in the trough more than the 00hr fields in the TIROS-N forecasts. This feature was propagated along with the trough out to 24hrs. However, the geostrophic jet maxima were not underestimated in the 12 and 24hr forecasts. Overall, the forecasts using only satellite upper air data did better than expected in forecasting the 500mb height field with the NOAA-6 forecasts being slightly better in positioning the 500mb trough and the TIROS-N forecasts being slightly better in describing the magnitudes of the height fields.

b. The 700-300mb layer

The control and verification 700-300mb thickness and thermal wind isotach analyses are shown in Figure 7 and the thickness difference fields between the same two thickness fields are shown in Figure 8. The effects of the initialization on the 700-300mb field was once again a reduction of the gradient as indicated by the 700-300mb thermal wind pattern. The 12hr forecast shows the western thickness trough moving too fast resulting in large negative thickness differences over the Dakotas and positive differences on the western side of the trough. At both 12 and 24hrs, the center of the maximum thickness gradient is properly located. However,

ORIGINAL PAGE IS
OF POOR QUALITY

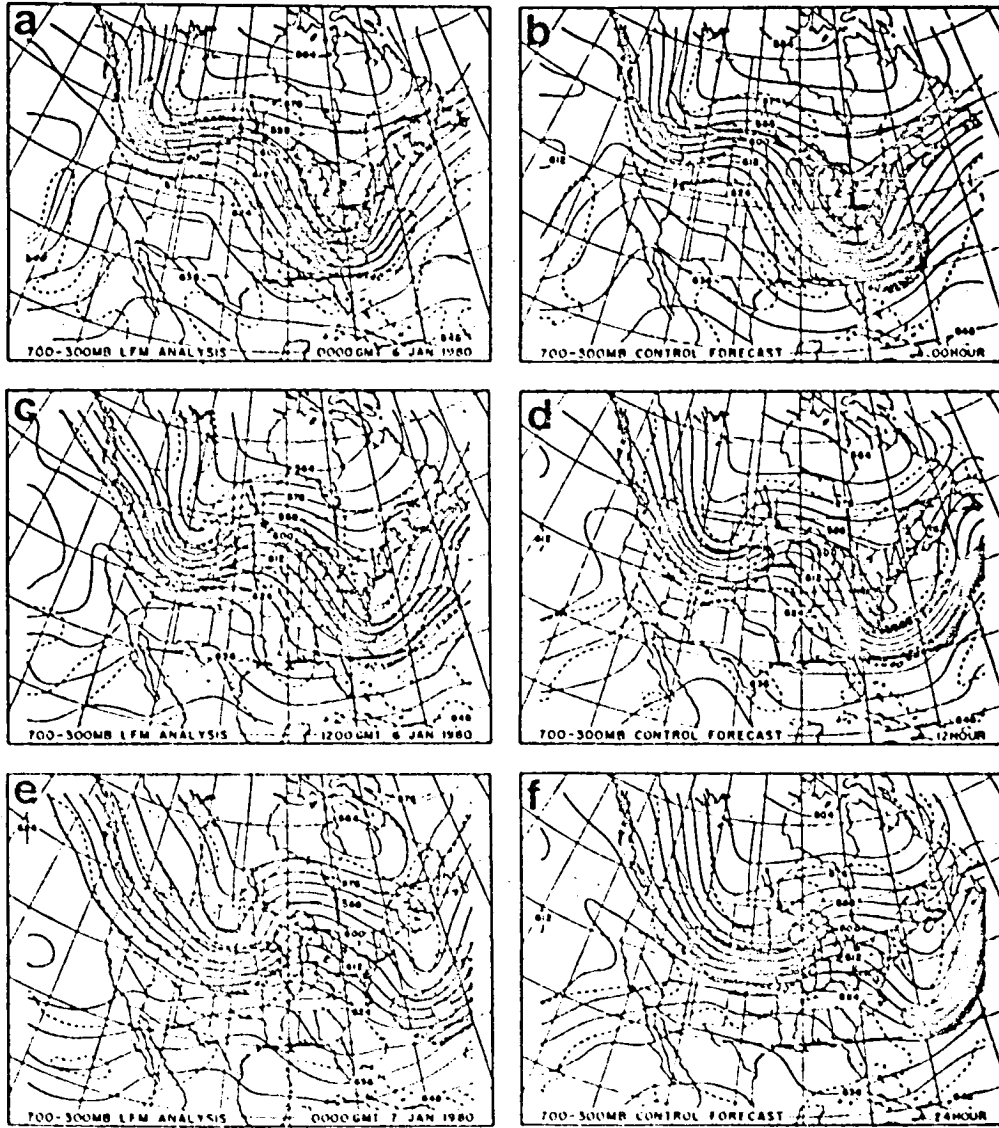


Figure 7: 700-300mb thickness (solid, dam) and thermal wind isotach (dashed, 20 m s⁻¹ interval) analyses for the LFM analysis (a,c,e) and control forecast (b,d,f). Isotach values greater than 40 m s⁻¹ are shaded.

ORIGINAL PAGE IS
OF POOR QUALITY

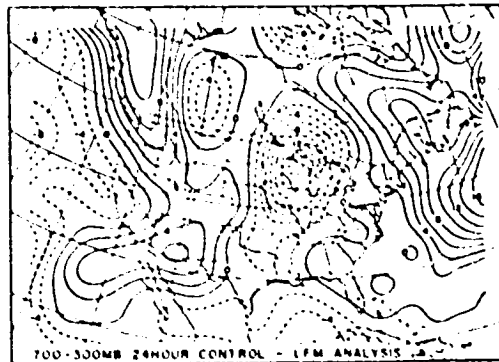
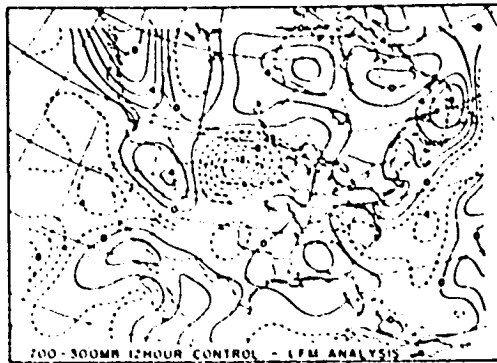
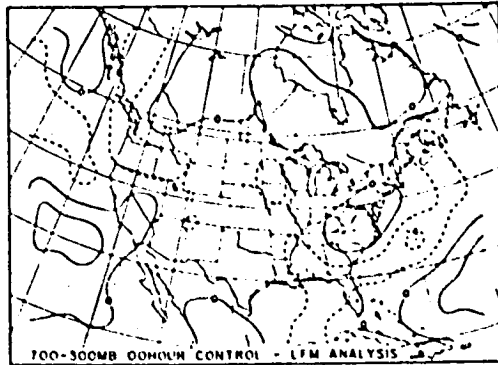


Figure 8: Control forecast minus LFM analysis thicknesses differences (dam). Negative differences are dashed.

the 12hr forecast overestimates the gradient at the base of the western trough. At 24hrs, the thickness trough has become too broad with a slight indication of a short wave trough developing on its eastern side. The geostrophic jet maximum associated with this pattern has a greater east-west extent.

Since the TIROS-N and NOAA-6 700-300mb 00hr forecasts shown in Figures 9b and 10b have no 40m s^{-1} thermal wind maximum in the western trough, it is apparent that the satellite underestimated the thickness gradients. This is also shown in Figures 11a and b. The 700-300mb satellite minus control thickness difference fields show that for both satellites the western trough axis is initially defined by a region of positive thickness anomalies surrounded by negative thickness differences, resulting in the underestimation of the thickness gradient in the satellite data. For both TIROS-N and NOAA-6, the resulting overestimation of heights are propagated with the trough through 24hr. Despite the underestimation of the gradient in the 00hr forecast, the thermal wind jet maxima in the 12 and 24hr forecasts are of nearly the same magnitude in the satellite forecasts as in the control forecast. However, in both the TIROS-N and NOAA-6 forecasts there is a tendency for the maximum gradient to be located on the west side of the trough as opposed to being located in the base of the control trough. Both satellite forecasts maintain the ridge north of Lake Superior better than the control forecast in the 24hr forecasts. (Compare Figures 9f and 10f.) Thus, the trough is not as broad as the control forecast yet still broader than the verification.

Even though both satellite forecasts are similar, certain differences exist. In all the TIROS-N forecasts, the magnitude of the thickness field more closely resembles the control forecasts and verifying analyses than the NOAA-6 forecast. In the TIROS-N forecast, anomalous troughing is indicated off Baja, Mexico at 12hrs and moves inland at 24hrs. (See Figures 11c and e.) This is probably due to slightly incorrect initial data along the fixed boundary which continuously produced errors through the forecast period. At 24hrs both the TIROS-N and NOAA-6 forecasts have developed indications of a short wave thickness trough over the Midwest as did the control forecast. However, the short wave trough in the NOAA-6 forecast is considerably more pronounced. (Figures 9f and 10f.)

c. Statistical evaluations

The statistical evaluation of the forecast was performed using layer mean temperatures for the three layers, 1000-700mb, 700-300mb and 300-100mb. Bias, standard deviation and SI scores were calculated. (See Table 1.) The verification

ORIGINAL PAGE IS
OF POOR QUALITY

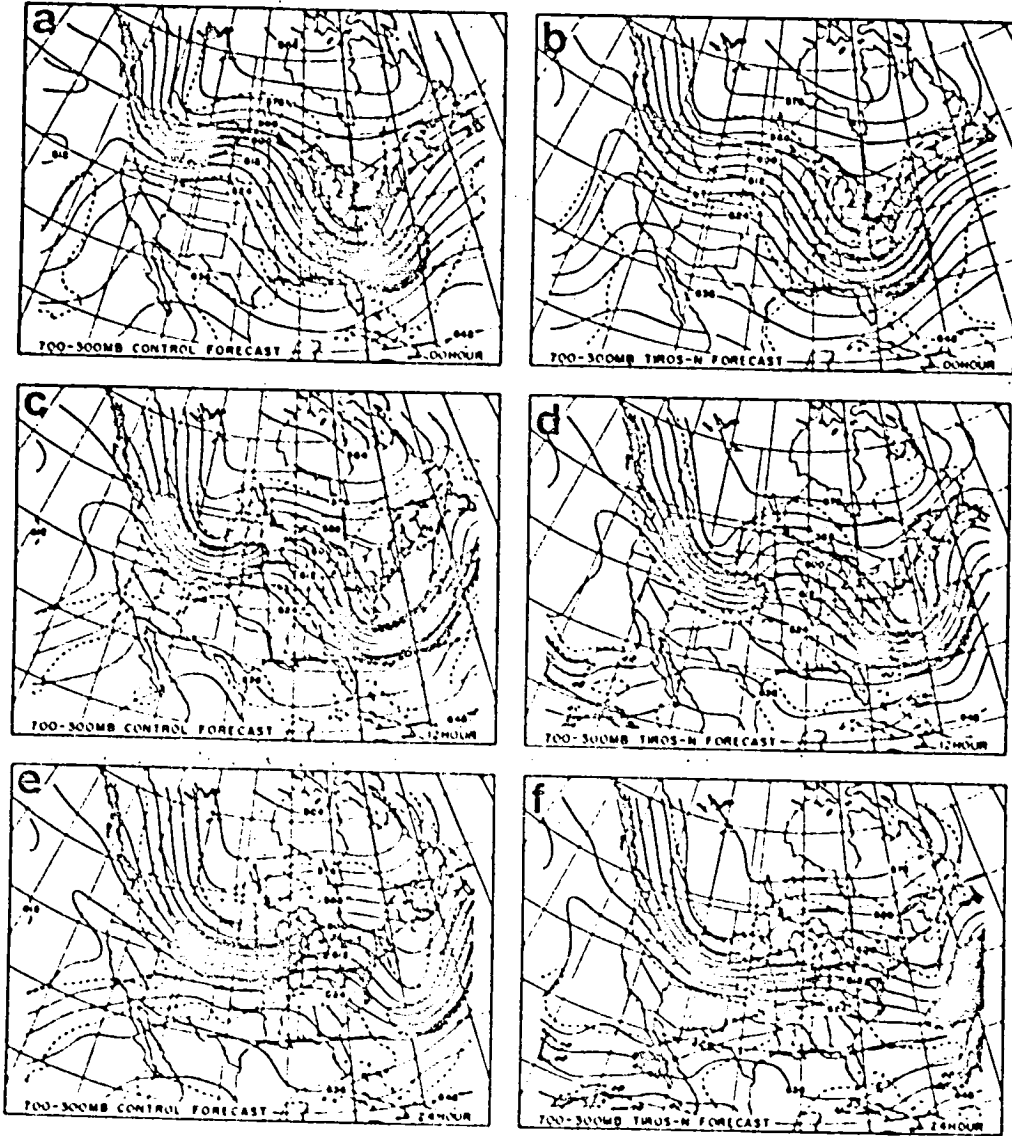


Figure 9: Same as Fig. 7 except for control (a,c,e) and TIROS-N (b,d,f) forecasts.

ORIGINAL PAGE IS
OF POOR QUALITY

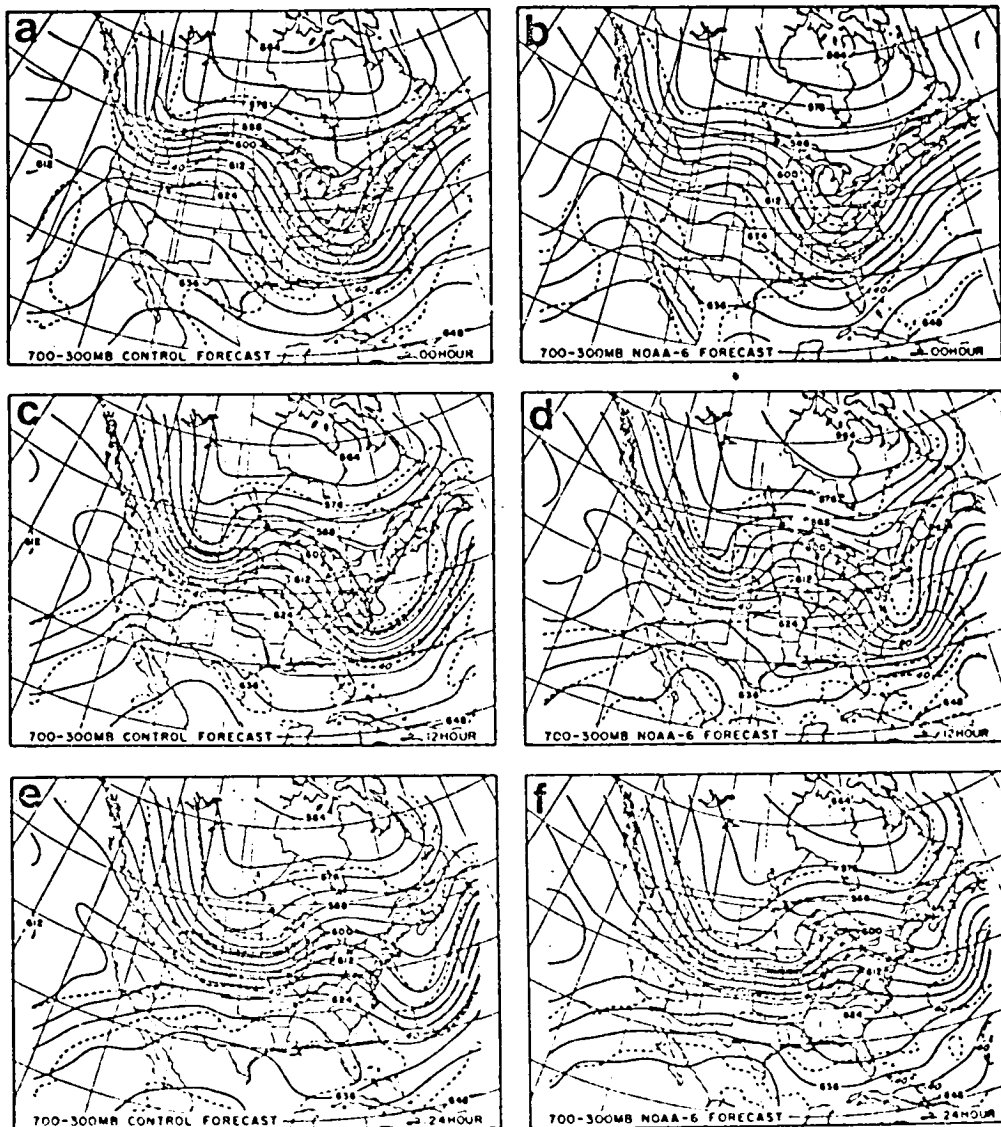


Figure 10: Same as Fig. 7 except for control (a,c,e) and NOAA-6 (b,d,f) forecasts.

Table 1: Layer mean temperature comparisons between the control, TIROS-N and NOAA-6 forecasts and the LPM analyses (top three lines of a, b, and c). Also compared were the TIROS-N and NOAA-6 forecasts with the control forecasts (last two lines of a, b, and c).

a. BIAS

	1000-700MB			700-300MB			300-100MB		
	00 HOUR	12 HOUR	24 HOUR	00 HOUR	12 HOUR	24 HOUR	00 HOUR	12 HOUR	24 HOUR
CONTROL VS ANAL.	.43	.14	-.35	-.36	-.03	-.19	.26	-1.69	-2.73
TIROS-N VS ANAL.	-.15	-.81	-1.83	-.79	-1.00	-1.77	1.33	-.81	-1.87
NOAA-6 VS ANAL.	.71	.01	-.71	-.90	-.58	-1.13	1.44	-.52	-1.40
TIROS-N VS CONTROL	-.58	-.96	-1.48	-.43	-.97	-1.57	1.07	.88	.85
NOAA-6 VS CONTROL	.28	-.13	-.36	-.54	-.54	-.94	1.18	1.18	1.32

b. STANDARD DEVIATION

	1000-700MB			700-300MB			300-100MB		
	00 HOUR	12 HOUR	24 HOUR	00 HOUR	12 HOUR	24 HOUR	00 HOUR	12 HOUR	24 HOUR
CONTROL VS ANAL.	.79	1.87	2.22	.43	1.33	1.62	.50	1.30	1.73
TIROS-N VS ANAL.	1.44	2.17	3.12	1.17	1.81	2.10	1.26	1.53	3.02
NOAA-6 VS ANAL.	2.07	2.57	2.81	1.71	2.07	1.74	1.92	1.90	2.70
TIROS-N VS CONTROL	1.32	1.54	2.40	1.03	1.66	2.41	.98	1.56	2.63
NOAA-6 VS CONTROL	2.18	2.37	2.52	1.59	1.87	1.69	1.62	2.02	2.49

c. S1

	1000-700MB			700-300MB			300-100MB		
	00 HOUR	12 HOUR	24 HOUR	00 HOUR	12 HOUR	24 HOUR	00 HOUR	12 HOUR	24 HOUR
CONTROL VS ANAL.	17.0	33.0	39.9	10.3	28.9	32.1	11.7	31.6	38.3
TIROS-N VS ANAL.	36.0	43.9	56.0	25.0	34.0	43.7	24.7	34.8	56.2
NOAA-6 VS ANAL.	46.2	51.0	53.3	32.4	36.8	41.7	36.7	40.4	55.5
TIROS-N VS CONTROL	30.2	30.6	36.6	21.6	34.0	45.0	21.0	37.2	47.4
NOAA-6 VS CONTROL	41.1	40.3	39.4	28.8	37.2	38.7	31.7	43.8	52.6

region previously shown in Figure 1 was chosen to be over an area rich in conventional data and was positioned to minimize the more severe boundary effects. In conducting the statistical comparisons, every third grid point was used in order to make the results reasonably compatible with those done on the LFM subset grid used by Schmidt et al. (1981). Recall that the LFM grid spacing is 190.5km compared with 67.56km used in the ANMRC model. The satellite forecasts are verified against both the LFM analyses and the control run. Verification against the control run was intended to reduce the effects on the statistics of the basic model errors and consistent errors resulting from the simplified experimental design.

The 00hr comparisons of the control versus the LFM analyses reveals the effect of the initialization and post-processing on the conventional data. For all three statistics, the smallest initialization and post-processing errors are located in the 700-300mb layer. Thus, the earlier choice of the 700-300mb layer based on the poor sounding quality below 700mb and above 300mb is further justified by the small effects of initialization and post-processing in this layer.

In the 300-100mb layer during the 24hr forecast period, the bias changes by nearly 3°C (from positive to negative values) in all three forecasts when compared to the LFM analyses. (See top three lines of Table 1a.) Closer inspection of the data (not shown) reveals that a large part of this bias change was in the 200-100mb layer. It is likely that much of this feature is due to the previously mentioned inconsistency in the initialization of the top sigma level.

In all cases when the forecasts were compared to the LFM analysis, the control forecast had lower standard deviations and S1 scores than the satellite forecasts. This implies, as expected, that the satellite analyses are less accurate than the conventional LFM analysis. However, it is encouraging that the standard deviations of the satellite forecasts versus the LFM analyses are only about 1°C greater than the corresponding control versus LFM analysis values. Also, the S1 scores for the 12hr forecasts in the 700-300mb layers (lines 2 and 3 in Table 1c) are certainly respectable. The lowest layer, 1000-700mb, appears to have abnormally large standard deviations and S1 scores. However, when the satellite forecasts are compared to the control forecasts these differences are generally reduced. This indicates that much of the difference may be a result of the initialization, post-processing or modelling errors, rather than satellite data errors.

In comparing the two satellites with each other an interesting feature is noted. At 00 and 12hr the TIROS-N forecasts are distinctly superior, but at 24hr, the NOAA-6 forecast is somewhat better. Inspection of the 700-300mb thickness difference fields in Figure 11 reveals that much of the decrease in the TIROS-N forecast skill between 12 and 24 hr is probably due to the large area of negative differences in the Southwest States. As mentioned previously, this error was probably due to the incorrect specification of the thermal structure along the fixed boundary. In the 12hr forecast the area is still far enough west to be mostly out of the verification region.

In summary, the results involving 500mb height fields, 700-300mb thickness fields and statistical parameters are consistent. While the major troughs and ridges are reasonably positioned in the satellite forecasts, the troughs are too warm and the ridges are too cold. As a result the overall gradients are somewhat reduced from those in the LFM analyses and the control forecasts. These patterns are similar to those found in the analyses based only on satellite data. (See Schmidt et al., 1981.) However, the maximum gradients tend to be of the same magnitude as the control forecast, but somewhat misplaced. Also, the forecasts unfortunately appear to be influenced by the use of fixed boundaries, especially the TIROS-N forecasts.

6. Conclusions

Using a high resolution limited area model, twenty-four hour forecasts have been produced from initial fields based only upon TIROS-N and NOAA-6 satellite upper air data and conventional surface data. These forecasts were evaluated against forecasts made using conventional data under the same constraints as used in making forecasts based on the satellite data. The evaluation of the information content of the satellite data in a numerical forecast situation was allowed by the complete separation of satellite and conventional upper air data and consistent preparation of the initial fields. Since two separate initial fields were derived using temperature data from two different satellites, an intercomparison between the two satellite forecasts was also possible.

The initial fields as described by the satellite data contained temperature gradients which were weaker than those in the conventional analyses. As shown by Schmidt et al. (1981) in a more complete study of the basic satellite analyses, this situation results from the overestimation of the temperature in troughs. This has been a persistent problem found in many previous studies (e.g. Koehler, 1981,

ORIGINAL PAGE IS
OF POOR QUALITY



Figure 11: TIROS-N minus control (a,c,e) and NOAA-6 minus control (b,d,f) forecast 700-300mb thickness differences (dam) with negative values dashed.

using Nimbus-6 data and Schlatter, 1981, using TIROS-N data). In the satellite forecast, this characteristic of the temperature field was propagated along with the synoptic features. However, in the forecasts the maximum temperature gradients were not generally underestimated but rather they were somewhat incorrectly located. Despite the initial underestimation of the temperature gradients, the satellite forecasts were still able to define the location of the major trough and ridge positions with a reasonable degree of accuracy under fairly severe limitations.

The satellite forecasts along with the control forecast were limited by the use of initial geostrophic winds, fixed boundary conditions and very limited parameterization. The lack of parameterization is unlikely to have severely affected the forecasts. The use of initial geostrophic winds undoubtedly had a detrimental effect on the forecasts. However, since the control forecast was similarly degraded, comparisons to the control forecast may have reduced the detrimental effect of using initial geostrophic winds. Unfortunately this is not true for the boundary conditions. Since fixed boundary conditions were used, an initial error in the boundary data may continue to generate errors throughout the forecast period. An excellent example of this is shown along the western boundary. The errors produced by the improper initial boundary values were able to propagate well into the Southwest United States in twenty-four hours. Not only were the TIROS-N forecasts degraded by the initial data along the western boundary, but also problems probably existed along the northern boundary as shown by the appearance of a secondary trough at 500mb. Since LFM, TIROS-N and NOAA-6 analyses were available for 1200 GMT 6 January and 0000 GMT 7 January, it may have been better to nest the forecasts using these analyses to update the boundary values.

Comparisons between the TIROS-N and NOAA-6 forecasts were difficult, since it appears that the TIROS-N forecast was more severely degraded by poor initial values along the fixed boundary. Statistically the TIROS-N data initially and at 12hr produced a better forecast than the NOAA-6 data. By 24hr the errors resulting from initial errors along the boundary had propagated inward far enough to severely effect the statistics. Thus, at 24hr the TIROS-N statistics were sufficiently degraded causing the NOAA-6 forecast statistics to be relatively superior. Subjectively, both satellites provided reasonable forecasts considering the synoptic situation. The NOAA-6 forecasts generally were slightly better at locating the synoptic features, while TIROS-N forecasts better described the magnitude of the temperature field. Considering the similarity of the initial fields it is not surprising that many aspects of the satellite forecasts were more

similar to each other than to the control or verifying analyses. It is also possible that differences in the satellite data and the conventional data were not only a result of satellite data errors, but also the satellite data may have resolved features not found in the conventional data.

The similarity in forecasts and initial fields further demonstrates that the satellite errors are not random but rather highly correlated to the synoptic situation. Correlated errors are more likely to be incorporated into the model forecasts than random errors. Therefore, the operational satellite data appear unlikely to produce a positive impact on numerical forecasts in a relatively data dense region unless the correlated nature of the data errors is either reduced or corrected using a thorough understanding of the correlated error structure. It should be noted that satellite soundings were not intended to completely replace conventional data but rather to provide supplementary information in data poor regions. In these regions, the satellite data are likely to contain enough additional information to improve numerical forecasts, if the difficult problem of combining data sources with differing error characteristics can be solved.

Acknowledgements

We wish to thank all those who took an active part in this study. Special thanks go to Brian Schmidt who contributed significantly in preparing the satellite sounding data, to Geary Callan, Graham Mills and Dr. Robert Schlesinger who helped with the ANMRC model runs, and to Eva Singer who typed the final manuscript. The ANMRC model runs were completed on the Cray-1 computer at the National Center for Atmospheric Research in Boulder, Colorado. This research was supported by NASA Grant NSG-5252.

References

- Blechman, A.G., and L.H. Horn, 1981: The influence of higher resolution Nimbus-6 soundings on locating jet maxima. Case Studies Employing Satellite Indirect Soundings Dept. of Meteor., U. of Wis., Final Report for NOAA Grant 04-4-158-2, 1-30.
- Bonner, W.D., K. Van Haaren and C.H. Hayden, 1976: Operational type analyses derived without radiosonde data from Nimbus 5 and NOAA 2 temperature soundings. NOAA Tech. Memo., NWS NMC 58, 17 pp.
- Gerrity, J.P., Jr., and J. Newell, 1976: Post processing the LFM forecasts. Technical Procedures Bulletin No. 174, NOAA, National Weather Service, Silver Spring, Md.
- Ghil, M., M. Halem, and R. Atlas, 1979: Time continuous assimilation of remote sounding data and its effect on weather forecasting. Mon. Wea. Rev., 107, 140-171.
- Halem, M., M. Ghil, R. Atlas, J. Susskind and W.J. Quirks, 1978: The GISS sounding temperature impact test. NASA Tech. Memo. 78063, NASA Goddard Space Flight Center, Greenbelt, Md., 421 pp.
- Horn, L.H., R.A. Peterson and T.M. Whittaker, 1976: Intercomparisons of data derived from Nimbus-5 temperature profiles, rawinsonde observations and initialized LFM model fields. Mon. Wea. Rev., 104, 1362-1371.
- Kelly, G.A.M., G.A. Mills, and W.L. Smith, 1978: Impact of Nimbus-6 temperature soundings on Australian region forecasts. Bull. Amer. Meteor. Soc., 59, 1225-1240.
- Koehler, T.L., 1981: A case study of height and temperature analyses derived from Nimbus-6 satellite soundings. Evaluations of Satellite Temperature Soundings Using Analyses and Model Forecasts. Dept. of Meteor., U. of Wis., Final Report for NASA Grant NSG-5252, 1-50.
- McGregor, J.L., L.M. Leslie and D.J. Gauntlett, 1978: The ANHRC limited area model: consolidated formulation and operational results. Mon. Wea. Rev., 106, 427-438.
- Mills, G.L., L.M. Leslie, J.L. McGregor and G.A.M. Kelly, 1981: A High Resolution Numerical Analysis/Forecast System for Short Term Prediction over the North American Region. Unpublished manuscript. Australian Numerical Meteorology Research Centre.
- Ohring, G., 1979: Impact of satellite temperature sounding data on weather forecasts. Bull. Amer. Meteor. Soc., 60, 1142-1157.
- Petersen, R.A., and L.H. Horn, 1977: An evaluation of 500mb height and geostrophic wind fields derived from Nimbus-6 soundings. Bull. Amer. Meteor. Soc., 1188-1197.

- Phillips, N., L. McMillin, A. Gruber, and D. Wark, 1979: An evaluation of early operational temperature soundings from TIROS-N. Bull. Amer. Meteor. Soc., 60, 1106-1197.
- Schlatter, T.W., 1981: An assessment of operational TIROS-N temperature retrievals over the United States. Mon. Wea. Rev., 109, 110-119.
- Schmidt, E.D., T.L. Kochler and L.H. Horn, 1981: Evaluation of TIROS-N and NOAA-6 satellite data: comparisons of colocated soundings and analyses for a January case. Evaluations of Satellite Temperature Soundings Using Analyses and Model Forecasts. Dept. of Meteor., U. of Wis., Final Report for NASA Grant NSC-5252, 51-81.
- Streit, D.F., and L.H. Horn, 1981: Intercomparisons of TIROS-N satellite soundings, radiosonde data and NMC analyses in tracking jet streaks. Synoptic-Dynamic Applications of Meteorological Satellite Data. Dept. of Meteor., U. of Wis., Final Report for NOAA Grant NA79AA-E-00011.
- Tracton, M.S., A.J. Desmarais, R.J. van Haaren and R.D. McPherson, 1980: The impact of satellite soundings upon the National Meteorological Center's analysis and forecast system - the Data Systems Test results. Mon. Wea. Rev., 108, 543-586.
- Tracton, M.S., A.J. Desmarais, R.J. van Haaren and R.D. McPherson, 1981: On the system dependency of satellite sounding impact - comments on recent impact test results. Mon. Wea. Rev., 109, 197-200.

ORIGINAL PAGE IS
OF POOR QUALITY

END

DATE

FILMED

MAY 13 1982